Mass spectrometry - recent applications in chemistry, pharmacology and biology

Bigler, L

MASS SPECTROMETRY – RECENT APPLICATIONS IN CHEMISTRY, PHARMACOLOGY AND BIOLOGY

Habilitationsschrift

Submitted by

Laurent Bigler, PhD

Institute of Organic Chemistry

University of Zurich

Zurich, 2008

ACKNOWLEDGMENTS

I would like to express my deepest gratitude to the following people who helped me in any capacity in the completion of this work:

Prof. J. Siegel for his generous support as well as his encouragements and for providing the opportunity to plan, conduct and presents various projects independently;

Prof. St. Bienz for his guidance, fruitful discussions, and advices in my daily life;

Urs, who supported me in the concretization of so many research projects;

Serge, Manuel and Silvan, for their friendship, and their great job in my mass lab;

Armin, curator of the institute's unique collection of natural products, for his advisements and for the shared moments;

Dr. R. Ha and Prof. Follath for the close and productive collaboration in the amiodarone project;

Prof. H. Möhler, and PD. Dr. R. Stendel for the interesting pharmacokinetic task;

PD. Dr. C. Ringli, Prof. E. Martinoia, and D. Santelia for providing me a fundamental introduction in plant biology and the fruitful cooperation in the flavonoid project;

The institute of organic chemistry for support and confidence;

Prof. M. Hesse for his support and his enthusiasm that convinced me to start this habilitation work;

My family, in particularly my wife, for her support in hard and stressed time;

And finally to all those persons who somehow contributed to the realization of this work.

SUMMARY

Over the past decade, mass spectrometry has undergone tremendous technological improvements allowing for its application to proteins, peptides, carbohydrates, DNA, drugs, and many other molecules relevant to material chemistry and chemical biology. Due to ionization methods such as electrospray ionization and matrix-assisted laser desorption, mass spectrometry has become an irreplaceable tool in molecular and life sciences.

In this treatise, a general history with the milestones of developments in mass spectrometry and their inventors is first presented. In the second part, the basics of mass spectrometry – ionization source, analyzer, and their combination with chromatographic methods – are shortly discussed. In the third part, analytical methods that were developed in our department and the context of the research projects are described and an outlook for future research is given in chapter 4. Finally, four selected applications in different research domains were chosen to show the versatility of analytics based on mass spectrometry (Chap. 5).

Structure elucidation of natural products will be exemplified with the characterization of polyamine derivatives found in spider venoms (Chap. 5.1). The analysis of such samples is a challenge, because structure elucidation of new natural products is performed directly from a complex mixture of sometimes more than thirty similar compounds having frequently same molecular weights.

In order to obtain confident interpretations, fundamental knowledge of molecular fragmentation reactions occurring in tandem mass spectrometry was necessary. To identify the origin of unexpected fragment ions, the ESI-MS/MS spectra of three synthetic ^{15}N-labeled polyamine derivatives were recorded on a triple quadrupole mass spectrometer (Chap. 5.2). The detailed knowledge of fragmentation mechanisms is essential, particularly when co-eluting isomeric compounds within complex mixtures such as spider venom are investigated.

Quantification of taurolidine in human blood plasma and whole blood will illustrate the application of mass spectrometry in pharmacology. Recently, this drug was found to exert an anti-neoplastic effect that could be applied to the treatment of glioblastoma. A new quantification method based on HPLC-ESI-MS/MS in the "multiple reaction monitoring" mode that allows pharmacokinetic studies was developed (Chap. 5.3). During repetitive infusions in patients, we could show that the calculated serum concentrations of taurolidine strongly increased after the start of each infusion and continued to increase until the end of the infusion, followed by a rapid decline. These results indicate that a repetitive infusion of taurolidine is the therapeutically adequate mode of administration for the indication of glioblastoma multiforme.

Finally, an example concerning the profiling – determination of structure and relative amounts – of glycosylated flavonol derivatives in Arabidopsis plants is given (Chap. 5.4). These experiments allowed the study of the function of these secondary metabolites in order to understand plant growth and development. We could demonstrate that subtle changes in the composition of flavonol glycosides can have a tremendous impact on plant development through auxin-induced and auxin-dependent processes.

TABLE OF CONTENTS

‡ equal contribution of both authors to this work

Curriculum Vitae

BIGLER LAURENT

Personal Data

Born:	Mai 8, 1968 in Meyriez (Switzerland)
Nationality:	Swiss citizen
Marital status:	Married, 4 children
Office address:	University of Zurich, Institute of Organic Chemistry, Winterthurerstr. 190, 8057 Zurich, Switzerland. Phone: (++41) 44-635 42 86; FAX: (++41) 44-635 68 12. Email: lbigler@oci.uzh.ch URL: http://www.oci.uzh.ch/service/ms.php
Private address:	Im Stüdli 9, 8627 Grüningen Phone: (++41) 43-833 91 22; FAX: (++41) 43-833 91 23 Email: l.bigler@bluewin.ch

Education and Academic Degrees

1983-1987	College “St-Michel“ in Fribourg, Matura (Sciences) 1987.
1987-1991	Studies in Chemistry at the University of Fribourg. Diploma in organic chemistry under the supervision of Prof. Dr. R. Neier entitled: **"Contribution à la synthèse du squelette de composés du type γ-Lycoran" (Tandem-Reaktionen Diels-Alder /Aldol-Kondensation)**. Diploma in physical chemistry under the supervision of Prof. Dr. P. Suppan entitled: "**Etude de la photolyse de dérivés halogénés de l'anthracène**".
1992-1996	PhD thesis in organic chemistry at the institute of organic chemistry at the University of Zurich under the supervision of Prof. Dr. M. Hesse and entitled: **"Anwendungen der Elektrospray-Ionisations-Massenspektrometrie. Strukturuntersuchungen an Polyamin-Derivaten und Korrelation von Metall-Ligand-Wechselwirkungen in Lösung und in der Gasphase"**.

Teaching and Research Experiences

1990-1991	Teacher in mathematic and physic at the “Gymnasium Gambach“ in Fribourg.
Since 1996	Scientific co-worker at the institute of organic chemistry at the University of Zurich.
2002	Organizer of the practical course "Praktische Einführung in die Massenspektrometrie inclusive GC/MS und HPLC/MS" for graduate students.
Since 2002	Head of the mass spectrometry department at the institute of organic chemistry and responsible for acquisition, operation, maintenance, and education. Habilitation work at the institute of organic chemistry. Lecturer (undergraduate) on "Anwendung spektroskopischer Methoden in der Chemie" (module CHE214.1; MS-part) together with T. Fox und St. Bienz. Guidance and formation of PhD students.
Since 2005	Lecturer (graduate) on "Spectroscopic Methods II" (module CHE431.1; MS-part) together with O. Zerbe, N. Walch and S. Jurt.

Further Tasks und Activities

- Wittnessing analyst with supervision and expertise of B-sample investigations in over fifteen doping cases related to the “Federation Equestre Internationale” (FEI), “Deutschen Reiterlichen Vereinigung” and the “Schweizerischen Pferde-Verband”.
- Committee Member of the “Swiss Group for Mass Spectrometry”
- Member of the “Swiss Chemical Society”, incl. “Division of Analytical Chemistry”
- Member of the “American Society for Mass Spectrometry”
- Member of the “Deutsche Gesellschaft für Massenspektrometrie”

Scientific Collaborations (October 2007)

- Prof. St. Bienz, Institute of Organic Chemistry, University of Zurich – Mass spectrometry as most sensitive tool for structure elucidation of natural products.
- Dr. H.R. Ha / Prof. Dr. F. Follath, Cardiovascular Therapy Research, Department of Internal Medicine, University Hospital of Zurich – Metabolism of Amiodarone, an antiarrhythmic drug.
- Prof. E. Martinoia, Institute of Plant Biology, University of Zurich. – Flavonoids and Auxin Flux.
- PD. Dr. C. Ringli, Institute or Plant Biology, University of Zurich. – Flavonol Glycosylation Profile and Plant Growth.
- Dr. S. Miescher Schwenninger, Institute of Food Science and Nutrition, ETH Zurich. – Synergisms effects between lactic acid bacteria and propionic acid bacteria.

Publication List

1. Baak, M.; Rubin, Y.; Franz, A.; Stoeckli-Evans, H.; Bigler, L.; Nachbauer, J.; Neier, R. (1993). "An unexpected tandem reaction between *N*-butadienyl-*N*-alkylketene *N,O*-trimethylsilyl acetals of propionamide and activated dienophiles like *N*-phenylmaleimide or acryloyl chloride" *Chimia* **47**, 233-240.
2. Chapeaurouge, A.; Bigler, L.; Schäfer, A.; Bienz, S. (1995). "Correlation of stereoselectivity and ion response in electrospray mass-spectrometry. Electrospray ionization-mass spectrometry as a tool to predict chemical behavior?" *J. Am. Soc. Mass Spectrom*. **6**, 207-211.
3. Bigler, L.; Hesse, M. (1995). "Neighboring group participation in the electrospray ionization tandem mass spectra of polyamine toxins of spiders. Part 1: α,ω-diaminoalkane compounds." *J. Am. Soc. Mass Spectrom*. **6**, 634-637.
4. Faessler, J.; Huber, P.; Bratovanov, S.; Bigler, L.; Bild, N.; Bienz, S. (1995). "Neighboring-group participation in the gas phase. Loss of benzaldehyde from [(benzyloxy)methyl]dialkylsilyl-substituted 1,3-dithianes." *Helv. Chim. Acta* **78**, 1855-1862.
5. Bigler, L.; Baumeler, A.; Werner, C.; Hesse, M. (1996). "Detection of noncovalent complexes of hydroxamic-acid derivatives by means of electrospray mass spectrometry", *Helv. Chim. Acta* **79**, 1701-1709.
6. Bigler, L.; Schnider, C. F.; Hu, W.; Hesse, M. (1996). "Electrospray-ionization mass spectrometry. Part 3. Acid-catalyzed isomerization of *N,N′*-bis[(*E*)-3-(4-hydroxyphenyl)prop-2-enoyl]spermidines by the *zip* reaction." *Helv. Chim. Acta* **79**, 2152-2163.
7. Fischer, B.; Vom Orde, M.; Leidenberger, K.; Pacheco, A.; Bigler, L. (1997). "Interactions of hydrogenated pterins with metal complexes; probes for the reaction centers in pterin-dependent metalloenzymes." *Chem. Biol. Pteridines Folates, Proc. Int. Symp. Pteridines Folates*, 23-28.
8. Youhnovsky, N.; Bigler, L.; Werner, C.; Hesse, M. (1998). "Online coupling of high-performance liquid chromatography to atmospheric pressure chemical ionization mass spectrometry (HPLC/APCI-MS and MS/MS). The pollen analysis of *Hippeastrum x hortorum*." *Helv. Chim. Acta* **81**, 1654-1671.
9. Bernasconi, G.; Bigler, L.; Hesse, M.; Ratnieks, F. L. W. (1999). "Characterization of queen-specific components of the fluid released by fighting honey bee queens" *Chemoecology*, **9**, 161-167.
10. Chesnov, S.; Bigler, L.; Hesse, M. (2000). "The spider *Paracoelotes birulai*: detection and structure elucidation of new acylpolyamines by on-line coupled HPLC-APCI-MS and HPLC-APCI-MS/MS." *Helv. Chim. Acta* **83**, 3295-3305.
11. Ha, H. R.; Bigler, L.; Binder, M.; Kozlik, P.; Stieger, B.; Hesse, M.; Altorfer, H. R.; Follath, F. (2001). "Metabolism of amiodarone (Part I): Identification of a new hydroxylated metabolite of amiodarone." *Drug Metab. Dispos.* **29**, 152-158.

12. Ha, H. R.; Kozlik, P.; Stieger, B.; Bigler, L.; Follath, F. (2001). "Metabolism of amiodarone II. High-performance liquid chromatographic assay for mono-*N*-desethylamiodarone hydroxylation in liver microsomes." *J. Chromatogr., B: Biomed. Sci. Appl.* **757**, 309-315.

13. Horsch, P.; Bigler, L.; Altorfer, H. R. (2001). "Influence of radiation sterilization on the stability of trifluorothymidine" *Int. J. Pharm.* **222**, 205-215.

14. Nezbedová, L.; Hesse, M.; Drandarov, K.; Bigler, L.; Werner, C. (2001). "Phenol oxidative coupling in the biogenesis of the macrocyclic spermine alkaloids aphelandrine and orantine in Aphelandra sp." *Planta* **213**, 411-417.

15. Kozlic, P.; Ha, H. R.; Stieger, B.; Bigler, L.; Follath, F. (2001). "Metabolism of amiodarone (Part III) : identification of rabbit cytochrome P450 isoforms involved in the hydroxylation of mono-*N*-desethylamiodarone." *Xenobiotica* **31**, 239-248.

16. Chesnov, S.; Bigler, L.; Hesse M. (2001). "The acylpolyamines from the venom of the spider *Agelenopsis aperta*" *Helv. Chim. Acta* **84**, 2178-2197.

17. Chesnov, S.; Bigler, L.; Hesse, M. (2002). "Detection and characterization of natural polyamines by HPLC-APCI(ESI)-MS" *Eur. J. Mass Spectrom*. **8**, 1-16.

18. Manov, N.; Tzouros, M.; Chesnov, S.; Bigler, L.; Bienz, S. (2002). "Solid-phase synthesis of polyamine spider toxins from the center and correlation with the natural products by HPLC-MS/MS" *Helv. Chim. Acta* **85**, 2827-2846.

19. Zikmundová, M.; Drandarov, K.; Bigler, L.; Hesse, M.; Werner, C. (2002). "Biotransformation of 2-benzoxazolinone (BOA) and 2-hydroxy-1,4-benzoxazin-3-one (HBOA) by endophytic fungi isolated from *Aphelandra tetragona* (Acanthaceae)" *Appl. Environ. Microbiol*. **68**, 4863.

20. Manov, N.; Tzouros, M.; Bigler, L.; Bienz, S. (2004). "Solid-phase synthesis of ^{15}N-labeled acylpentamines as reference compounds for the MS/MS investigation of spider toxins" *Tetrahedron* **60**, 2387-2391.

21. Tzouros, M.; Bigler, L.; Bienz, S.; Hesse, M.; Inada, A.; Murata, H.; Inatomi, Y.; Nakanishi, T.; Darnaedi, D. (2004). "Two new Spermidine Alkaloids from *Chisocheton weinlandii*" *Helv. Chim. Acta* **87**, 1411-1425.

22. Quaglino, D.; Ha, H. R.; Duner, E.; Bruttomesso, D.; Bigler, L.; Follath, F.; Realdi, G.; Pettenazzo, A.; Baritussio, A. (2004). "Effects of metabolites and analogs of Amiodarone on alveolar macrophages: structure-activity relationship." *Am. J. Physiol. Lung Cell Mol. Physiol*. **287**, L438-L447.

23. Kozlick, P.; Baehler, M.; Puentener, C.; Zerbe, O.; Bigler, L.; Altorfer, H. R., *J.* (2004). "*N*-Nitrosylation potential of mono-*N*-desethylamiodarone at physiological pH" *Pharm. Biomed. Analysis* **34**, 399-407.

24. Tzouros, M. ; Manov, N. ; Bienz, S. ; Bigler, L. (2004). "Tandem Mass Spectrometric Investigation of Acylpolyamines of Spider Venoms and their ^{15}N-Labeled Derivatives" *J. Am. Soc. Mass Spectrom.* **15**, 1636-1643.

25. Zerbe, K.; Woithe, K.; Li, D. B.; Vitali, F.; Bigler, L.; Robinson, J. A. (2004). "An Oxidative Phenol Coupling Reaction Catalyzed by OxyB, a Cytochrome P450 from the Vancomycin-Producing Microorganism" *Angew. Chemie* **116**, 6877-6881.

26. Ha, H.R.; Bigler, L.; Wendt, B.; Hesse, M.; Follath, F. (2005). "Identification and Quantitation of Novel Metabolites of Amiodarone in Plasma of Treated Patients" *Eur. J. Pharm. Sciences* **24**, 271-279.

27. Tzouros, M.; Chesnov, S.; Bienz, S.; Hesse, M.; Bigler, L. (2005). "New Linear Polyamine Derivatives in Spider Venoms" *Toxicon* **46**, 350-354.

28. Wenger, K.; Bigler, L.; Suter, M.J.-F.; Schönenberger, R.; Gupta, S.K.; Schulin, R. (2005). "Effect of Corn Root Exudates on the Degradation of Atrazine and its Chlorinated Metabolites in Soils" *J. Environ. Qual.* **34**, 2187-2196.

29. Krauss, J.; Härri, S.A.; Bush, L.; Husi, R.; Bigler, L.; Power, S.A.; Müller, C.B. (2007). "Effects of Fertilizer, Fungal Endophytes and Plant Cultivar on the Performance of Insect Herbivores and Natural Enemies" *Functional Ecology* **21**, 107-116.

30. Bigler, L.; Spirli, C.; Fiorotto, R.; Pettenazzo, A.; Duner, E.; Baritussio, A.; Follath, F.; Ha, H.R. (2007). "Synthesis and Cytotoxicity Properties of Amiodarone Analogues" *Eur. J. Med. Chem.* **42**, 861-867.

31. Eichenberger, S.; Bigler, L. Bienz, S. (2007). "Structure Elucidation of Polyamine Toxins in the Venom of the Spider *Larinioides folium*" *Chimia* **61**, 161-164 – Prize for the best poster presentation at the SCS fall meeting 2006.

32. Stendel, R.; Scheurer, L.; Schlatterer, K.; Stalder, U.; Fiss, I.; Möhler, H.; Bigler, L. (2007). "Pharmacokinetics of Taurolidine following Repetitive Intravenous Infusions Measured by HPLC-MS/MS of the Derivatives Taurultame and Taurinamide in Glioblastoma Patients" *Clin. Pharmacokinet.* **46**, 513-524.

33. Schellenberg, B.; Bigler, L.; Dudler, R. (2007). "Identification and analysis of genes involved in the biosynthesis of glidobactins, a family of antitumor antibiotics" *Environ. Microbiol.* **9**, 1640-1650.

34. Ringli, C.; Bigler, L.; Leiber, R.-M.; Diet, A.; Santelia, D.; Frey, B.; Pollmann, S.; Klein, M. "The Modified Flavonol Glycosylation Profile in the Arabidopsis *rol1* Mutants Results in Auxin-induced and Auxin-independent Alterations in Plant Growth and Cell Shape Formation" *in preparation*.

35. Santelia, D; Vincenzetti, V.; Sauer, M.; Bigler, L.; Klein, M.; Youngsook, L.; Friml, J.; Geisler, M.; Martinoia, E. "Flavonoids redirect polar auxin fluxes during gravitropic responses", *in preparation*.

36. Tzouros, M.; Chesnov, S.; Bigler, L.; Bienz, S.; Hesse, M.; Eichenberger, S. "Characterization of free long-chained polyamines from the venom of the spider *Paracoelotes birulai*" in preparation.

37. Deillon, C. A.; Hoffmann S. R. K.; Gutte B.; Bigler, L. "The *retro*-GCN4 leucine zipper has ribonuclease activity", in preparation.

38. Bigler, L.; Stalder, U.; Patzelt, H. "Taxonomy of Archaea by Mass Spectrometry", in preparation.

I. GENERAL HISTORY AND DEVELOPMENTS

The history of mass spectrometry begins already at the end of the 19th century in the Cavendish Laboratories of the University of Cambridge, England. Joseph J. Thomson discovered that electrical discharges in gases produced ions and these rays of ions would adopt different parabolic trajectories according to their mass when passed through electromagnetic fields.

Figure 1.1. J.J. Thomson

The apparatus he used consisted of a highly evacuated glass tube, fitted with electrodes (figure 1.2). Electrons were produced by electrical heating of a tungsten filament (C). Electrons were accelerated and force to form a beam by passing through discs A and B. Finally, they were passed through electric and magnetic fields where they were deviated and finally detected on a zinc sulfide screen (Thomson 1913; Dahl 1997).

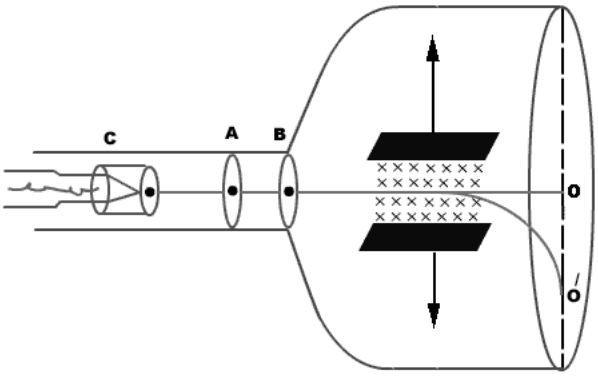

Figure 1.2. System used by J.J. Thomson for determination of the *m/z* ratio of electrons

These experiments allowed the determination of the mass-to-charge ratio (*m/z*) of electrons, the first charged particles that could be measured. J.J. Thomson was awarded for his pioneer works with the Physic Nobel Prize in 1906. A few years later, Thomson was able to determine the *m/z* values of the first atoms, the ^{20}Ne and ^{22}Ne isotopes, as well as those of the ionized O_2, N_2, CO, CO_2, and $COCl_2$ molecules.

It was Thomson's student Francis William Aston who designed several subsequent mass spectrographs in which ions were dispersed by mass and focused by velocity. The use of electromagnetic focusing led to improvements in mass resolving power, and the subsequent discovery of not less than 212 of the 287 naturally occurring isotopes. It was Aston's research that gave a proof for the fact that most natural occurring elements are composed of several natural isotopes. The characterization of the elements chlorine with isotope of masses 35 and 37, bromine with mass 79 and 81, and krypton with mass 78, 80, 82, 83, 84, and 86 got him rewarded with the Nobel in Chemistry in 1922 (Aston 1919).

Figure 1.3. F.W. Aston

The development of modern sector field mass spectrometers, characterized with an extended mass range, was achieved 1917 by Arthur J. Dempster at the university of Chicago who developed a magnetic analyzer that focused ions formed by electron impact (EI) onto an electrical collector (Dempster 1917). EI-MS allowed physicists to identify compounds by the mass of elements that constitute molecules, and to determine the isotopic composition of these elements. Dempster's mass spectrometer was over 100 times more accurate than previous versions (e.g. from Aston) and their design is still used to this day. Dempster's research led in 1935 to his discovery of the radioactive uranium isotope ^{235}U.

In the 1930's started at the University of California, Berkeley, the carrier of an outstanding personality, Ernest O. Lawrence. He is best known for his invention, utilization, and improvement of an ion storage device, the cyclotron (Lawrence 1934).

Figure 1.4. Ernest O. Lawrence

Through the construction of machines with increasing size, Lawrence was able to provide the crucial equipment needed for experiments in high-energy physics. Around the cyclotron, Lawrence built up his Radiation Laboratory, which would become one of the foremost laboratories for physics research. In 1939, Lawrence was awarded with the Nobel Prize in Physics for his work on the cyclotron and its application. State-of-the-art, Fourier-transform ion cyclotron resonance mass analyzers, based on Lawrence's ion storage principle, represent the highest performance in terms of resolution, accuracy, and sensitivity.

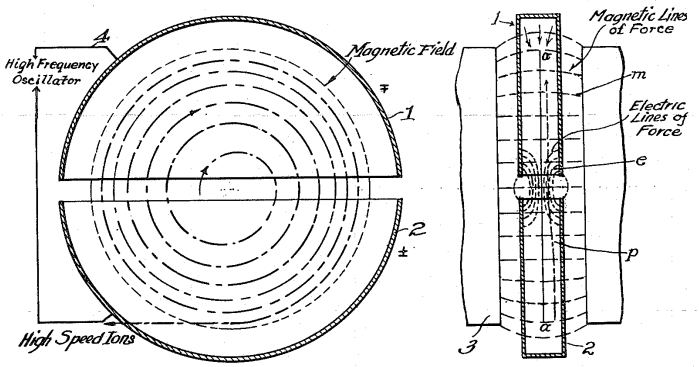

Figure 1.5. Diagram of cyclotron operation from Lawrence's 1934 patent

The early 1940s saw the rise of synthetic organic chemistry's demand for instruments able to characterize organic molecules. For this purpose, Joseph Mattauch and his student Richard Herzog, as well as Kenneth Bainbridge, Alfred Nier, and others focused their efforts on the improvement of Dempster's mass analyzer. They developed double-focusing mass spectrometers combined with the incorporation of the latest vacuum technologies and electronics of the time, which led to the first commercial mass spectrometers (Mattauch et al. 1934; Johnson et al. 1953).

During the 1940's, William Stephens invented the time-of-flight (TOF) mass analyzer. Ions are separated based on differences in their velocities as they are accelerated down a linear flight tube (Stephens 1946). This concept was much cheaper and simpler than sector field instruments. Furthermore, TOF apparatuses have principally an unlimited mass range and excellent sensitivity. The relevance of Stephens's idea came out only in the nineties when the matrix-assisted laser desorption ionization source for the characterization of macromolecules was developed.

Quadrupole mass spectrometers were developed by Wolfgang Paul of the University of Bonn emerged in the 1950s. Therein separation of ions is reached by applying quadrupolar electric fields comprising radiofrequency and direct-current components. At that time, the challenge was the coupling of mass spectrometers to gas chromatographs in order to analyze mixtures (Paul et al. 1953). Later, Paul and Hans G. Dehmelt from the University of Washington created also the quadrupole ion trap. Both were awarded in 1989 with the Nobel Prize in Physics for their work on ion trapping. Quadrupoles are the most widespread mass analyzers nowadays, mainly in combination with gas and liquid chromatographic devices.


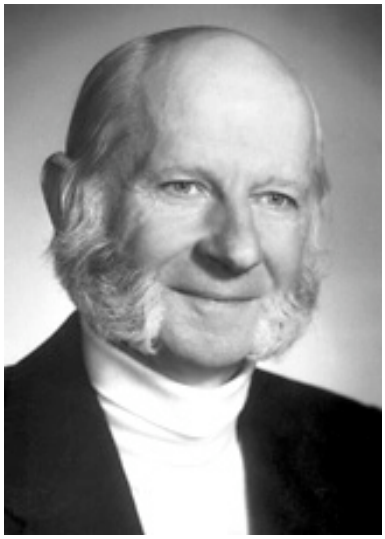

Figure 1.6. Wolfgang Paul and Hans G. Dehmelt

The field of mass spectrometric applications was importantly extended in 1956 from simple atom identification in molecules to the characterization of organic compounds. Thanks to Sir John H. Beynon and his development of fragmentation rules in EI-MS, the structure of organic molecules got amenable (Beynon 1956). At the same time, Fred McLafferty proposed a hydrogen transfer reaction that will come to be known as the McLafferty rearrangement (McLafferty 1956; McLafferty 1959).

By the 1960s, mass spectrometry had become an established technique for the characterization of organic compounds. This breakthrough was favored by the introduction of the chemical ionization (CI) source invented by Munson and Field in 1966 (Munson et al. 1966). Nonetheless, new ion sources were demanded, because EI-MS led often to many fragment ions or decomposition of thermally labile compounds. In such cases, molecular ions ($M^{\bullet+}$) could not be detected and the molecular weight of the compounds remained unknown.

Chemical ionization is based on ionization through proton transfer reactions. Small and polar molecules as e.g. α-D-glucose, could now be transfer to the gas phase, and ionized to quasi-molecular ions (e.g. $[M+H]^+$ or $[M–H]^–$) without dissociation reactions.

Other so-called "soft ionization" methods emerged a few years later including field desorption, secondary ionization MS (or SIMS), plasma desorption, and laser desorption MS (Gross 2004).

Until now, only fragment ion spectra obtained from EI mass spectra of pure samples could be used for structure elucidation. The analysis of crude mixture components required the

development of a new technology, tandem mass spectrometry (MS/MS). This type of instruments is using two stages of mass analysis, and is based on collision-induced dissociation procedures. Its relevance is also closely related to the development of soft ionization techniques and that lack of structure information contained in such mass spectra (Yost et al. 1978).

In 1974, Alan G. Marschall and Melvin B. Comisarov developed a Fourier-transform ion cyclotron mass spectrometer (FT-ICR MS) on the basis of E. Lawrence's work (Comisarow et al. 1974). A major advantage of FT-ICR MS is that it allows many ions to be detected simultaneously in a non-destructive way. These mass spectrometers also achieve the highest mass resolution and accuracy, allowing the study of chemical reactivity in the gas phase as well as ion fragmentations.

Major technical developments were not only related to the design of new mass analyzers. Also innovative ionization methods allowed the extension to new application domains. A important effort was given to develop a method for the direct transition of ions from a solution to the gas phase. In 1975, E. C. Horning came initially to the idea of using heat for evaporation of the solvent and a corona discharge for the ionization of the molecules (Carroll et al. 1975). The atmospheric pressure chemical ionization (APCI) was born.

Ionization techniques capable of efficiently ionizing biological molecules were developed in the 1980's. First, Michael Barber invented the fast atom bombardment (FAB) technique, which uses a source of neutral heavy atoms to ionize compounds from the surface of a liquid matrix (Barber et al. 1981). Some years later, John B. Fenn and colleagues at Yale University refined an electrospray ion source originally reported by Malcolm Dole of Northwestern University almost two decades earlier (Dole et al. 1968). The first experiments dealt with the formation of a molecular beam from a small supersonic free jet that contained a variety of ionic species (Yamashita et al. 1984; Yamashita et al. 1984). Later, ions of biological macromolecules were produced in the gas phase (Fenn et al. 1989), a development that was rewarded in 2002 with the Nobel Prize in Chemistry.

John Fenn shared his award with Koichi Tanaka who was able to vaporize and ionize macromolecules such as proteins by laser irradiation. The problem of the ionization method is that the direct irradiation of an intense laser pulse on a macromolecule causes cleavage of the analyte into tiny fragments and the loss of its structure. In 1987, Tanaka found that by using a mixture of ultra fine metal powder in glycerol as a matrix, an analyte

could be ionized without dissociation (Tanaka et al. 1987). This technique became known as soft laser desorption (SLD).

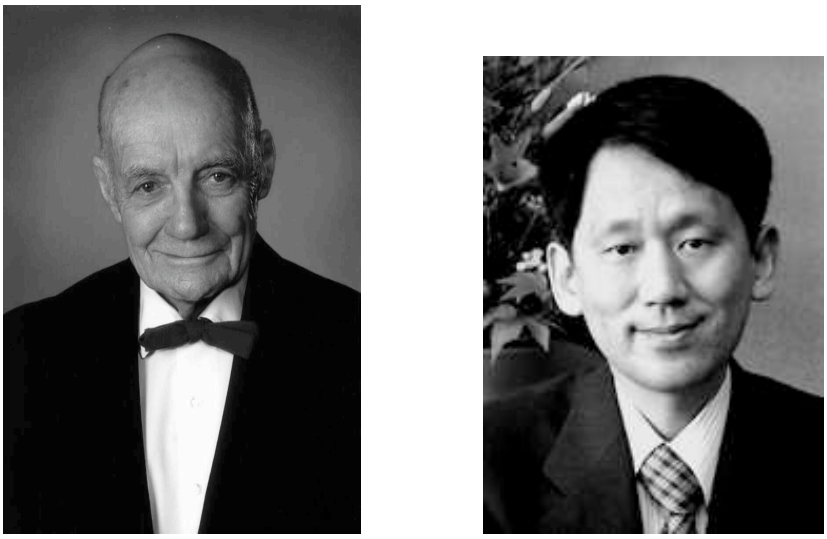

Figure 1.7. John B. Fenn and Koichi Tanaka

Tanaka's part of the Nobel Prize raised polemics in the scientific community because the contributions of two German scientists, Franz Hillenkamp and Michael Karas were important enough for being also included as prizewinners. In their technique, first reported in 1985, a laser desorbs molecules from a solid surface covered with a matrix of crystalline organic compound of low molecular weight (Karas et al. 1988). This procedure increases significantly the sensitivity and is called matrix-assisted laser desorption ionization (MALDI). Furthermore, Tanaka's SLD is not used currently for biomolecules analysis, meanwhile MALDI is widely used in mass spectrometric research laboratories. Proteins, oligonucleotides, polymers, polyaromatic hydrocarbons, oligosaccharides, etc. are characterized with this method. However, while MALDI was developed prior to SLD, it was not used to ionize proteins until after Tanaka's report.

Mass spectrometry's characteristics have it to an outstanding position among analytical methods. In particular, the tremendous development of ESI and MALDI in the last fifteen years enabled to introduce biological molecules exceeding 1 million Daltons into mass spectrometers as stable gas-phase ions. The impact of the soft ionization techniques as irreplaceable tools in the biological sciences can be illustrated by the increase of the number of publications in the last years. From the over 15'000 papers related to mass spectrometry in 2005, more than 40% are dealing with ESI or with MALDI.

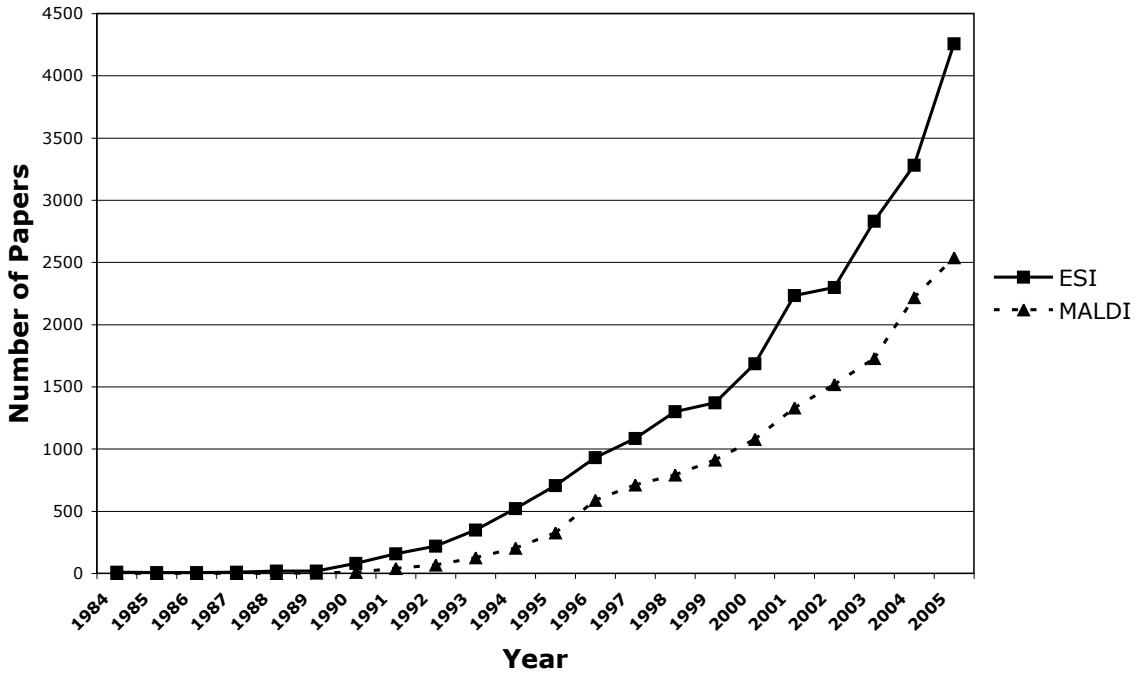

Figure 1.8. Number of articles including the words "electrospray" and "matrix assisted laser desorption" in the title, abstracts, or key words published each year obtained from the SciFinder database.

II. SURVEY OF THE VARIOUS METHODS

2.1. Basics

The importance of mass spectrometry lies above the simple determination of the molecular weights of organic molecules. Information related to structure or quantities of traces of compounds within complex samples can also be obtained by mass spectrometric methods. For successful analyses, several aspects, which are connected one to another, have to be considered: objectives of the investigation, fundamentals (physics), technical realization, and mass spectral interpretation.

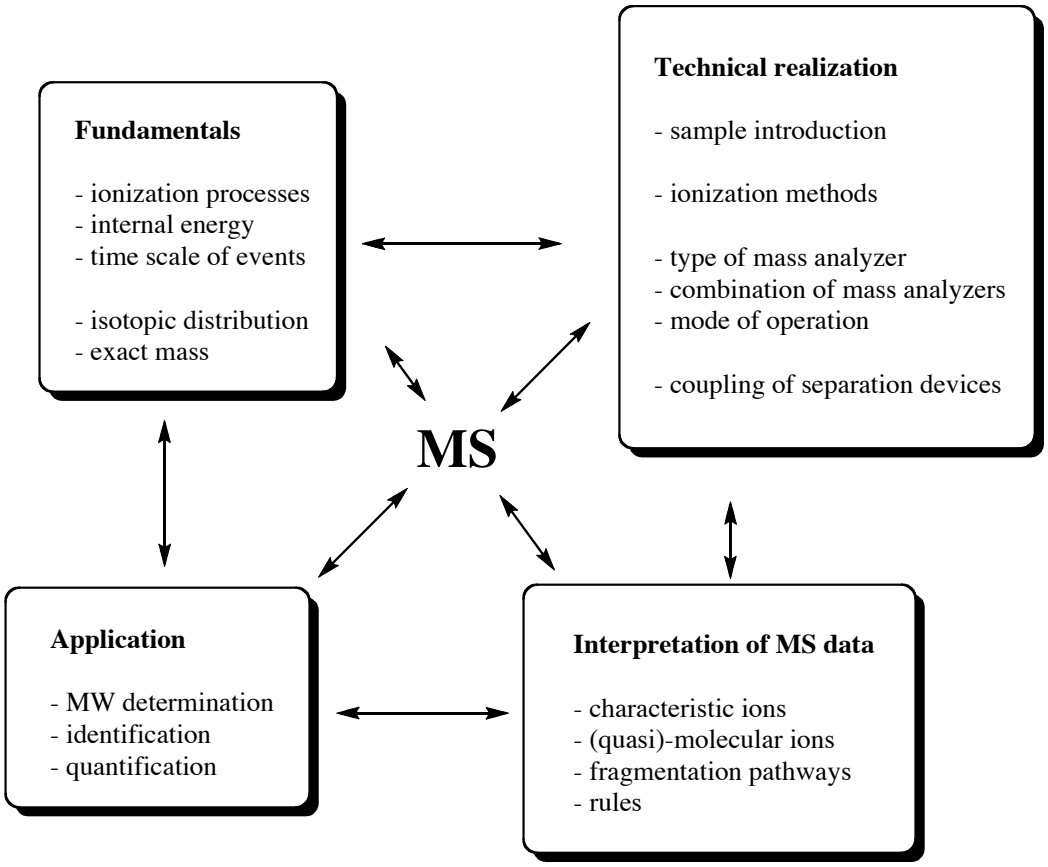

Figure 2.1. Interactions needed for a successful investigation using mass spectrometry. Adapted from (Gross 2004).

The basic method to carry out an analysis is common across all mass spectrometers. First, an organic compound or a metal complex is introduced through a sample inlet into the mass spectrometer. Once inside the instrument, the sample molecules are converted into ions in the ionization source, before being electrostatically accelerated into the mass analyzer, where they are separated according to their mass-to-charge (*m/z*) ratio. The ions collide with the detector and the resulting impact energies are converted into electrical signals. These signals are transmitted to a computer and converted into *m/z* and intensities (Koppenaal et al. 2005). The separation of the ions and their detection occur mandatorily in a high vacuum region, because collisions between ions and neutral molecules or atoms have to be avoided.

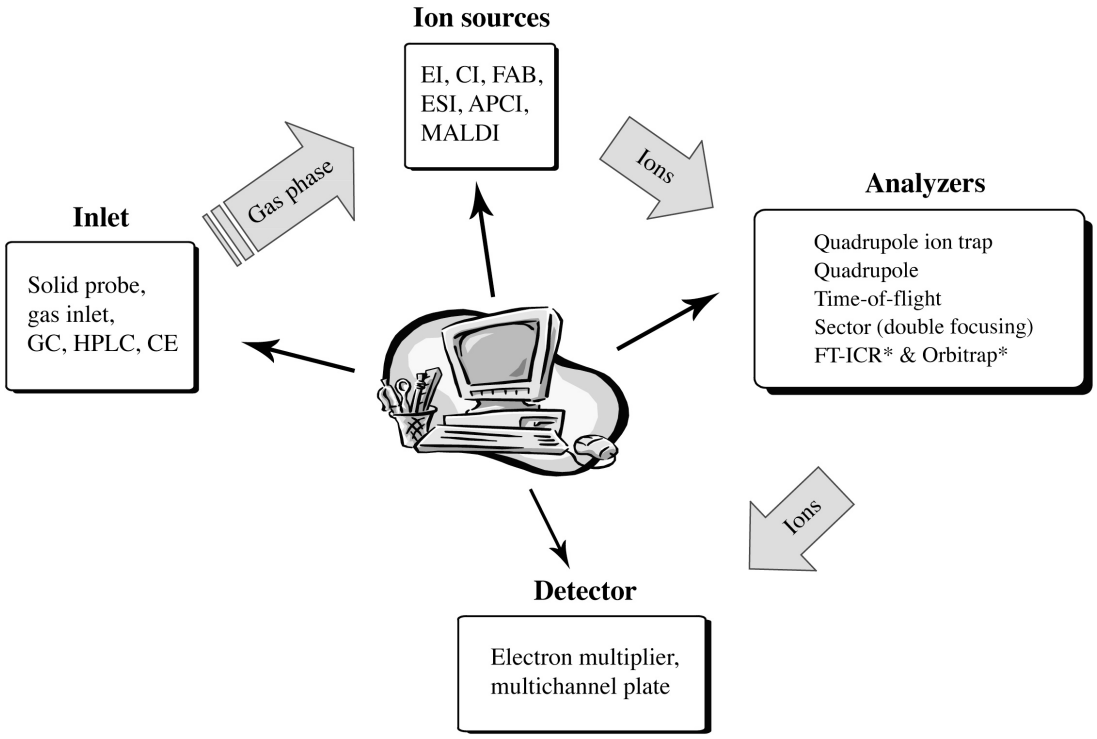

Figure 2.2. Basic components of a typical mass spectrometer. *FT-ICR and Orbitrap do not use a standard destructive detector.

For many years, only samples containing pure compounds delivered useful data. Because samples are often mixtures and to gain efficiency and sensitivity, hyphenated methods based on gas chromatography (GC), high performance liquid chromatography (HPLC), and capillary electrophoresis (CE) on-line coupled to mass spectrometers were developed. In the next three chapters, the most important ionization methods, mass analyzers and chromatographic systems are briefly presented.

2.2. Ion Sources

Independent of the method, samples can only be investigated by mass spectrometry when two conditions are fulfilled: the molecules have to be in the gas phase and charged. To that end, several techniques based on three main physical processes – evaporation, desorption and spraying – were developed.

2.2.1. Ionization Following Evaporation

Electron-impact (EI). Molecules in the gas phase are bombarded with a beam of electrons that carry 70eV energy in a "near-miss" trajectory. This leads to interaction with electrons of the molecules, and one of them is ejected. During the collision, the molecule absorbs part of the kinetic energy (10-12 eV in average) and fragment ions are formed.

$$M + e^-_{70eV} \longrightarrow M^{\bullet +} + e^-_{60eV} + e^-_{thermal}$$

In organic molecules, lone-pairs electrons are most easily ionized, followed by π- and σ-electrons, respectively. Moreover, not the weak bonds of a molecule are broken during the ionization process, but rather stable fragment ions are formed.

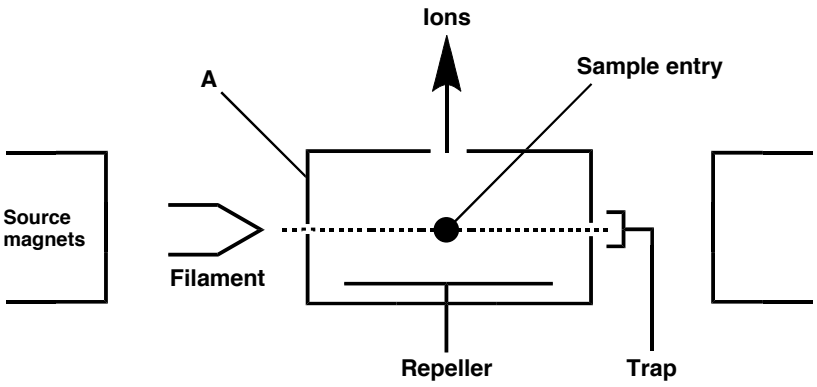

Figure 2.3. Electron-impact ion source

Chemical Ionization (CI). The CI-method was developed to overcome the problem of too heavy fragmentation often observed in EI-MS, particularly with labile sample molecules. Glycoside derivatives, for example, do not show molecular ions ($M^{\bullet+}$) under EI-MS conditions. However, chemical ionization allows the formation of quasi-molecular ions by protonation in the positive ionization mode (formation of $[M+H]^+$-ions) or deprotonation in the negative ionization mode ($[M-H]^-$-ions), and thus the determination of the molecular weight of the rather labile molecules.

The quasi-molecular ions are formed by proton-transfer reactions (or ion/molecule reactions) with a reactant gas (e.g. methane, *iso*-butane, ammonia) that was ionized by electron impact at 200 eV. The change from EI- to CI-MS mode is easy, as the same ion source is used. Only the "ion volume" where the ionization takes place (A, figure 2.3) has to be exchanged and filled with reactant gas.

The main drawback of EI- and CI-MS is that the samples to be investigated have to be transferred into the gas phase by evaporation (heating) before the ionization and transfer to the analyzer. This cannot be achieved for many polar, non-volatile and large molecules – as most of the biologically interesting biopolymers and other natural products – by heating without decomposition of the samples.

2.2.2. Ionization by Desorption

Desorption methods were developed for non-volatile compounds. The idea was to deposit the sample on a solid support, in some cases together with a matrix, to transfer the support in the mass spectrometer, and to apply a particle beam rich in energy. The type of ionization depends on the nature of the falling particles and the matrix.

Fast-Atom Bombardment (FAB). Samples are mixed with a low-volatile fluid (e.g. glycerin, thioglycerin, or 3-nitrobenzyl alcohol), and a thin layer of the solution is brought onto a plate and fixed in the ion source. The sample is then ionized by bombardment with fast neutral atoms like Ar or Xe. Usually, protonated and/or sodiated quasi-molecular ions ($[M+H]^+$ and/or $[M+Na]^+$) are formed in the positive ionization mode, and deprotonation occurs in the negative mode ($[M-H]^-$-ions). With the development of FAB, peptides with MW up to 3000 Da could be investigated with MS for the first time.

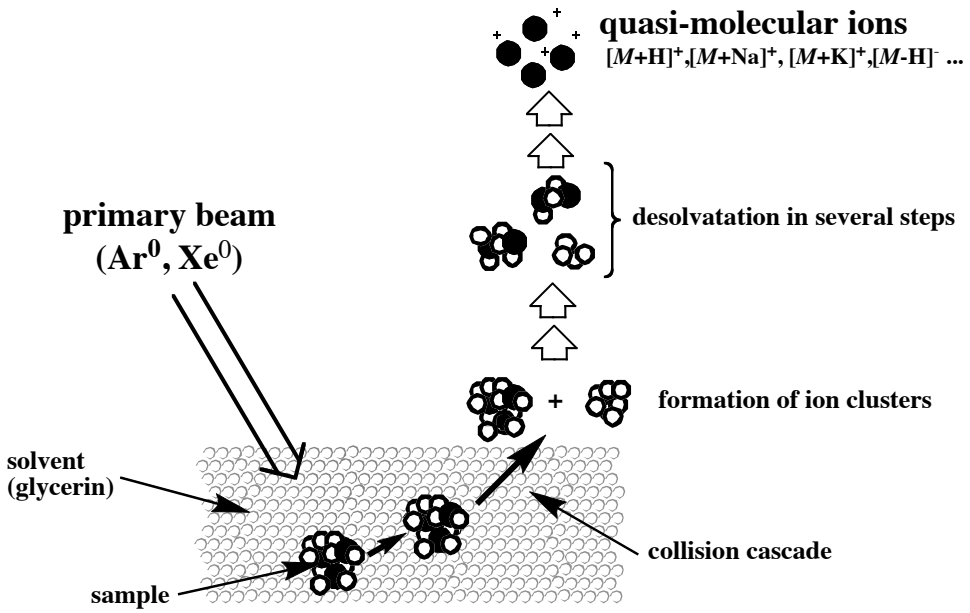

Figure 2.4. Fast-atom bombardment mechanism

The relevance of FAB-MS strongly decreased the last few years. The principal reason is the emergence of other two further ionization methods, ESI and APCI, that are easier in handling and more versatile to apply.

Matrix-Assisted Laser Desorption Ionization (MALDI). MALDI is an efficient and extremely sensitive technique with a wide application range. The measurements are performed in two steps. First, the sample is dissolved in a mixture of solvent and matrix. The most widely used matrices are α-cyano-4-hydroxycinnamic acid (HCCA), 2,5-dihydroxybenzoic acid (DHB), or sinapinic acid (SA), depending the class of compounds under investigation. In a second step, the crystals that were built are irradiated with short and strong laser pulses, leading to the formation of ions.

The role of the matrix is to co-crystallize with the sample molecules and to absorb laser energy. Therefore, the matrix molecules contain a chromophore with absorption maximum at the wavelength of the laser (e.g. the matrices given above are used for a N_2-laser at 337nm). The exact mechanism of material ablation and formation of charged matrix and molecules in the Maldi process are still poorly understood (Hillenkamp et al. 2007). It is generally accepted that the matrix absorb the laser energy, evaporate and transfer some energy to sample molecules. Quasi-molecular ions are formed by proton-transfer reactions during the evaporation process. Mainly $[M+H]^+$, $[M+Na]^+$, $[M+2H]^{2+}$, or $[M-H]^-$ -ions are observed.

The major drawback of Maldi-MS is the formation of very intensive matrix signals in the low mass range. A new approach has been developed recently to overcome ion suppression effects when low molecular weight compounds are analyzed. This method is based on dense arrays of single-crystal silicon nanowires (Go et al. 2005). Such a solid support absorbs the laser energy and transfers it to the sample molecules without evaporating. Only sample molecules are protonated and transferred to the gas phase.

Because the laser beam is pulsed, MALDI do not produce continuously ions. A pulsed ion beam, together with the formation of mostly singly charged quasi-molecular ions, makes time-of-flight (TOF) the best type of mass analyzer. TOF is very sensitive and has an unlimited mass range, essential properties required for the analysis of large biomolecules.

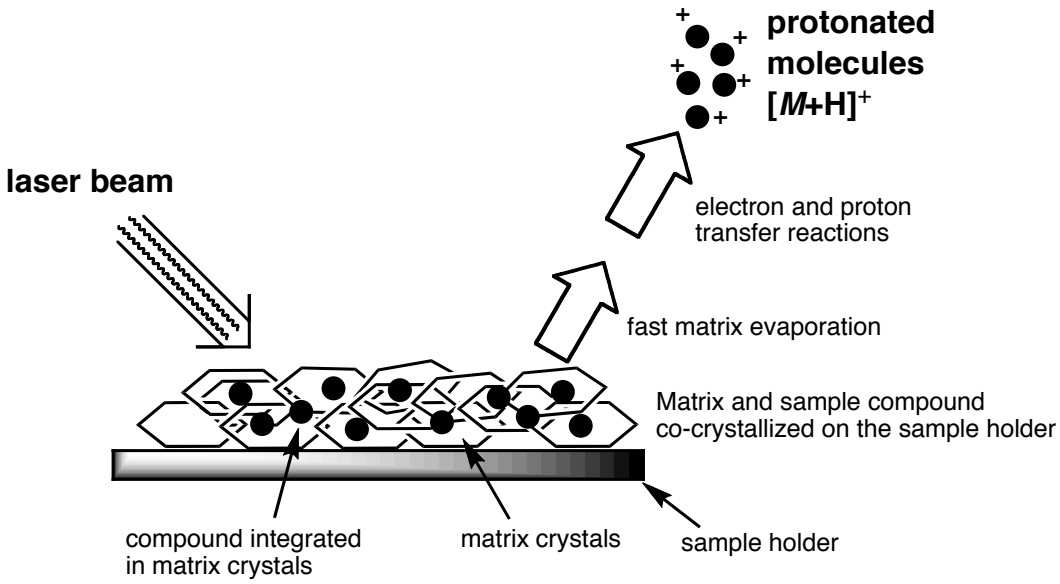

Common matrices:

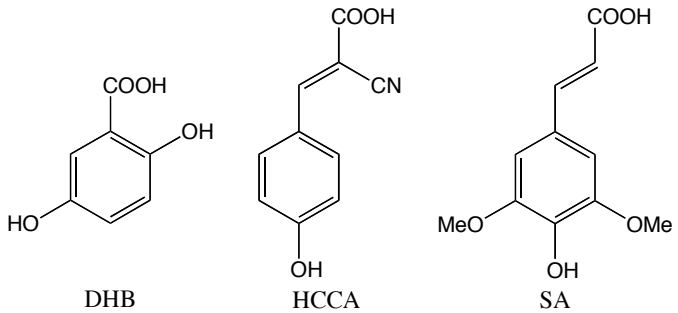

Figure 2.5. Matrix-assisted laser desorption ionization

MALDI became an unique method in many different domains such as proteomics and genomics, for the analysis of oligosaccharides, synthetic polymers, lipids, and even non-covalent complexes of large molecules or taxonomy of bacteria (Hillenkamp et al. 2007).

2.2.3. Ionization via Spraying

The demand for liquid chromatography-mass spectrometry (HPLC-MS) interfaces was the main motivation for the development of atmospheric pressure ionization methods in the 1970's and 1980's. Thermospray was the first commercially available spraying technique (Vestal 1983). Later, atmospheric pressure chemical ionization (APCI) and electrospray ionization (ESI) were developed because these methods offer better sensitivity and reproducibility. Today, over 99% of the HPLC-MS applications are based on these two ionization techniques.

Electrospray Ionization (ESI). A sample is dissolved in a rather polar solvent like, for example, H_2O, MeOH, i-PrOH, CH_3CN, or CH_2Cl_2, containing a volatile buffer like HCOOH, CH_3COOH, TFA, NH_4OAc, or Et_3N. A high voltage (typically 3-4 kV) is applied to this solution that contain the preformed ions, and emerge from a thin capillary at a flow rate of around 0.5-500µl·min^{-1}. The electrical fields cause the solvent to brake into fine threads that subsequently disintegrate into small droplets (figure 2.6). Quasi-molecular ions are generated from these droplets by a variety of ionization processes (Cole 1997).

a) ESI

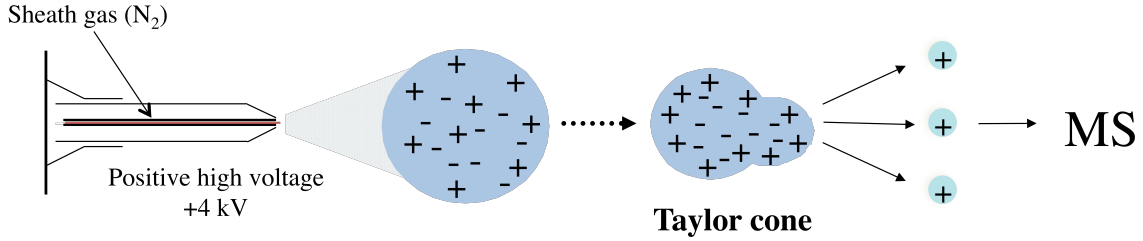

b) APCI

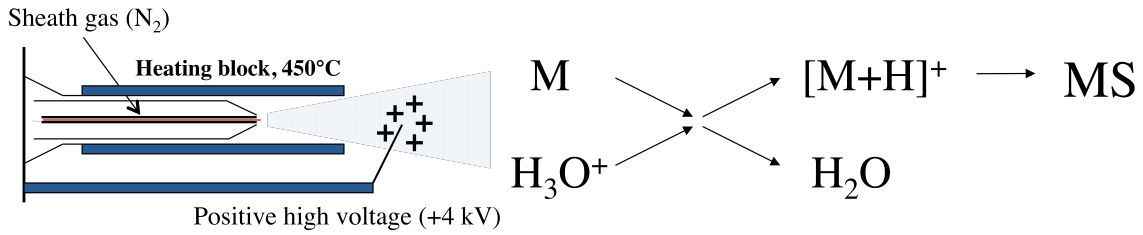

Figure 2.6. Direct comparison of a) ESI and b) APCI

Initially, ESI-MS investigations were focused on small polar molecules. The method became essential only when the group of Fenn showed in 1988 that multiple-charge ions can be generated from proteins by ESI (Fenn et al. 1990). This allows the analysis of

molecules with MW > 100'000 using 'conventional' mass analyzers (e.g. quadrupole, ion trap, sector field instruments) with a mass range of 100-3'000 *m/z*.

Electrospray is the mildest of all ionization methods allowing investigations of thermal labile molecules, metal complexes, or the study of non-covalent interactions. It is also often connected to liquid chromatograph for the analysis of complex mixtures like biological fluids or protein digests.

Atmospheric-Pressure Chemical Ionization (APCI). A sample solution (flow rate 200-1000 µl·min^{-1}, same solvents and buffers as in ESI) is sprayed at atmospheric pressure trough a heated capillary (250-450°C) with N_2 as sheath gas. A corona needle (3-5 kV) ionizes first N_2 that is in excess, the formed $N_2^{\bullet+}$ ions react with gaseous solvent molecules, and acidic species like e.g. $CH_3OH_2^+$ or H_3O^+ are formed. These acids finally ionize the sample molecules *via* proton-transfer reactions in the gas phase. Because protonation occurs in the gas phase, APCI may form quasi-molecular ions from sample molecules with lower proton affinities than with ESI.

Practically, the change from ESI to APCI with a given mass spectrometer is very easy because only the front of the ion source containing sprayer and corona needle has to be exchanged. This operation can be done without venting the instrument.

The choice of the ionization mode, ESI or APCI, is made according the polarity and the molecular weight of the sample:

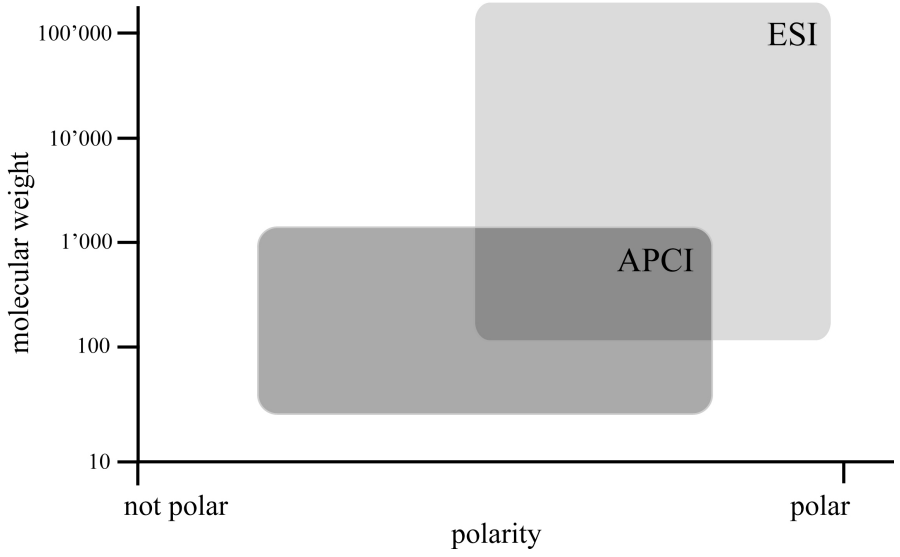

Figure 2.7. ESI versus APCI in function of the molecule properties

2.2.4. Overview of the ionization methods

The ionization method is chosen according to the following criteria:

- For volatile, not too polar samples, EI-MS is generally appropriate. If no molecular ions are observed by this method, then CI-MS is used, which normally allows the determination of the molecular weight of the sample molecule.
- For macromolecular compounds contained in only a few microliters of sample solution, MALDI-MS is the method of choice.
- ESI/APCI-MS has a broad spectrum of application. They are used for various organic molecules, from simple to complex. The only prerequisite is that the sample molecules contain at least one functional group. Furthermore, ESI is the best method for the study of non-covalent interactions or complex formation.

	Ionisation method	**Ionisation agent**	**Results**	**Typical applications**
Evaporation	**EI** Electron Impact	70 eV Electrons	Reproducible spectra containing many fragment ions	Volatile compounds with low MW. **Structure elucidation.**
	CI Chemical Ionization	Ions in the gas phase (NH_4^+)	Protonated molecules	Volatile compounds with low MW. **MW determination**
Desorption	**FAB, MALDI**	Beam of energy rich atoms, ions, or photons	Entire Quasi-molecular ions formed via redox or acid/base reactions	None volatile compounds from middle (FAB) up to high MW. **MW determination**
Spraying	**ESI, APCI** Electrospray, Atmospheric Pressure Chemical Ionization	Electrical field on micro-droplets or vapor.	Entire Quasi-molecular ions (several time charged in ESI)	None volatile, mid- to polar compounds with low to high MW. **MW determination**

2.3. Analyzers

There are three fundamental ways to separate ions. In all cases, ions are separated according to their mass-to-charge ratios (*m/z*). A beam of charged particles can be deviated by electric or magnetic fields, ions can be trapped and mass selectively ejected or they can be separated by time-of-flight.

Modern mass analyzers were always sophisticated apparatuses produced from elements that approach the state-of-the-art in electronics, vacuum systems, magnet design, precision machining, and computerized data acquisition, and processing. They are the core of a mass spectrometer and its most expensive part.

The most widely used analyzers will shortly be presented hereafter.

2.3.1. Deflection of ion beams

A continuous ion beam can be deflected by momentum in a magnetic field, by electric fields, or by linear radio frequency.

Sector-Field Instrument. Sector-field instruments are typically fitted with EI-, CI-, or FAB-ion sources. They represent the earliest MS-instruments and are still in use because of their performance in mass resolution and accuracy. Typically two sectors, which are magnets or strong electrostatic analyzers, are coupled in series.

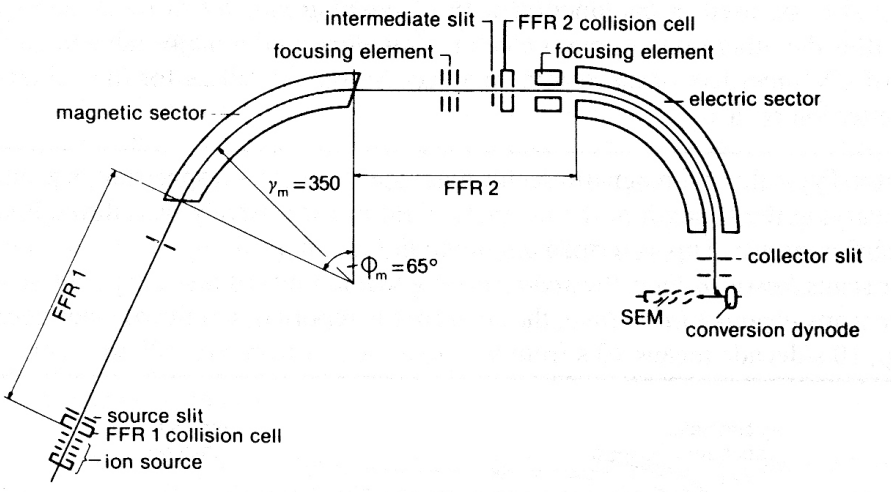

Figure 2.8. Finnigan MAT95 two-sector-field instrument (Brunnée 1997)

Sector-field analyzers have high resolution and high accuracy capability. These performances allow the determination of chemical formula of the sample molecules investigated by EI-, CI-, or FAB-MS. Beside organic mass spectrometry, sector-field instruments are widely used in isotope ratio determination. With this type of experiments, the origin or age of a sample can be determined. This ability is applied in archeology (age of a finding), in food industry (geographic origin of an additive), or in doping analysis (distinction between natural or synthetic steroids anabolic).

Linear Quadrupole. Four parallel rods build a quadrupole analyzer. A direct current (DC) is applied on an opposite pair of these rods, and a radiofrequency (RF) voltage on the other.

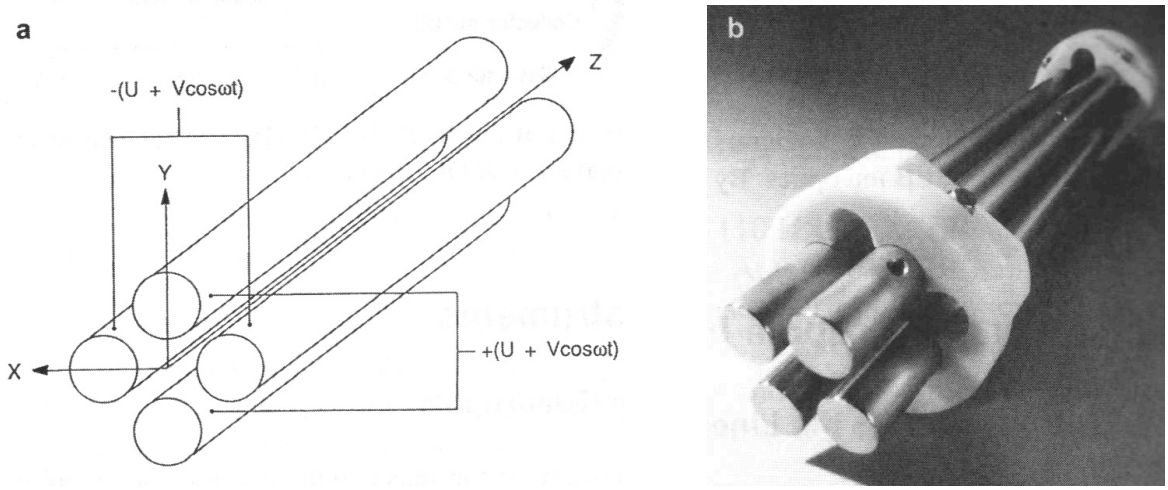

Figure 2.9. Schematic view and picture of a quadrupole mass analyzer (Gross 2004)

At a defined DC and RF voltage, only the beam of ions with a specific mass-to-charge ratio has a stable trajectory (*m/z* 100 in figure 2.10). This means that only ions of this *m/z* reach the detector and that all other ions are filtered out.

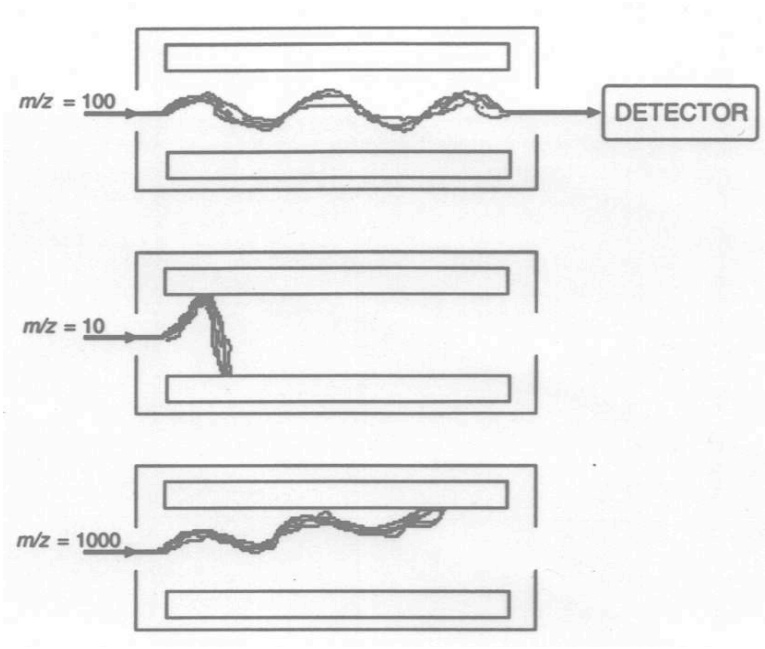

Figure 2.10. Quadrupole at specific voltage

The linear quadrupole analyzers were initially developed to being coupled to gas chromatographs. Today, they are most used systems because of their relatively cheap prize, robustness, and versatility. They are generally fitted with EI-, CI-, ESI-, as well as APCI-ion sources, and often coupled to gas and liquid chromatographic systems. Quadrupoles are also used in tandem mass spectrometry (MS/MS) as filters, collision cells, or analyzers.

2.3.2. Trapping Ions

Three methods of trapping ions are established: the quadrupole ion trap, operating at normal resolution, and Fourier-transform ion cyclotron resonance (FT-ICR) and orbitrap, both as high-end mass spectrometers.

Since in trapping analyzers all ions are collected simultaneously over a variable duration, they are very sensitive. However, space-charge effects due to overloading have to be avoided otherwise resolution and accuracy will be lost. Modern ion-trapping instruments have an implemented automatic gain control to overcome this drawback.

Quadrupole Ion Trap (QIT). A ring together with a gap and an end cap electrode build a quadrupole ion trap. This three dimensional arrangement is partially filled with an inert

gas, typically He at $3\text{-}5 \cdot 10^{-5}$ mbar. This gas is used for cooling the ions once they have entered the trap and before the mass analysis is performed.

With such an instrument, several steps are necessary to record a mass spectrum. After the trap was emptied, charged particles are collected at a specific DC- and RF-voltage and gathered in the center of the analyzer. Then, the ions are mass selectively ejected to the detector.

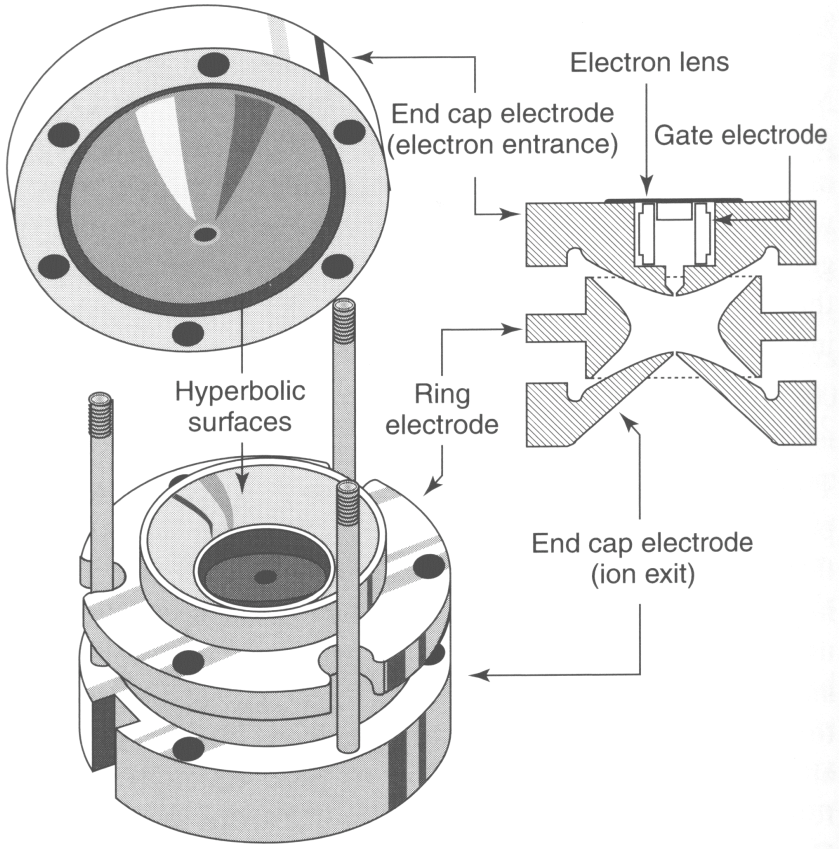

Figure 2.11. Quadrupole ion trap (March 2000)

If required, automatic MS/MS experiments can be performed. In this case, all the charged particles that enter the mass spectrometer are collected. Then the precursors ions are isolated, excited and dissociation reactions occurs as the trap is filled with He. Finally, the formed fragment ions are mass selectively ejected and recorded. With quadrupole ion trap, up to the 10^{th} generation of product ions (MS^{10}) can be studied. This is particularly useful when, for example, glycosyl derivatives are investigated with ESI-MS^n. The first generation of product ions (or MS^2) shows often only the loss of the glycosyl group. If structure information concerning the core of the molecule, e.g. an alkaloid, a flavonoide, or a steroid is required, then further generations of products ions could to be generated.

Because of their mass range from 40 up to 3'000 or even 6'000 *m/z* for some instruments, EI-, CI-, ESI-, and APCI-ion sources are the ionization methods that best fit QIT mass analyzers. Automatic gain control, automatic MS/MS experiments, and high scan rates are the reasons for the broad application spectrum of QIT, in particularly in combination with GC and HPLC.

Linear Ion Trap (LIT). Linear ion traps are available since 2002 (Hager 2002). They combine the principals of operation and the properties of linear quadrupoles and QIT. They can accumulate charged particles, excite them axially or linearly, and they can act as normal scanning mass analyzer. They are fast, extremely sensitive because of less space-charge-effects compared to QIT, and they are often used as MS/MS device coupled to high-end FT-ICR or orbitrap analyzers.

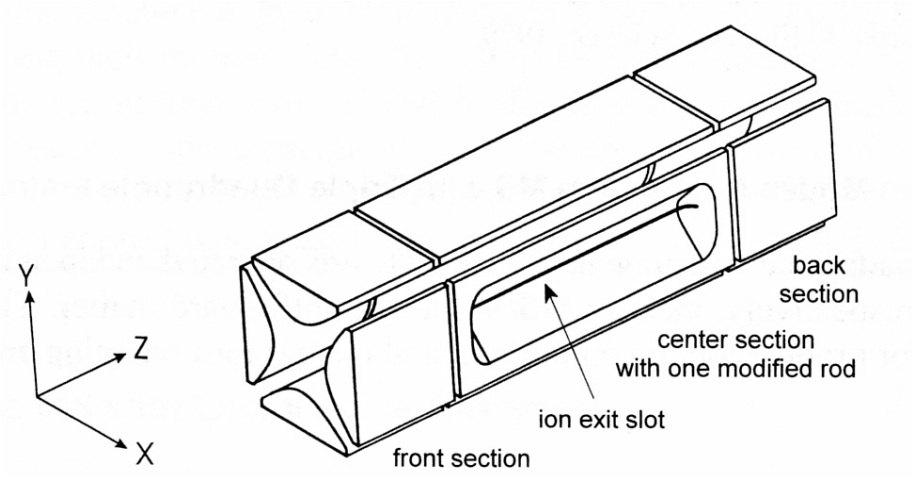

Figure 2.12. Linear ion trap

Fourier-Transform Ion Cyclotron Resonance (FT-ICR). Together with the orbitrap, FT-ICR are the only instruments that record mass spectra in a non-destructive way. The charged particles are collected in the center of a cubic or cylindrical cell, which is placed in the center of a superconducting magnet. After excitation, ions with different *m/z* ratios rotate at different frequencies around the axis of the cell. A detection electrode finally records the magnetic fields they induce. The sum of the frequencies is 'Fourier-transformed' and a mass spectrum is generated.

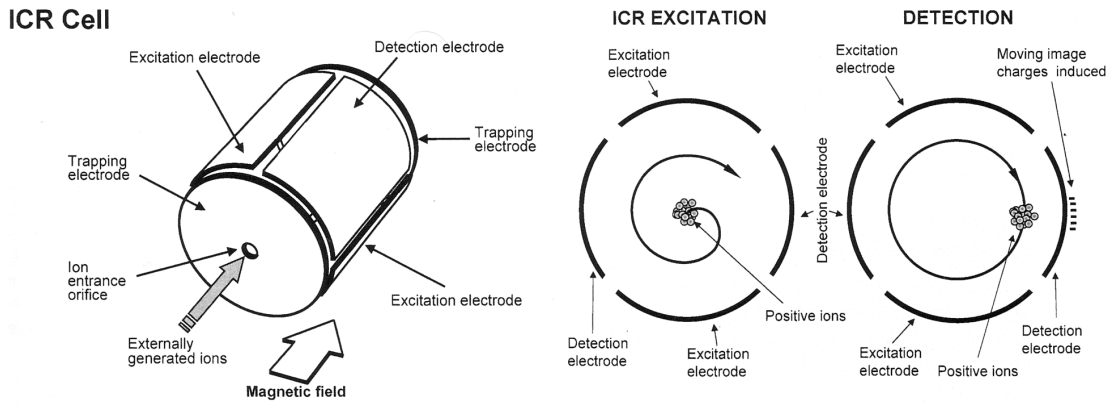

Figure 2.13. Fourier-transform ion cyclotron resonance analyzer (Marshall et al. 1998)

Despite the costs of FT-ICR instruments, which are proportional to the strength of the magnet, this relatively old technology is still in use because of its unequaled performances in resolution and accuracy (sub-ppm with external calibration). As a highlight, over 11'000 compositionally distinct components of a single ESI-FT-ICR-MS of crude oil in the mass range 200-1000 *m/z* could be resolved (Hughey et al. 2002).

Orbitrap. The orbitrap mass analyzer is the only instrument based on a fully new mode of operation that was invented the last 20 years. It was invented by Makarov in 2000, was first connected in 2003 to a high performance liquid chromatograph and already commercialized in 2004 (Makarov 2000). The ions are trapped and analyzed by rotation around a central rod. As for FT-ICR, different ions have distinctive frequencies, and the magnetic fields they induce are recorded and 'Fourier transformed'. Finally, software transforms the ion frequencies to a *m/z* scale.

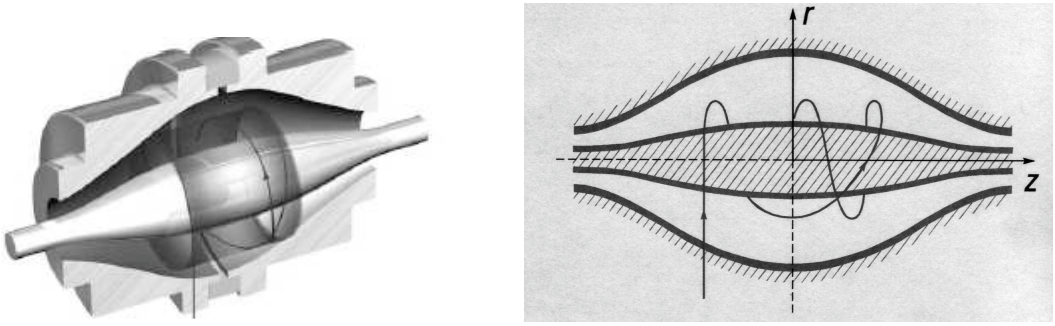

Figure 2.14. Orbitrap mass analyzer (Hu et al. 2005)

Orbitrap instruments reach resolutions and accuracies that are close to those obtained from FT-ICR instruments; however, they have a higher scan rate and they operate without superconducting magnets. Therefore, they are lower in price and easier to maintain.

Orbitraps are offered in combination with a LIT, which allows several types of experiments as, for example, full scan MS and MS/MS at normal and high accuracy, to be performed in a single HPLC run.

2.3.3. Time-of-flight

The linear time-of-flight (TOF) mass analyzer is the simplest of all the mass analyzers. An analysis is based on the acceleration of a group of ions toward a detector by an accelerating potential, giving all of the ions the same kinetic energy. As the ions have the same energy but different masses, the ions of lower mass reach the detector first due to their higher velocity. Hence, the analyzer is called time-of-flight because the mass is determined from the ions' time of arrival.

TOF has enjoyed a renaissance with the development of delayed extraction and reflectron technologies that led to an increase of performance. The delayed extraction is a technique applied in MALDI, which allows ions to be extracted from the ionization source after cooling and focusing (Brown et al. 1995). The reflectron is an electrostatic mirror which effects higher resolution by increasing the path length and through kinetic energy focusing (Mamyrin 2001).

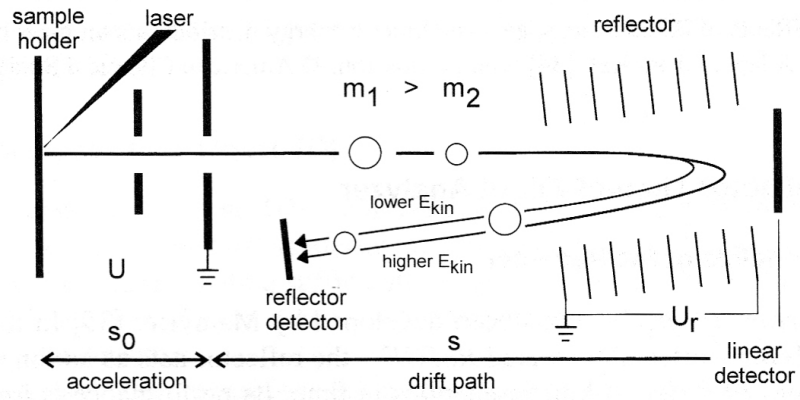

Figure 2.15. Reflectron time-of-flight mass analyzer (Wollnick 1993)

Today, TOF instruments are widely used for MALDI-, HPLC/ESI-, and GC/EI-MS applications. They have high scan rates (up to 100 Hz), high sensitivity and good resolution. Their mass range is principally only limited by the energy liberated when ions collide with the detector.

2.3.4. Hybrid Instruments

Individual mass spectrometers can be constructed by combining different types of mass analyzers into a single instrument. The driving force to do so is to get powerful MS/MS instruments by combination of the advantageous properties of each mass analyzer they are composed of.

Table2.1. Most extensively used hybrid instruments

MS1	MS2	Comment
Sector field	Quadrupole or QIT	Were first developed but fastidious maintenance
Quadrupole	TOF	Sensitive, good resolution
LIT	FT-ICR	Ultrahigh resolution and mass accuracy
LIT	Orbitrap	High resolution, mass accuracy and sensitivity

The best-established hybrid mass analyzer is probably the quadrupole time-of-flight. This analyzer is typically coupled to ESI ion sources, because it combines the stability of a quadrupole analyzer with the high sensitivity, and accuracy of a time-of-flight reflectron mass analyzer. The quadrupole can either act as an analyzer in an ordinary quadrupole instrument to scan across a specified *m/z* range, or it can also be used to selectively isolate a precursor ion that is then directed to a collision cell to induce fragmentation. The TOF reflectron mass analyzer then analyzes the resulting fragment ions.

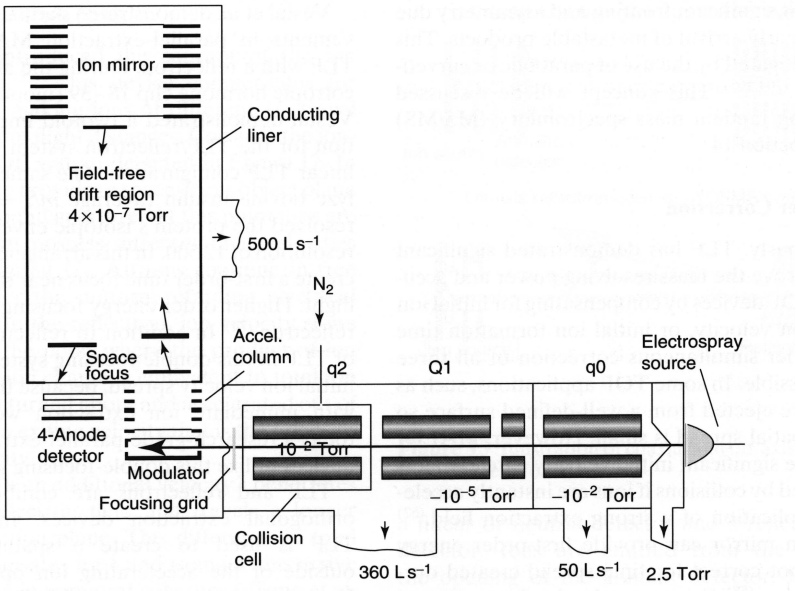

Figure 2.16. Hybrid quadrupole time-of-flight mass analyzer

2.4. Hyphenated Methods

Chromatographic detectors, such as flame ionization detector frequently used in GC or variable wavelength detector in HPLC, deliver a chromatogram that represent the mass flow eluting from the chromatographic column. Using a mass spectrometer instead, offers an additional dimension of information about the structure of the analyte.

Often, the analysis of complex mixtures requires the combination of separation techniques and mass spectrometry. The first hyphenated method was the coupling of gas chromatography with mass spectrometry (GC-MS), and soon, GC-MS became a routine instrumentation (Message 1984). The desire to couple HPLC with MS was the driving force for the development of the atmospheric-pressure ionization methods (ESI and APCI). Coupling of capillary zone electrophoresis, and capillary electrochromatography to MS followed (Shintani et al. 1997).

Mass analyzers are highly selective, and coupling of chromatographic systems increase their sensitivity by concentrating the sample on the column. Such an additional beneficial effect allows effective quantification work. Therefore, GC- and HPLC-MS are widely used, for example, in food and environment chemistry, medicine, and forensics.

2.4.1. Gas Chromatography – Mass Spectrometry (GC-MS)

GC columns consist of coated glass capillaries of usually 0.22mm ID. In GC-MS, they are directly interfaced to EI/CI ion sources. The separation of the components occurs through interactions of the analyte with the stationary phase of the column (different polarity) and by elevating the temperature of the oven (different vapor pressure). Helium gas is usually used as carrier gas. The compounds eluting from the GC column are then quantitatively transferred into the ion source during a short time interval, just sufficiently long to acquire a few mass spectra. This allows the analysis of samples in the low nanogram region.

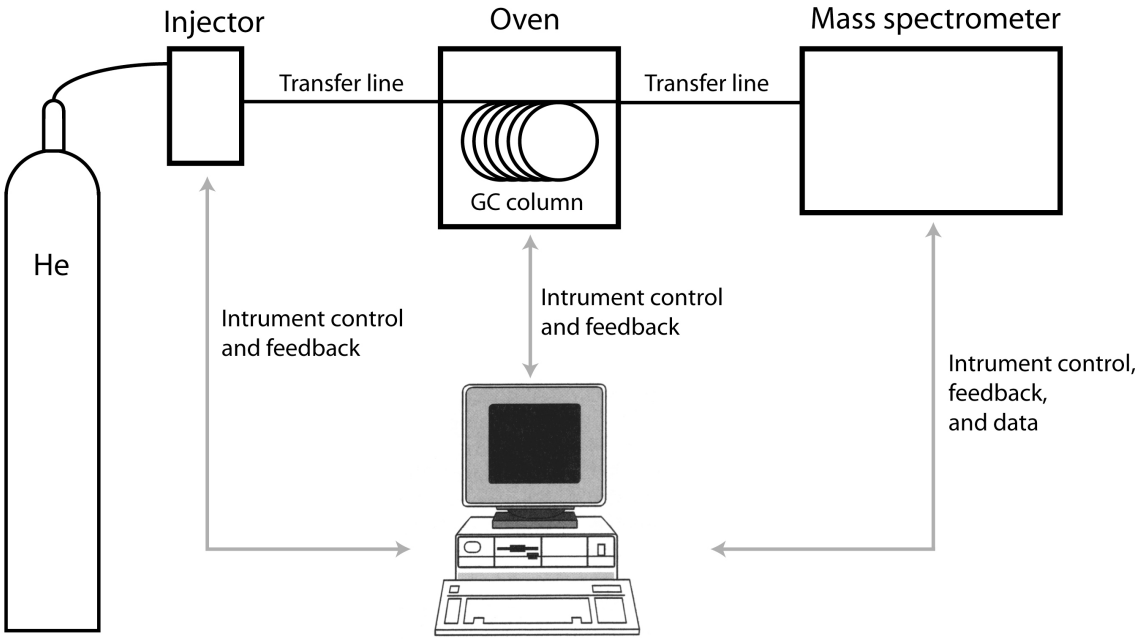

Figure 2.17. GC-MS instrument

The injector of the chromatograph and the transfer line are always at high temperature, even when the oven containing the column is not hot. The technique requires therefore a certain level of volatility and thermal robustness of the analyte. In order to adapt a substance to these properties, derivatization is well established. The most frequent procedures are silylation, acetylation, methylation, and fluoralkylation of XH groups. These derivatizations usually lead to a decrease of polarity and to enhanced volatility of the sample compounds.

2.4.2. Liquid Chromatography – Mass spectrometry (HPLC-MS)

Investigations into the coupling of HPLC and MS started some 30 years ago, in the early 1970's. During the first 20 years most of the attention had been given to finding solutions to interface problems or developing new technologies; today, focus is almost exclusively given to the application of the available techniques. Technological problems appear to be solved, and from the wide variety of interfaces developed over the past years, basically only two remained, ESI and APCI (Niessen 2006).

In HPLC, the general principal of chromatographic separation is based on a liquid/liquid or solid/liquid repartition of analytes between a particular stationary phase in a HPLC column (or capillary) and a mobile phase that is pumped through the column. The variation of the

mobile phase composition throughout a chromatographic separation is called gradient elution; it normally allows a better and faster separation of components.

After the HPLC pump, a UV detector at variable wavelengths (to obtain chromatograms) or photodiode array (to obtain chromatograms and absorption spectra of the components) is often coupled prior to an MS instrument. With such an instrumental setup, information about chromophores, molecular weight and structure (MS/MS analyzer is required) of mixture components can be obtained in a single HPLC run.

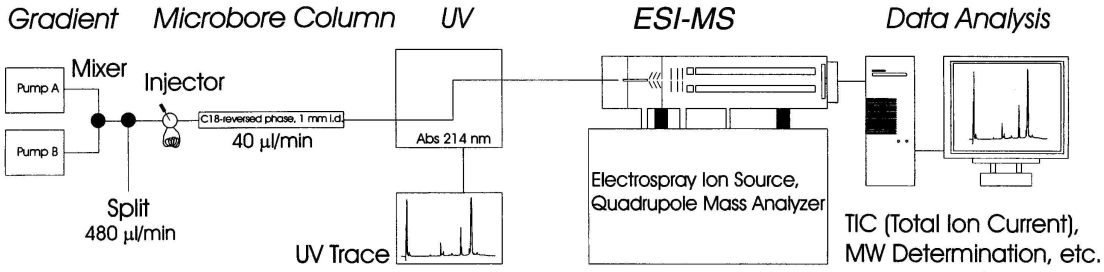

Figure 2.18. Standard HPLC-UV-ESI-MS instrument fitted with a microbore HPLC column

In order to increase the sample concentration at the detector, HPLC instruments working with lower flow rates have been developed. For a defined amount of sample injected, the limit of detection is more than three orders of magnitude lower if nanoHPLC is used instead of standard chromatography. For this reason, the nano-HPLC-MS coupling is routinely established in most of the proteomic laboratories that analyze digests of protein samples.

Table2.2. Effect of the HPLC column diameter on the sensitivity

Type	Column ID	Injection vol. [µl]	Flow	Detector conc.$_{rel.}$
Standard	4.6 mm	5-20	1000 µl·min^{-1}	1
Narrowbore	1-2 mm	0.5-5	40-300 µl·min^{-1}	20-5
microHPLC	300 µm	0.1-0.3	4 µl·min^{-1}	235
nanoHPLC	75 µm	0.05-0.1	200 nl·min^{-1}	3800

2.4.3. Tandem Mass Spectrometry (MS/MS)

Whereas the ionization techniques and mass analyzers developed in the mid-1980s are crucial to the application of MS to biological compounds, the technique of MS/MS is an equally important factor in the contribution to the field. As the name implies, MS/MS involves two stages of MS. In the first stage, ions of a desired *m/z* are isolated from the rest of the ions emanating from the ion source. These isolated ions (so-called precursor ions or parent ions) are then induced to undergo chemical reactions by increasing their internal energy, usually via collision with an inert gas (He or Ar). This process is called 'collision induced dissociation' (CID). Finally, the fragment ions are separated and recorded.

There are two types of MS/MS instruments, namely 'tandem in space' and 'tandem in time'. 'Tandem in space' instruments are consisting of more than one mass analyzer and each step of the MS/MS investigation is performed at a different place in the instrument (MS I and MS II). Beam-type analyzers like triple quadrupole, time-of-flight, or sector-field quadrupole are used in tandem-in-space instruments.

Ion traps and FT-ICR are instruments performing 'tandem-in-time' experiments. The various stages of MS/MS – ion collection, isolation, excitation, and analysis of the fragment ions – are performed in the same analyzer but separated in time. Tandem-in-time instruments have the advantage of being able to do multiple stages of MS/MS (MS^n) experiments with a single mass analyzer.

MS/MS experiments are often used for structure elucidations when soft ionization techniques (e.g. ESI, APCI, or Maldi) are in employed. These ion sources generate mainly quasi-molecular ions, and the spectra contain only low structure information. It is noteworthy that for HPLC-MS applications, other scan modes are possible that significantly improves the selectivity (figure 2.19). For example, the monitoring of certain collision-induced fragmentation reactions by selected reaction monitoring (SRM) – in this case MS I and MS II are fixed at reaction specific *m/z* values – lead to chromatograms with a greatly improved S/N ratio. This technique was applied for the quantification of taurolidine in human plasma (see Chap. 5.3).

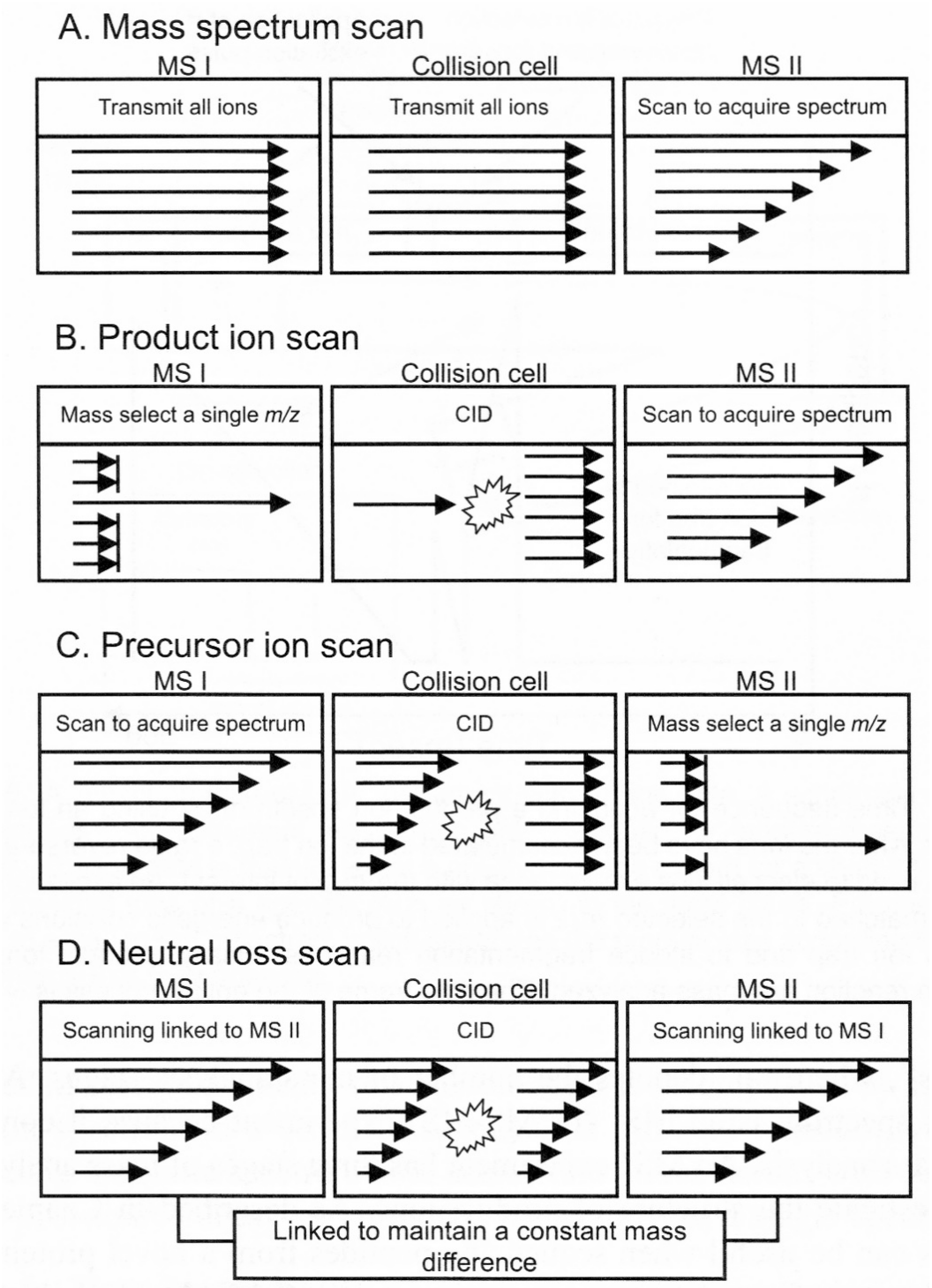

Figure 2.19. Analysis mode in tandem MS (Kinter et al. 2000).

Although SRM is the method of choice in quantitative bioanalysis, precursor-ion and neutral-loss analysis modes are particularly useful in quantitative analysis and screening of food or environmental samples for contaminants. For example, when a glycosylated peptide is dissociated, one of the product ions is *m/z* 204, which is a glycosyl fragment. By setting MS II to only *m/z* 204, MS I can be scanned to sequentially pass all the ions emitted

from the ion source, but only those ions that dissociate to *m/z* 204 will be detected (precursor ion scan). This means that the glycosyl derivatives will be the only components of the mixture that show a signal on the HPCL-MS/MS chromatogram. Precursor-ion scans or neutral-loss scans have to be performed on tandem-in-space instruments. Thus, for screening mixtures, beam instruments (e.g. triple quadrupoles) have a definite advantage over ion trap instruments.

Today, tandem mass spectrometry is an established method with plentiful applications, e.g. in elucidation of structures, determination of fragmentation mechanisms, determination of elementary compositions, applications to high-selectivity and high-sensitivity analysis and observation of ion-molecule reactions. In proteomic applications for example, the sensitivity levels are so low that sequencing and identification of proteins can be accomplished on the same amounts of material used by biomedical investigators in routine experiments (Kinter et al. 2000).

III. OWN DEVELOPMENTS

Coupled with different separating methods such as gas chromatography (GC) or high-performance liquid chromatography (HPLC), mass spectrometry gained a capacity to solve problems that were inadequately addressed by other analytical tools. A large number of ionization methods and type of analyzers have been developed and combined in various ways (see above). Nowadays, to a great part, the challenge in MS is the selection, depending on the material of interest, of the best combination of separating and detecting methods to suite actual needs.

The success of MS-analyses is strongly dependent on the procedure of sample preparation. In the works presented hereafter, the analytes were of medium to high polarity and low volatility, and part of complex mixtures. In order to reduce sample degradation, to minimize contamination and to increase sensitivity and efficiency, sample preparations were chosen as straightforward as possible. A method based on GC-MS has never been taken in account because the polar compounds of interest, an extraction step followed by derivatization reactions would have been necessary. This is difficult to achieve without discrimination of some of the components, in particular, when the analytes are highly soluble in water and have to be quantified.

For these reasons, methods based on the analyses of crude mixtures, HPLC chromatographic separation, on-line recording of UV-absorption spectra and mass spectrometry, were developed. The choice of the MS instrument was mainly dependent on the instrument performance. The performance can typically be defined by the following characteristics: accuracy, resolution, mass range, tandem analysis capabilities, and scan speed. In combination with liquid chromatography, two types of ions sources, ESI and APCI, can be considered. In the following table, the mass analyzers typically used for electrospray and their performances are displayed.

Table 3.1. General comparison of ESI-mass analyzers and their properties

	Quadru-pole	**Ion Trap**	**Time-of-Flight Reflectron**	**Magnetic Sector**	**FT-ICR**	**Q-TOF**
Accuracy	100 ppm	100 ppm	< 5 ppm	< 3 ppm	< 1 ppm	< 5 ppm
Resolution	2'000	4'000	15'000	30'000	100'000	10'000
m/z range	4'000	4-6'000	10'000	8'000	10'000	10'000
Scan Rate	~2 Hz	~5 Hz	50 Hz	0.1 Hz	~1 Hz	~20 Hz
MS/MS	MS^2 (QqQ)	MS^n	MS	MS^2	MS^n	MS^2
Comments	Low cost, Ease of pos/neg ions switching	Low cost, Ease of pos/neg ions switching	Good accuracy and resolution	High accuracy but low scan rate	High resolution & accuracy, expensive	Good accuracy and resolution

All experiments were performed with a triple stage quadrupole (QqQ) and with a quadrupole ion trap (QIT), both couple to a HPLC system. These highly automated systems are able to produce even hundreds of analyses per day. Such automation requires samples of the same type to be treated by an analytical protocol that has been carefully elaborated by an expert before. A successful and straightforward data interpretation is strongly dependent from the quality of the data obtained. Sample preparation procedure, choice of the HPLC conditions (column, gradient, and solvents), selection of the ionization method, MS parameters, and, if necessary, MS/MS experiments have to be well thought-out for a good method optimization.

Recently, we have developed several analytical methods for the structure elucidation of unknown natural products or the study of biosynthesis pathways in plants (Chesnov et al. 2002). For example, more than 80 polar organic compounds could be identified from 10mg pollen of *Hippeastrum* flowers, or labeled precursor molecules were added to the growth medium and labeled biotransformed products detected after there were assimilated from *Aphelandra* plants.

The experimental setup shown in Scheme 3.1 consists of an HPLC on-line coupled with an ultraviolet diode array detector (UV-DAD) and either APCI-, or ESI-MS and MS/MS. Such systems are particularly advantageous for the analysis of substances that are available only in traces. Additionally, the analysis of crude material decreases the probability of

material loss or oxidation (formation of artifacts) during the handling of the sample before it is introduced into the mass spectrometer. HPLC-UV(DAD)-ESI-MS gives important primary information about the structural nature of the compounds, i.e. the type of chromophores present, and, of course, the molecular weight of the analyzed compounds. ESI- and APCI-MS are soft and sensitive ionization techniques and usually yield quasi-molecular ions with low fragmentation. This is particularly suitable for the investigation of thermolabile compounds such as e.g. polyamines, flavonol, or peptide/protein derivatives. The present work will give an insight into a selection of HPLC-UV(DAD)-ESI-MS and MS/MS applications. After adaptation of the experimental setup, investigations as versatile as structure elucidation, metabolomic profiling, or pharmacokinetic studies of thermally unstable compounds can be performed.

The central research performed in our laboratories will be shortly introduced hereafter. All studies were done using hyphenated mass spectrometric methods, and mass spectrometry was a key tool for solving the problem.

Scheme 3.1. Mass spectral fragmentation of the terminal part of the $[M + H]^+$ ions of the *IndAc* pentamine derivatives

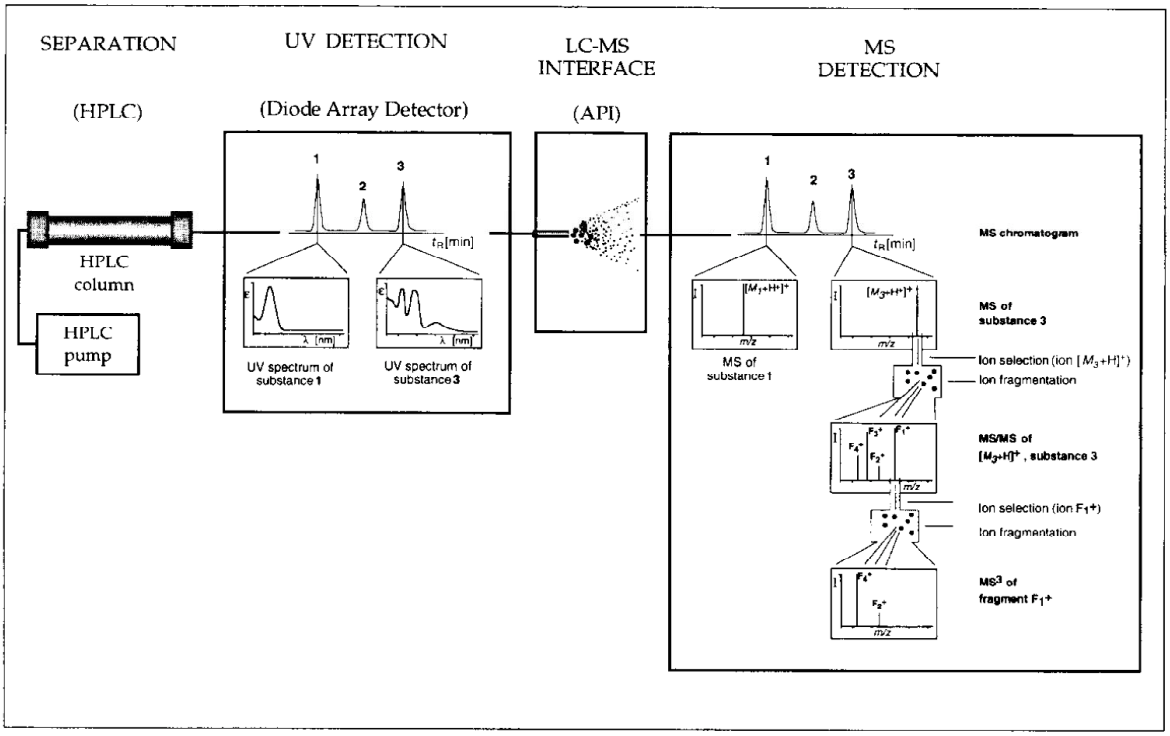

A) Structure elucidation of natural products – Polyamine derivatives from spider venom

Biologically active compounds from different natural sources have attracted the attention of scientists for hundred of years. Their constituents were isolated and their further use as possible medicines tested. A more sophisticated separation, characterization and synthesis of natural compounds could be achieved with the development of modern analytical and organic chemistry. Nevertheless, it was only possible to analyze those substances that were present in at least milligram amounts. The separation and characterization of minor components that were present in natural objects in trace amounts was unlikely by classical methods.

In the last twenty years, spider venoms were widely investigated with the aim to elucidate their structures and to test their biological activity (Escoubas et al. 2000; Rash et al. 2001). Interesting results were obtained during these studies. In spider venom, depending on the species, one could find in different ratios various compounds, such as amino acids, purine bases, polyamines, acylpolyamines, peptides, polypeptides and proteins.

In our laboratories, methods based on HPLC, on-line coupled with UV-diode array detection, and APCI- or ESI-MS/MS (scheme 3.1), were used for the first time to characterize low-molecular-weight compounds, in particularly polyamine derivative, present in spider venoms (Chesnov et al. 2000; Horni et al. 2000; Chesnov et al. 2001). After injection, the sample is separated into its components on the column according to their polarity. After separation, they pass through the UV(DAD) detector, and the chromophores present are determined from the UV spectra that are recorded continuously during the whole measurement. The sample is sprayed into the mass spectrometer as soon as it has passed the UV cell. The molecular weight of a substance can then be estimated instantly from the quasi-molecular ions $[M+H]^+$. Of course, all the collected information, – the mass spectra of separated or partly-separated compounds with their retention times, as well as their UV spectra – is rather incomplete because mild ionization prevents any structural information from being obtained, other than the molecular weight and the chromophores.

More data could be obtained using the technique of MS/MS. Fragment ions obtained by collision-induced dissociation (CID) of the quasi-molecular ions, give additional structural

information. Our first tandem mass spectrometry experiments were performed on a triple-stage quadrupole mass spectrometer (QqQ) in the product ion scan mode. The selected precursor ions collided with an inert gas (Ar), got more internal energy and fragmented. A connected second mass spectrometer (Q3) analyzed the fragment ions.

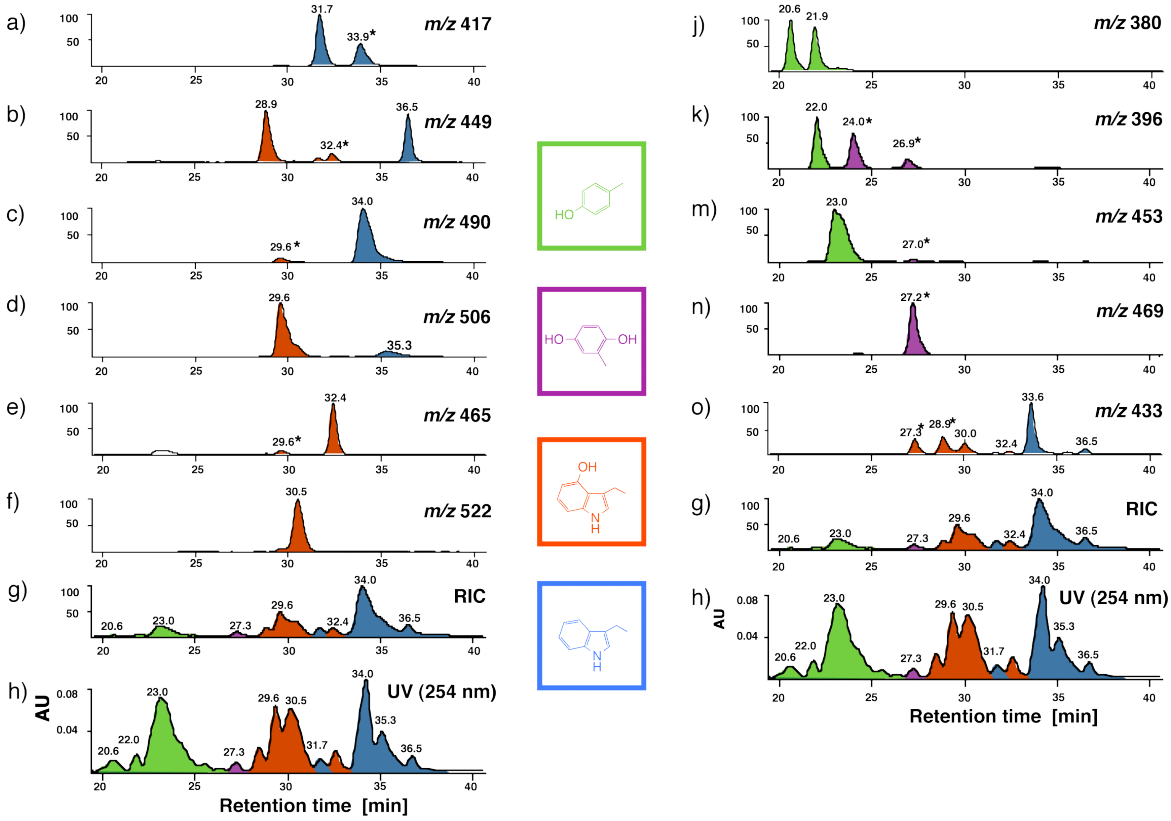

Figure 3.1. Agelenopsis aperta venom: acylpolyamine-containing fraction analyzed by HPLC-UV(DAD)/APCI-MS. **a)–g)** and **j)–o)** (EIC) of quasi-molecular ions m/z 417, 449, 490, 506, 465, 522, 380, 396, 453, 469, 433. **g)** RIC; **h)** UV Detection at 254 nm. AU = arbitrary unit. The starred signals belong to compounds co-eluting with the major constituents, where the chromophore type was suggested from MS/MS data.

If an HPLC is connected to a triple quadrupole instrument, structure elucidation of the interesting compounds has to be performed in two steps. The masses of interest have been to be determined in one run and then, structure elucidation of a unique *m/z* value can be performed in a second run.

Investigations of the venom of *Agelenopsis aperta* spider, shown in figure 3.1 demonstrate how laborious such analyses can become if a complex sample is investigated (Chesnov et al. 2001). This approach, nevertheless, allowed the characterization of no less than 38 acylpolyamines with 11 different molecular weights in the venom of *A. aperta* spiders ((Manov et al. 2002); for a general structure, see e.g. ARG636 in figure 3.2).

Only 11 acylpolyamine derivatives were known in this venom before (Quistad et al. 1990). The structures of these main components were elucidated after an extensive procedure of first fractionation/purification of the whole venom by HPLC, then individual fraction analyses by fast atom bombardment (FAB) mass spectrometry.

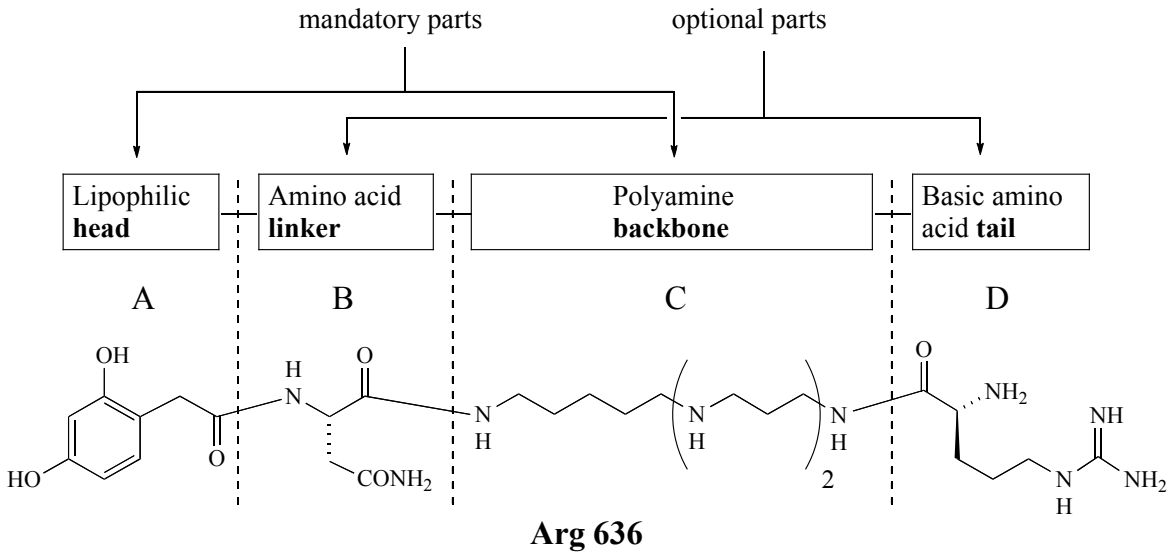

Figure 3.2. Structures of polyamine spider toxins exemplified by **Arg 636**.

The next improvement of the analytical procedure was achieved with the use of quadrupole ion trap mass analyzer. This type of mass spectrometer is able to select and to fragment automatically precursor ions registered during ESI-MS in the full scan mode. Quasi-molecular ions are trapped, the product ions of interest segregated by mass and further fragmented by collision with He. This makes structure elucidation of unknowns in complex mixtures much faster and more sensitive. Information about the molecular weight and structure of many unknowns can be gained from a single HPLC run.

A few milligrams of lyophilized crude venom of *Larinioides folium* spiders containing also salts, peptides, or proteins, was necessary for the study its polyamine derivatives content by HPLC-UV(DAD)-MS/MS (Eichenberger et al.). Combined with H/D-exchange experiments for the determination of the number of exchangeable protons, and amino acid analysis, as many as 41 polyamine derivatives could be identified in this complex venom (figure 3.3).

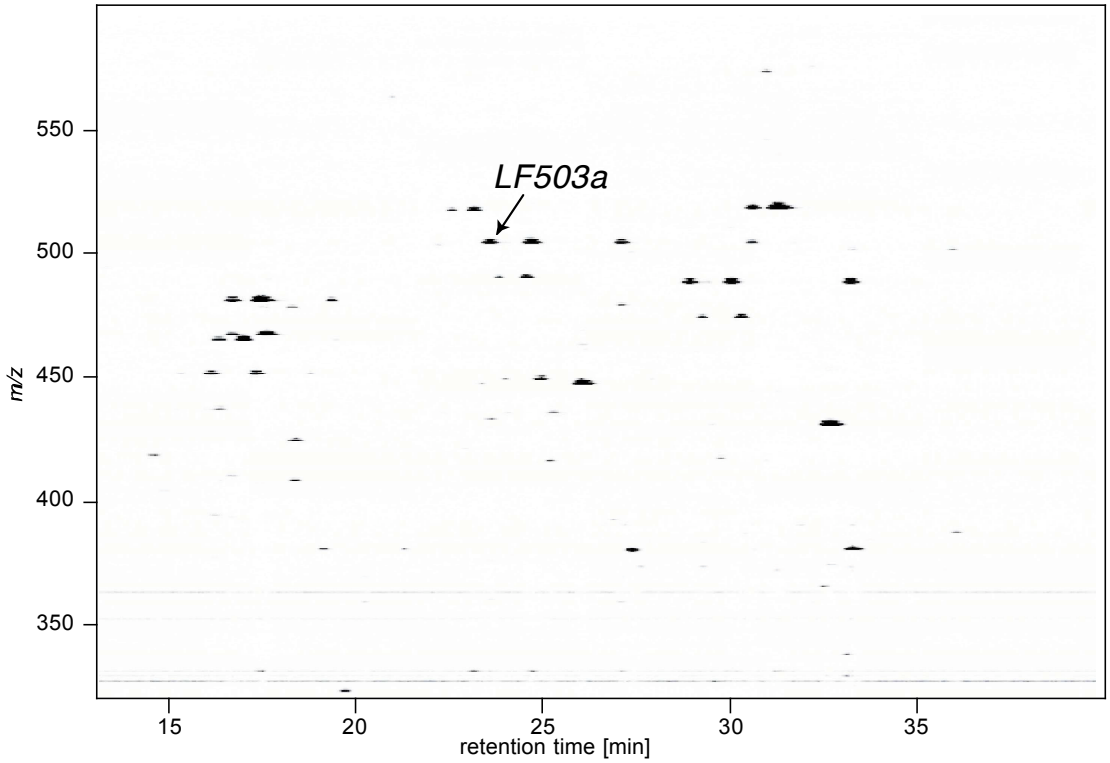

Figure 3.3. 3D-Plot of retention time (t_R) *vs m/z* and rel. int. of an HPLC-ESI-MS run with the lyophilized spider venom of *L. folium*.

The next level of difficulty is defined by the characterization of free linear polyamine derivatives containing four, five, or six N-atoms, and is presented in Chap. 5.1 hereafter. Some of constituents found there were *N*-hydroxylated, guanidylated, or acetylated with a UV-inactive group. Only a few examples of non-acylated polyamines containing more than four N-atoms were known. Beside caldopentamine (PA3333[1]) in the silk glands and in the heads of the spiders *Nephila clavata* and *Araneus ventricosus* (Hamana et al. 1991), extended free polyamines were only found in bacteria (Hamana et al, 1992). They were characterized either by GC-MS after their derivatization with heptafluorobutyric anhydride (HFBA, (Niitsu et al. 1993)), or by HPLC and fluorescence detection of the *o*-phthalaldehyde (OPA) reaction products (Hamana et al. 1998).

[1] The abbreviation PA stands for polyamine; the figures designate the number of methylene in-between the several N-atoms Bienz, S., Detterbeck, R., Ensch, C., Guggisberg, A., Häusermann, U., Meisterhans, C., Wendt, B., Werner, C. and Hesse, M. (2002). "Putrescine, Spermidine, Spermine, and Related Polyamine Alkaloids." *Alkaloids* **58**: 83-338..

Our approach of on-line HPLC-UV(DAD)-ESI/APCI-MS and MS/MS experiments became more difficult as soon as the lypophilic head was missing in the polyamine derivatives. First, the HPLC-UV detector does not register such compounds. Moreover, they are now particularly polar and therefore interactions with the C_{18}-chains of the reverse phase HPLC column extremely weak. The results are retention times close to the dead volume and problems of co-elution.

Only the introduction of end-capped C_{18}-columns of good quality with 3µm particle size, which are more or less stable under 100% aqueous conditions, allowed the separation and characterization of the free polyamines. In addition, discussion concerning the biosynthetical pathway leading to the formation of acylpolyamines in spider venoms became possible.

B) Mechanisms of Tandem Mass Spectrometric Fragmentations

Many natural products like peptides, oligonucleotides or saccharides are thermally labile compounds and failed to be investigated by long-established electron impact mass fragmentation at 70 eV. The same is true for polyamines (e.g. spermidine and spermine) and their derivatives. To render such molecules more heat resistant, they were first converted to their more stable N-acetyl derivatives (Bosshardt et al. 1974). The mass spectral fragmentation of the acetyl derivatives then allows the deduction of general rules for this class of compounds.

Because the available amounts of the toxins are often very small and they have high polarity, the above-mentioned acetylation method is not useful and analytical systems based on the soft ionization techniques ESI and APCI were developed. To obtain structural information from quasi-molecular ions $[M+H]^+$, $[M+nH]^{n+}$, or $[M+Na]^+$, low energy collision induced dissociation (CID) with argon in a triple stage quadrupole or with helium in an ion trap instrument is the method of choice (Biemann et al. 1987; Fenn et al. 1989). In fact, polyamines such as spermine are so reactive that they even decompose in the ESI ion source if the lens voltages are not very well optimized; under such inadequate conditions, they give similar spectra to those obtained from CAD experiments.

The reactivity of quasi-molecular ions under CID conditions has been studied in detail principally for proteins and peptides (Kinter et al. 2000). This research was catalyzed by the tremendous development of proteomic sciences in the nineties; however, the fragmentation behavior of polyamine derivatives was scarcely known, particularly because of a lacking of synthetic reference material. For this reason, new synthetic pathways based on solid phase technologies have been developed (Manov et al. 2002).

Measuring thoroughly characterized reference structures is not sufficient to obtain evidence of the mechanistic pathway of CID fragmentations. Therefore, reference compounds were labeled. The easiest labeling reaction is the H/D-exchange of all acidic H-atoms with deuterated solvent (e.g. CD_3OD or D_2O). After carefully flushing of the ESI ion source in order to avoid back exchange, MS/MS studies can be performed on molecules containing fully deuterated amine, amide, hydroxyl, or acidic groups (Bigler et al. 1995). These types of experiments allowed us to uncover an unexpected neighboring group participation fragmentation reaction in cinnamic acid derivatives of diamines

(Scheme 3.2). Existence of this mechanism was further confirmed by MS/MS analyses of the meta-substituted cinnamic acid as well as the diaminopropane and heptane derivatives. These compounds showed much stronger signals for the product corresponding to the four-center cleavage mechanism B, i.e. fragment ion *m/z* 93 having one deuterium atom less.

Scheme 3.2. Mass spectral fragmentation of the diamino cinnamic acid derivatives under CID conditions.

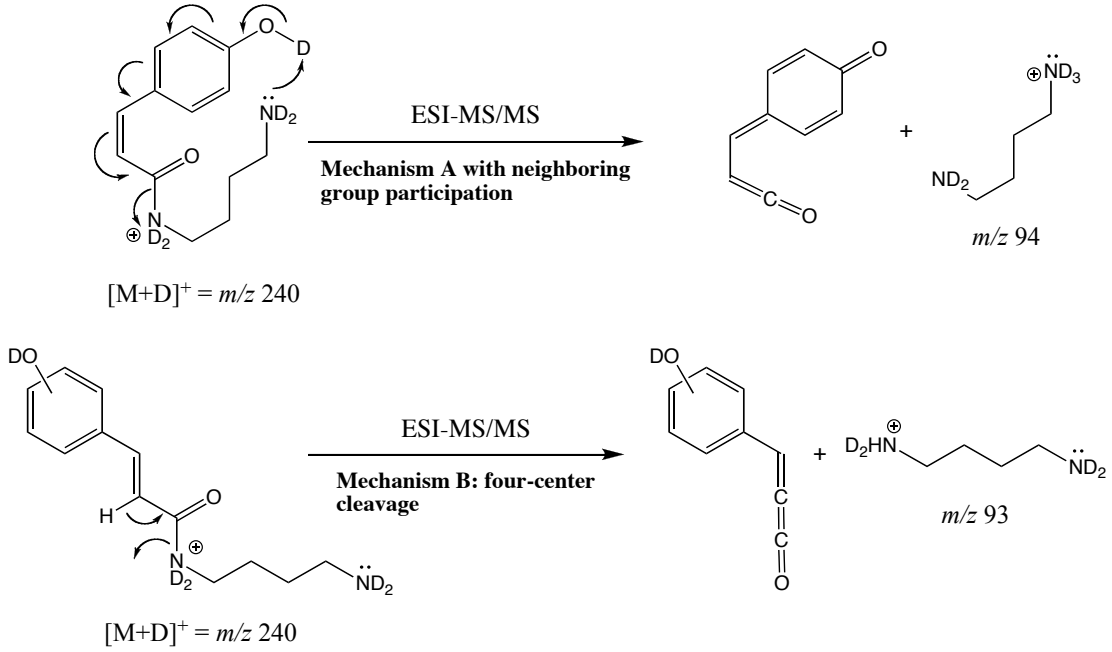

The synthesis of all acylpolyamines that could be considered in a spider venom sample is extremely time consuming. For this reason, a method for structure elucidation of acylpolyamines based on MS/MS data only is preferred, but requires a comprehensive understanding of fragmentation mechanisms.

For the first time, ^{15}N-labeled acylpentamines were synthesized by Bienz and coworkers (Manov et al. 2004). They were used to verify the hypothesis of (i) a trans-amidation reaction, (ii) a cascade of transamination reactions, or (iii) a stepwise fragmentation of the sample molecule.

Scheme 3.3.

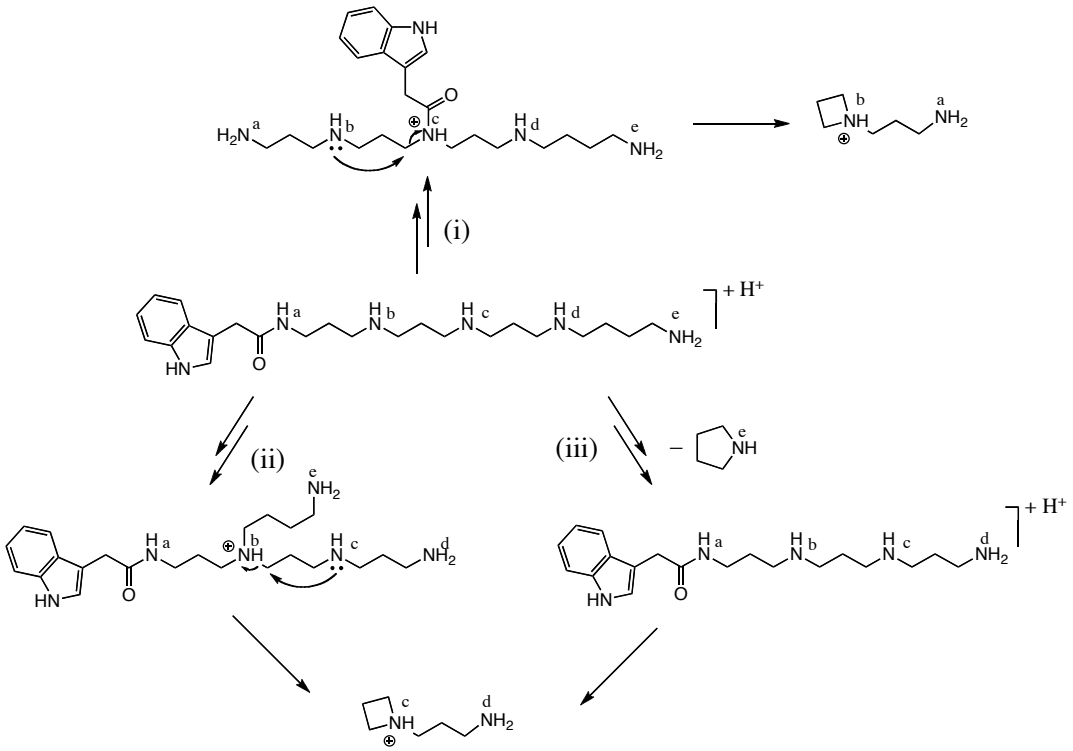

The MS/MS analyses of the ^{15}N-labeled materials revealed the presence of fragment ions of the internal portion of the acylpolyamine (in bold on figure 3.4), which excluded the mechanism of transamidation (i). However, the mechanisms (ii) and (iii) can still not be distinguished with the results obtained.

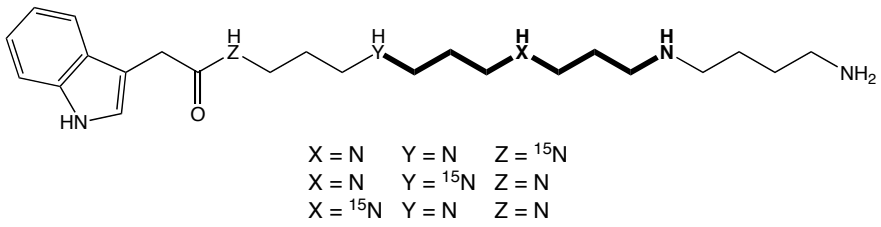

Figure 3.4. ^{15}N-Labeled polyamine derivatives.

To summarize, the 2nd paper demonstrates that structural elucidations of polyamines and their derivatives based on HPLC-UV(DAD)-APCI-MS and -MS/MS is only possible by comparison with synthetic material and require a profound knowledge of the fragmentation behavior under CID conditions, especially in the case of co-eluting isomers. Their identity, in such an extreme case, could only be revealed due to the specific fragmentation behavior of the several structural isomers that could only be studied, however, with the pure labeled compounds.

C) Drug Metabolism and Quantification

Nature is an excellent source of new drugs or, more commonly, of lead candidates to drugs. Of the 20 most important drugs in 1999, 9 of them were derived from natural products (Harvey 2000; Silverman 2004). One approach to pharmacological research is the study of drug metabolism and the isolation of metabolites, the drug degradation products. On the one hand, these compounds may show a stronger or a different interesting pharmacological activity and, on the other hand, they might be responsible for side effects.

Research in drug metabolism is strongly based on HPLC-MS and MS/MS. The investigations done in our laboratories on amiodarone (AMI) were chosen as an example. This compound, which was initially developed 40 years ago as an antianginal drug, is still considered as one of the most effective antiarrhythmic agents. However, AMI therapy is accompanied by a variety of severe adverse effects, including pulmonary toxicity, hepatotoxicity, and thyroid dysfunction. Since mono-*N*-desethylamiodarone (MDEA) was the only known metabolite of AMI in humans, we tried, in collaboration with the university hospital of Zurich, to study AMI metabolism more in detail.

Preliminary studies have shown that mammals, in particular rabbits, are biotransforming AMI to MDEA as well as to three other HPLC-UV-detectable compounds. Therefore, extracts obtained from rabbit liver microsomes were used first. The first compound that could be identified by HPLC-MS/MS was a hydroxylated derivative of MDEA (3'OH-MDEA). It is noteworthy that NMR was necessary to allege the exact position of the hydroxyl group (Ha et al. 2001; Ha et al. 2001). This new substance was then synthesized (Wendt et al. 2002) and finally tested for it effects on lung cell by looking for it toxicity toward alveolar macrophages (Quaglino et al. 2004).

Experiments with human plasma could also been performed succefully (Ha et al. 2005). Two further metabolites could be identified as di-*N*-desethylamiodarone (DDEA) and deaminated AMI (DAA) by HPLC-MS/MS. This analytical method was then modified so that all metabolites could be quantified from 1mL patient plasma in the nanogram range.

All these studies provide evidence that the metabolism of AMI is more complex than generally accepted: the unique formation of MDEA (scheme 3.4). Further investigations are needed to know whether the metabolites reported herein are synergistic to the therapeutic effect of the parent drug or are responsible for the undesired side effects observed in the AMI therapy.

Scheme 3.4. Metabolic pathway of amiodarone

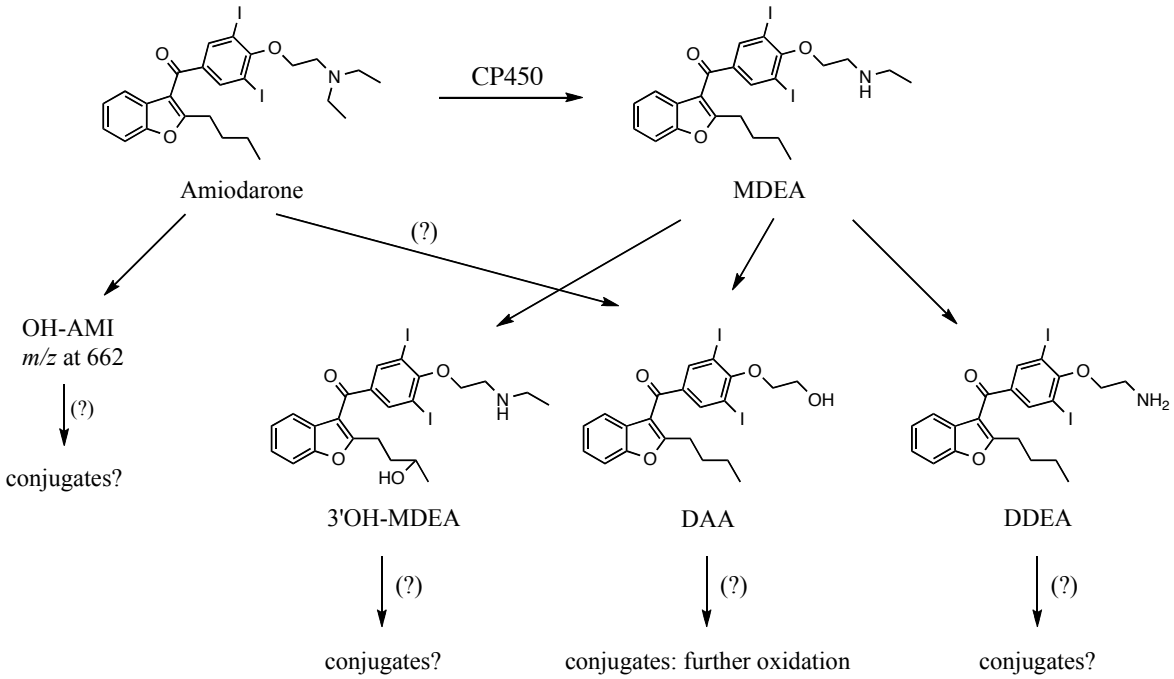

Another example of pharmacological studies that were performed using HPLC-ESI-MS/MS is presented in Part 3. Taurolidine has to be found to exert a selective antineoplastic effect that can be used for the treatment of brain tumors. The difficulty of the pharmacokinetic studies was that taurolidine is not stable in aqueous solutions and forms an equilibrium with degradation products. A new highly selective and sensitive quantification method based on ESI-MS/MS was developed. With this approach, the pharmacokinetics of taurolidine and its degradation products taurultame and taurinamide in plasma and *whole blood* in vitro as well as *in vivo* could be investigated.

D) Flavonoids and Plant Growth

The comprehensive analysis in which all the metabolites of an organism are identified and quantified is called metabolomics (Bino et al. 2004). This new methodology contributes to our understanding of the complex molecular interactions in biological systems. Gas chromatography-MS (GC-MS), HPLC-UV(DAD)-MS, and capillary electrophoresis (CE)-MS are the methods of choice for qualitative and quantitative metabolite profiling. An instantaneous snapshot of the physiology of a cell is obtained, giving a more complete picture of living organisms (Villas-Bôas et al. 2005).

Scheme 3.5. Main steps involved in sample preparation, analysis and processing during metabolome analysis.

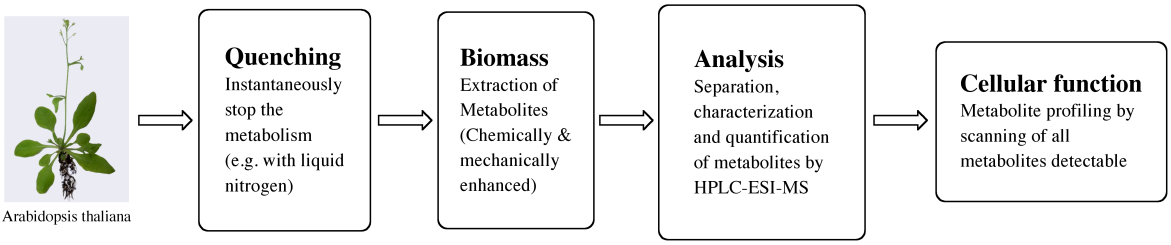

The major challenge of metabolite identification is rapid, sensitive and reliable elucidation of structural changes. This concerns immediate inactivation of the metabolism, extraction of the maximum number of metabolites in their original state and quantitative amount, identification of a maximum number of metabolites in a single analysis, and finally, principal component analyses in order to highlight the components of interest (scheme 3.5).

The combination of HPLC with MS enables the analysis of many classes of compounds, in particular non-volatile and thermally unstable metabolites that display a wide variety of polarities and molecular masses, without any derivatization. Plant and fungal secondary metabolites, amino acids, nucleotides and oligosaccharides have been identified and quantified from data obtained from a UV(DAD) detector or from MS^n experiments. Especially ion trap mass spectrometers with their multiple MS capabilities and sensitivity in full scan mode have proven to be excellent tools for this purpose.

Flavonoids are widely distributed in plants, fulfilling many functions including yellow or red/blue pigmentation in flowers and protection from attack by microbes and insects

(Andersen et al. 2006). They are divided in three main groups: flavones, flavanones, catechins, and anthocyanins.

Scheme 3.6. Main groups of flavonoids

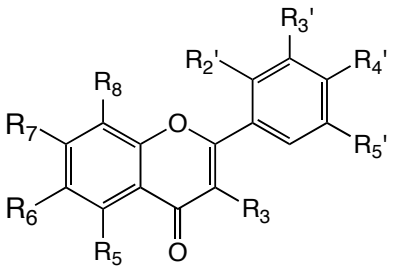

Flavone

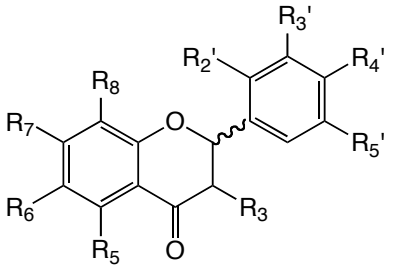

Flavanone

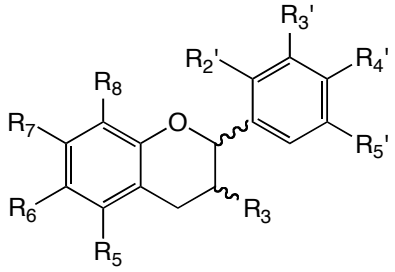

Catechin

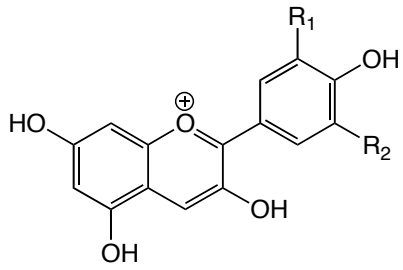

Anthocyanin

Flavonoids are secondary metabolites known to modulate plant growth and development. In the 4th research topic, we were interested in flavonols, a subgroup of flavones that are assumed to modify the auxin flux in the plant. Their study is complex because of the multiplicity and the similarity of the different molecular structures. For example, more than 350 derivatives evolving from a single flavonol aglycone, quercetin, have been described in plants, and most of this variability comes from glycosylation by one or several sugar moieties (Kerhoas et al. 2006).

In wild type and transgenic or mutant *Arabidopsis thaliana* plants, flavonols are glycosylated with up to four glucose and rhamnose substituants (Stobiecki et al. 2006). The HPLC-UV(DAD)-ESI-MS approach is well suited for their determination, providing molecular weight, general structure, and relative concentrations of the various constituents without derivatization.

IV. OUTLOOK

We plan to focus our next developments on improvements of analysis and data processing methods, and initiation of new research fields.

The application of high-resolution mass spectrometry in structure elucidation of natural products will be established for thermal labile molecules contained in complex mixtures. High accurate ESI-MS and MS/MS provide data that allow only a small number of theoretical elemental compositions for a sample ion, in most cases just a single hit. Once the elemental compositions of protonated sample molecules and their fragment ions is known, the interpretation of the fragmentation pattern, in combination with additional analytical data from H/D exchange experiments, amino acid analysis and UV/VIS spectroscopy, should allow a simplified and unambiguous structure determination of unknown natural products.

New data processing methods based on accurate masses will also allow the recognition of functional group in bioorganic molecules. The deviation of the exact mass compared to the nominal mass depends on the class of compounds and the molecular weight and was defined as "delta mass variation" (Juris 2006). This approach was successfully applied for the identification of amino acids. Functional groups of petroleum components were also identified by comparison of the delta mass to the theoretical exact masses in a so-called "Kendrick plot" allowing their classification and characterization.

The improvement of HPLC-MS data processing using statistical tools is another ongoing research domain. For the growing flow of information obtained from an increasing number of samples, an algorithm was developed that detect the relevant component in a set of analyses. This so-called "principal component analysis" (PCA) software provides information about variance in data sets and simultaneously highlights signals (R_t-*m/z* pairs in HPLC-MS chromatograms) responsible for variation. This straightforward approach, particularly when complex HPLC-MS data have to be processed as e.g. in the characterization of polyamine derivatives found in spider venom (Chap. 5.1), or flavonoid

profiling as presented in chapter 5.4, will improve the detection rate of unknown natural products, or drug metabolites.

The development of mass spectrometry as a platform for strategies that study non-covalent interactions between small organic molecules or metal ions, and receptors like e.g. proteins, or RNA will be followed. The method will be based on the soft ionization techniques MALDI and ESI. This so-called SAR (structure-activity relationship) approach allows the identification and optimization of high-affinity ligands (compounds that bind to receptors) by quantification of binding affinity, stoichiometry, and specificity over a wide range of ligand binding energies. A set of diverse compounds, in particular polyamine derivatives will be measured by ESI- or APCI-MS in order to identify those that bind to receptor, e.g. a strain of RNA. Competition experiments will be used to identify the ones that bind to the same site and those that do not, and to estimate stoichiometry and binding constants of the complexes.

For example, it is planned to study the interactions between synthetic or newly identified natural products, e.g. polyamine derivatives that are synthesized in the laboratory of Prof. S. Bienz at the University of Zurich, and DNA and RNA strains. ESI- and MALDI-MS-based methods will be used as they have been successfully employed to measure DNA or RNA complexes with proteins, drugs or other ligands (Beck et al. 2001; Hofstadler et al. 2001). We hope with this approach to gain insights into the understanding of biological processes on a molecular level. Furthermore, this approach has a potential to allow the design of drugs that specifically bind selected DNA sequences in a combinatorial way.

A recently discovered novel and special field of application for mass spectrometry is the taxonomy of microorganisms (Fenselau et al. 2001). Increasing numbers of highly halophilic (= salt-loving) microorganisms - both Archaea and Bacteria - are isolated from salt lakes and saline marshes in many parts of the world. These organisms, which grow well at NaCl concentration up to 4M, appear to play a vital ecological role in their habitats and show great promise for applications in environmental biotechnology. The de-replication and ultimately the taxonomic characterization of halophilic cells from natural isolates, however, still remain laborious and expensive.

In collaboration with Prof. H. Patzelt from the Sultan Qaboos University in the Sultanate of Oman, new methods based on MALDI-MS are currently developed for the taxonomic characterization of halophilic Archaea. A fingerprint comparison of whole-cell MALDI mass spectra would allow their rapid and facile identification.

Literature

Andersen, O. M. and Markham, K. R. (2006). *Flavonoids : chemistry, biochemistry and applications*. Boca Raton, Fla., CRC Press.

Aston, F. W. (1919). "The Mass Spectra of Chemical Elements." *Phil. Mag.* **XXXVIII**: 707.

Barber, M., Bordoli, R. S., Sedgwick, R. D. and Tyler, A. N. (1981). "FAB of Solids as an Ion Source in Mass Spectrometry." *Nature* **293**: 270-5.

Beck, J. L., Colgrave, M. L., Ralph, S. F. and Sheil, M. M. (2001). "Electrospray ionization mass spectrometry of oligonucleotide complexes with drugs, metals, and proteins." *Mass Spectrom. Rev.* **20**: 61-87.

Beynon, J. H. (1956). "The Use of the Mass Spectrometer for the Identification of Organic Compounds." *Microchimica Acta* **44**: 437.

Biemann, K. and Scoble, H. A. (1987). "Characterization by Tandem Mass-Spectrometry of Structural Modifications in Proteins." *Science* **237**: 992-998.

Bienz, S., Detterbeck, R., Ensch, C., Guggisberg, A., Häusermann, U., Meisterhans, C., Wendt, B., Werner, C. and Hesse, M. (2002). "Putrescine, Spermidine, Spermine, and Related Polyamine Alkaloids." *Alkaloids* **58**: 83-338.

Bigler, L. and Hesse, M. (1995). "Neighboring Group Participation in the Electrospray Ionization Tandem Mass Spectra of Polyamine Toxins of Spiders. Part 1: α,ω-Diaminoalkane Compounds." *J. Am. Soc. Mass Spectrom.* **6**: 634-637.

Bino, R. J., Hall, R. D., Fiehn, O., Kopka, J., Saito, K., Draper, J., Nikolau, B. J., Mendes, P., Roessner-Tunali, U., Beale, M. H., Trethewey, R. N., Lange, B. M., Wurtele, E. S. and Sumner, L. W. (2004). "Potential of metabolomics as a functional genomics tool." *Trends in Plant Science* **9**: 418-425.

Bosshardt, H. and Hesse, M. (1974). "Massenspektrometrische Wechselwirkung zwischen den funktionellen Gruppen mehrfach substituierter Alkane." *Angew. Chem.* **86**: 256-270.

Brown, R. S. and Lennon, J. J. (1995). "Mass Resolution Improvement by Incorporation of Pulsed Ion Extraction in a Matrix-Assisted Laser Desorption/Ionization Linear Time-of-Flight Mass Spectrometer." *Anal. Chem.* **67**: 1998.

Brunnée, C. (1997). "50 Years of MAT in Bremen." *Rapid Commun. Mass Spectrom.* **11**: 694-707.

Carroll, D. I., Dzidic, I., Stillwell, R. N., Haegele, K. D. and Horning, E. C. (1975). "Atmospheric-Pressure Ionization Mass-Spectrometry - Corona Discharge Ion-Source for Use in Liquid Chromatograph Mass Spectrometer-Computer Analytical System." *Anal. Chem.* **47**: 2369-2373.

Chesnov, S., Bigler, L. and Hesse, M. (2000). "The Spider *Paracoelotes birulai*: Detection and Structure Elucidation of New Acylpolyamines by on-line coupled HPLC-APCI-MS and HPLC-APCI-MS/MS." *Helv. Chim. Acta* **83**: 3295-3305.

Chesnov, S., Bigler, L. and Hesse, M. (2001). "The Acylpolyamines from the Venom of the Spider *Agelenopsis aperta*." *Helv. Chim. Acta* **84**: 2178-2197.

Chesnov, S., Bigler, L. and Hesse, M. (2002). "Detection and Characterization of Natural Polyamines by High-Performance Liquid Chromatography-Atmospheric Pressure Chemical Ionization (Electrospray Ionization) Mass Spectrometry." *Eur. J. Mass Spectrom.* **8**: 1-16.

Cole, R. B. (1997). *Electrospray Ionization Mass Spectrometry: Fundamentals, Instrumentation, and Applications*. New York, Wiley Intersciences.

Comisarow, M. B. and Marshall, A. G. (1974). "Fourier Transform Ion Cyclotron Resonance Spectroscopy." *Chem. Phys. Lett.* **25**: 282.

Dahl, P. F. (1997). *Flash of the Cathode Rays: A History of J.J. Thomson's Electron*, Institute of Physics Publishing.

Dempster, A. J. (1917). "A New Method of Positive Ray Analysis." *Phys. Rev.* **XI**: 316.

Dole, M., Mack, L. L., Hines, R. L., Mobley, R. C., Ferguson, L. D. and Alice, M. B. (1968). "Molecular Beams of Macroions." *J. Chem. Phys.* **49**: 2240-2249.

Eichenberger, S., Tzouros, M., Bienz, S. and Bigler, L. *In preparation*.

Escoubas, P., Diochot, S. and Corzo, G. (2000). "Structure and pharmacology of spider venom neurotoxins." *Biochimie* **82**: 893-907.

Fenn, J. B., Mann, M., Meng, C. K., Wong, S. F. and Whitehouse, C. M. (1989). "Electrospray Ionization for Mass Spectrometry of Large Biomolecules." *Science* **246**: 64-71.

Fenn, J. B., Mann, M., Meng, C. K., Wong, S. F. and Whitehouse, C. M. (1990). "Electrospray Ionization-Principles and Practice." *Mass Spectrometry Reviews* **9**: 37-70.

Fenn, J. B., Mann, M., Meng, C. K., Wong, S. F. and Whitehouse, C. M. (1989). "Electrospray Ionisation for Mass Spectrometry of Large Biomolecules." *Science* **246**: 64-71.

Fenselau, C. and Demirev, P. (2001). "Characterization of Intact Microorganisms by MALDI Mass Spectrometry." *Mass Spectom. Rev.* **20**: 157-171.

Go, E. P., Apon, J. V., Luo, G., Saghatelian, A., Daniels, R. H., Sahi, V., Dubrow, R., Cravatt, B. F., Vertes, A. and Siuzdak, G. (2005). "Desorption/Ionization on Silicon Nanowires." *Anal. Chem.* **77**: 1641-1646.

Gross, J. H. (2004). *Mass Spectrometry - A Textbook*. Berlin Heidelberg, Springer-Verlag.

Ha, H. R., Bigler, L., Binder, M., Kozlik, P., Stieger, B., Hesse, M., Altorfer, H. R. and Follath, F. (2001). "Metabolism of amiodarone (part I): Identification of a new hydroxylated metabolite of amiodarone." *Drug Metab. Disp.* **29**: 152-158.

Ha, H. R., Bigler, L., Wendt, B., Maggiorini, M. and Follath, F. (2005). "Identification and quantitation of novel metabolites of amiodarone in plasma of treated patients." *Eur. J. Pharm. Sciences* **24**: 271-279.

Ha, H. R., Kozlik, P., Stieger, B., Bigler, L. and Follath, F. (2001). "Metabolism of amiodarone - II. High-performance liquid chromatographic assay for mono-N-desethylamiodarone hydroxylation in liver microsomes." *J. Chrom. B* **757**: 309-315.

Hager, J. W. (2002). "A New Linear Ion Trap Mass Spectrometer." *Rapid Commun. Mass Spectrom.* **16**: 512-526.

Hamana, K., Niitsu, M., Samejima, K., Itoh, T., Hamana, H. and Shinozawa, T. (1998). "Polyamines of the thermophilic eubacteria belonging to the genera *Thermotoga*, *Thermodesulfovibrio*, *Thermoleophilum*, *Thermus*, *Rhodothermus* and *Meiothermus*, and the thermophilic archaebacteria belonging to the genera *Aeropyrum*, *Picrophilus*, *Methanobacterium* and *Methanococcus*." *Microbios* **93**: 7.

Hamana, K., Niitsu, M., Samejima, K. and Matsuzaki, S. (1991). "Novel polyamines in insects and spiders." *Comp. Biochem. Physiol.* **100B**: 399-402.

Harvey, A. (2000). "Strategies for Discovering Drugs from Previously Unexplored Natural Products." *Drug Discovery Today* **5**: 294.

Hillenkamp, F. and Peter-Katalinic, J. (2007). *MALDI-MS – A Practical Guide to Instrumentation, Methods and Applications*. Weinheim, Wiley-VCH.

Hofstadler, S. A. and Griffey, R. H. (2001). "Analysis of Noncovalent Complexes of DNA and RNA by Mass Spectrometry." *Chemical Reviews (Washington, D. C.)* **101**: 377-390.

Horni, A., Weickmann, D. and Hesse, M. (2000). "The main products of the low molecular mass fraction in the venom of the spider Latrodectus menavodi." *Toxicon* **39**: 425-428.

Hu, Q., Noll, R. J., Li, H., Makarov, A., Hardman, M. and Cooks, R. G. (2005). "The Orbitrap: a New Mass Spectrometer." *J. Mass Spectrom.* **40**: 430-433.

Hughey, C. A., Rodgers, R. P. and Marshall, A. G. (2002). "Resolution of 11 000 Compositionally Distinct Components in a Single Electrospray Ionization Fourier Transform Ion Cyclotron Resonance Mass Spectrum of Crude Oil." *Anal. Chem.* **74**: 4145-4149.

Johnson, E. G. and Nier, A. O. (1953). "Angular Aberrations in Sector-shaped Electromagnetic Lenses for Focusing Beams of Charged Particles." *Phys. Rev.* **91**: 10.

Juris, M. (2006). "Mathematical tools in analytical mass spectrometry." *Anal. Bioanal. Chem.* **385**: 486-499.

Karas, M. and Hillenkamp, F. (1988). "Laser Desorption Ionization of Proteins with Molecular Mass Exceeding 10'000 Daltons." *Anal. Chem.* **60**: 2299.

Kerhoas, L., Aouak, D., Cingoz, A., Routaboul, J. M., Lepiniec, L., Einhorn, J. and Birlirakis, N. (2006). "Structural characterization of the major flavonoid glycosides from Arabidopsis thaliana seeds." *J. Agric. Food Chem.* **54**: 6603-6612.

Kinter, M. and Shermann, N. E. (2000). *Protein Sequencing and Identification Using Tandem Mass Spectrometry*. New York, Wiley-Interscience.

Koppenaal, D. W., Barinaga, C. J., Denton, M. B., Sperline, R. P., Hieftje, G. M., Schilling, G. D., Andrade, F. J. and Barnes, J. H. (2005). "MS Detectors." *Anal. Chem.* **77**: 418A-427A.

Lawrence, E. O. (1934). Method and Apparatus for the Acceleration of Ions. U. S. P. Office. United States**:** 1-7.

Makarov, A. (2000). "Electrostatic Axially Harmonic Orbital Trapping: A High-Performance Technique of Mass Analysis." *Anal. Chem.* **72**: 1156.

Mamyrin, B. A. (2001). "Time-of-flight Mass Spectrometry (Concepts, Achievements,

and Prospects)." *Int. J. Mass Spectrom.* **206**: 251-266.

Manov, N., Tzouros, M., Bigler, L. and Bienz, S. (2004). "Solid-phase synthesis of N-15-labeled acylpentamines as reference compounds for the MS/MS investigation of spider toxins." *Tetrahedron* **60**: 2387-2391.

Manov, N., Tzouros, M., Chesnov, S., Bigler, L. and Bienz, S. (2002). "Solid-phase synthesis of polyamine spider toxins and correlation with the natural products by HPLC-MS/MS." *Helv. Chim. Acta* **85**: 2827-2846.

March, R. E. (2000). "Quadrupole Ion Trap Mass Spectrometry: a View at the Turn of the Century." *Int. J. Mass Spectrom.* **200**: 285-312.

Marshall, A. G., Hendrickson, C. L. and Jackson, G. S. (1998). "Fourier Transform Ion Cyclotron Resonance Mass Spectrometry: a Primer." *Mass Spectom. Rev.* **17**: 1-34.

Mattauch, J. and Herzog, R. (1934). "Über einen neuen Massenspektrographen." *Zeitschrift für Physik* **89**: 786.

McLafferty, F. W. (1956). "Mass Spectrometric Analysis. Broad Applicability to Chemical Research." *Anal. Chem.* **28**: 306.

McLafferty, F. W. (1959). "Mass Spectrometric Analysis. Aromatic Acids and Esters." *Anal. Chem.* **31**: 82.

Message, G. M. (1984). *Practical Aspects of Gas Chromatography/Mass Spectrometry*. New York, John Wiley & Sons.

Munson, M. S. B. and Field, F. H. (1966). "Chemical Ionization Mass Spectrometry. I. General Introduction." *J. Am. Chem. Soc.* **88**: 2621.

Niessen, W. M. A. (2006). *Liquid Chromatography – Mass Spectrometry, 3rd ed.* Boca Raton, CRC Press.

Niitsu, M., Samejima, K., Matsuzaki, S. and Hamana, K. (1993). "Systematic analysis of naturally occurring linear and branched polyamines by gas chromatography and gas chromatography-mass spectrometry." *J. Chromatogr.* **641**: 115-23.

Paul, W. and Steinwedel, H. (1953). "Ein neues massenspektrometer ohne Magnetfeld." *Z. Naturforschung* **8a**: 448.

Quaglino, D., Ha, H. R., Duner, E., Bruttomesso, D., Bigler, L., Follath, F., Realdi, G., Pettenazzo, A. and Baritussio, A. (2004). "Effects of metabolites and analogs of amiodarone on alveolar macrophages: structure-activity relationship." *Am. J. Physiol.-Lung Cellular Mol. Physiol.* **287**: L438-L447.

Quistad, G. B., Suwanrumpha, S., Jarema, M. A., Shapiro, M. J., Skinner, W. S., Jamieson, G. C., Lui, A. and Fu, E. W. (1990). "Structures of paralytic acylpolyamines from the spider *Agelenopsis aperta*." *Biochem. Biophys. Res. Commun.* **169**: 51-56.

Rash, L. D. and Hodgson, W. C. (2001). "Pharmacology and biochemistry of spider venoms." *Toxicon* **40**: 225-254.

Shintani, H. and Polonsky, J. (1997). *Hanbook of Capillary Electrophoresis Applications*. London, Blackie Academic & Professional.

Silverman, R. B. (2004). *The Organic Chemistry of Drug Design and Drug Action*. Amsterdam, Elsevier Academic Press.

Stephens, W. (1946). "Pulsed Mass Spectrometer with Time Dispersion." *Bull. Am. Phys. Soc.* **21**: 22.

Stobiecki, M., Skirycz, A., Kerhoas, L., Kachlicki, P., Muth, D., Einhorn, J. and Mueller-Roeber, B. (2006). "Profiling of phenolic glycosidic conjugates in leaves of Arabidopsis thaliana using LC/MS." *Metabolomics* **2**: 197-219.

Tanaka, K., Ido, Y., Akita, S., Yoshida, Y. and Yoshida, T. (1987). "Protein and Polymer Analysis up to *m/z* 100'000 by Laser Ionization Time-of-flight Mass Spectrometry." *Rapid Commun. Mass Spectrom.* **2**: 151.

Thomson, J. J. (1913). *Rays of Positive Electricity and their Application to Chemical Analysis*. London.

Vestal, M. L. (1983). "Ionization Techniques for Non-Volatile Molecules." *Mass Spectrom. Rev.* **2**: 447-480.

Villas-Bôas, S. G., Mas, S., Akesson, M., Smedsgaard, J. and Nielsen, J. (2005). "Mass spectrometry in metabolome analysis." *Mass Spectrom. Rev.* **24**: 613-646.

Wendt, B., Ha, H. R. and Hesse, M. (2002). "Synthesis of two metabolites of the antiarrythmicum amiodarone." *Helv. Chim. Acta* **85**: 2990-3001.

Wollnick, H. (1993). "Time-of-Flight Mass Analyzers." *Mass Spectom. Rev.* **12**: 89-114.

Yamashita, M. and Fenn, J. B. (1984). "Electrospray Ion Source. Another Variation on the Free-jet Theme." *J. Phys. Chem.* **88**: 4451.

Yamashita, M. and Fenn, J. B. (1984). "Negative Ion Production with the Electrospray Ion Source." *J. Phys. Chem.* **88**: 4671.

Yost, R. A. and Enke, C. G. (1978). "Selected Ion Fragmentation with a Tandem Quadrupole Mass Spectrometer." *J. Am. Chem. Soc.* **100**: 2274.

V. SPECIFIC CASE STUDIES

5.1. New linear polyamine derivatives in spider venoms

Abstract

Linear free polyamines were characterized in the venom of the spiders *Agelenopsis aperta*, *Hololena curta*, and *Paracoelotes birulai* by RP-HPLC coupled to mass spectrometry. The several linear polyamines found were tetramine, pentamine, and hexamine derivatives. Some of these natural products were identified as N-hydroxylated, guanidylated, or acetylated compounds. In addition, the biosynthetical pathway leading to the formation of acylpolyamines in spider venoms is discussed.

Introduction

Spider venoms are known to be the source of a multitude of natural products and particularly of acylpolyamines (Schäfer et al. 1994; Itagaki et al. 2000; Chesnov et al. 2002). Although many acylpolyamines with rather uncommon polyamine backbones were found in spider venoms, information about the presence of the respective free non-derivatized bases is scarce in literature. Low molecular weight biogenic amines such as the ubiquitous putrescine (PA4)[1], cadaverine (PA5), spermidine (PA34), and spermine (PA343) were characterized in the mygalomorph spiders *Scodra griseipes* (Lange et al. 1992; Lange et al. 1992), the Sydney funnel-web spider *Atrax robustus* (Duffield et al. 1979), and the species *Dugesiella hentzi*, *Aphonopelma emilia* and two further *Aphonopelma* species (Cabbiness et al. 1980). The same biogenic amines along with histamine were also reported in nine typical Japanese spider species (Hagiwara et al. 1991). Caldopentamine (PA3333) was found, in addition to the more common biogenic amines, not in the venom but in the silk glands and in the heads of the spiders *Nephila clavata* and *Araneus ventricosus* (Hamana et al. 1991). Apart from this last example, no information about spider derived, non-acylated polyamines containing more than four N-atoms is found in literature. The only natural sources for such extended polyamines, namely pentamines and hexamines, are bacteria. For example, homocaldopentamine (PA3334) (Oshima et al. 1983) and isomeric thermopentamine (PA3343) (Hamana et al. 1990) were extracted from the thermophilic eubacteria *Thermus thermophilus* and homocaldohexamine (PA33334), thermohexamine (PA33343), and homothermohexamine (PA33433) in *Bacillus schlegelii* (Hamana et al. 1992). In these cases, also branched polyamines were characterized in addition to the linear compounds. These polyamines from bacteria were identified either by gas chromatography coupled to mass spectrometry (GC-MS) after their derivatization with heptafluorobutyric anhydride (HFBA) (Niitsu et al. 1993), or by liquid chromatography (LC) and fluorescence detection of the *o*-phthalaldehyde (OPA) reaction products (Hamana et al. 1998).

---

[1] The abbreviation PA stands for polyamine; the figures designate the number of methylene in-between the several N-atoms Bienz, S., Detterbeck, R., Ensch, C., Guggisberg, A., Häusermann, U., Meisterhans, C., Wendt, B., Werner, C. and Hesse, M. (2002). "Putrescine, spermidine, spermine, and related polyamine alkaloids." *Alkaloids* **58**: 83-338..

Recently, we have used high-performance liquid chromatography, on-line coupled with atmospheric-pressure chemical ionization mass spectrometry (HPLC-UV(DAD)-APCI-MS and MS/MS), to identify the acylpolyamine toxins contained in the venom of the spiders *Paracoelotes birulai* (Amaurobiidae) (Chesnov et al. 2000) and *Agelenopsis aperta* (Agelenidae) (Chesnov et al. 2001). This instrumental setup allowed us to detect and to elucidate the structure of polyamine derivatives directly, without an additional derivatization step. For example, a total of 38 compounds were characterized in *A. aperta* (Manov et al. 2002), and it was shown that for PA3343 and PA3334 all acylpentamine isomers of the type Acyl3334[2], Acyl3343, Acyl3433, and Acyl4333 were present in the toxin mixture. On the basis of this latter finding, we postulated that the biosynthetic precursors of the acylpolyamines in spider venom might be the parent linear polyamines that are 'statistically' mono-acylated at either terminal amino group of the molecule. To support these assumptions, we searched for free polyamines in the venoms of the aforementioned spiders *P. birulai* and *A. aperta*, as well as in *Hololena curta* (Agelenidae). Due to the absence of a chromophore on such compounds, UV detection was not appropriate. Reverse-phase HPLC-APCI-MS was selected as the method of choice for the separation and detection of linear polyamines.

Experimental

Lyophilized spider venom samples from *A. aperta*, *H. curta*, and *P. birulai* were purchased from Fauna Laboratories, Ltd. (Almaty, Kazakhstan). A portion of the crude venom (~100 μg) was dissolved in MeCN/H_2O (3:2) containing 0.1% of trifluoroacetic acid (TFA) and the stock solution stored at –20°C prior to use. Chromatographic separations were performed with an Interchim Uptisphere RP C_{18} column (UP3HDO–20QS, 3 μm, 4.6x200 mm) at a flow rate of 500 μl min^{-1} gradients of MeCN/H_2O/0.1% TFA from 0 to 10% over 5 min and from 10 to 15% over 10 min. The APCI-MS and MS/MS experiments were performed on a triple quadrupole instrument (Finnigan TSQ 700), and the base peak chromatograms (BPC) were obtained by monitoring the ions with *m/z* between 100 and 1000.

[2] The different acyl groups linked to the polyamine backbones were 4-OH-Benz, 2,5-$(OH)_2$-Benz, and IndAc.

Results and Discussion

The peaks observed in the chromatograms for the venom of the three spider species were distributed over three different regions (figure 1). The first fraction, containing the linear polyamines, eluted with retention times (t_R) close to 5 min. The second fraction, eluting with t_R between 10 and 12 min, was composed of pyrimidine and purine derivatives. This class of compounds was found in the venom of the spider *Latrodectus menavodi* and will not be further discussed here (Horni et al. 2000). The third fraction, eluting with t_R between 12 and 15 min, consisted of acetyl- and guanidino-substituted linear polyamines.

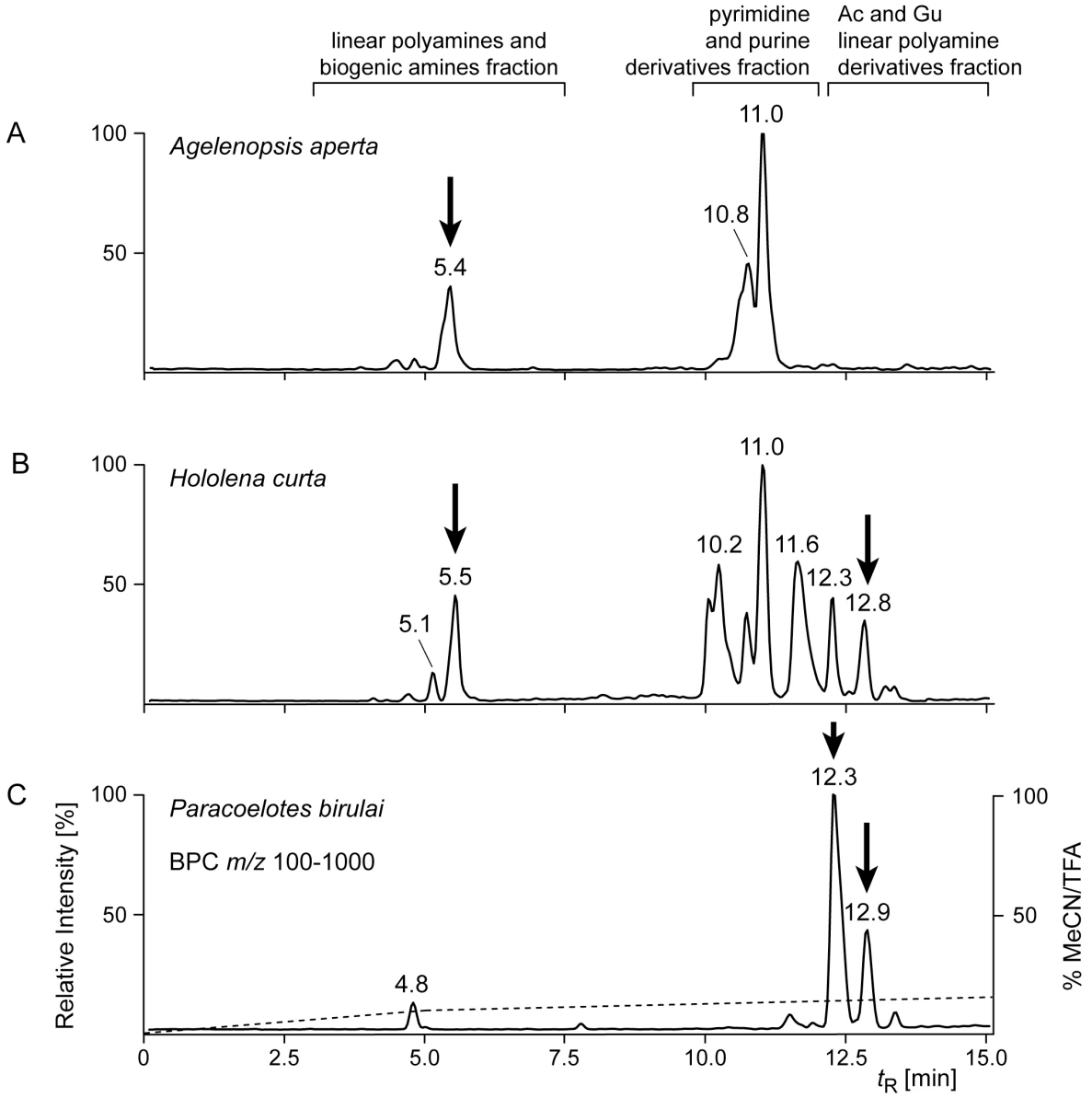

Figure 1. Reverse-phase HPLC-MS base peak chromatograms (BPC) of the venom of the spiders *A. aperta* (**A**), *H. curta* (**B**), and *P. birulai* (**C**) obtained with an Interchim UP3HDO–20QS column (4.6x200 mm, 500 µl min^{-1}) with a MeCN/H_2O/TFA gradient. An arrow indicates fractions containing linear polyamines and derivatives thereof.

The first fraction containing the polyamines is rather prominent in the venom of both Agelenidae species *A. aperta* and *H. curta*, but little abundant only in the venom of *P. birulai*. The mass spectra of the compounds co-eluting at t_R = 5.4 min in *A. aperta* (t_R = 5.5 min in the case of *H. curta*) gave rise to the quasi-molecular ions $[M + H]^+$ at *m/z* 203, 219, 260, 276, 317, and 333.

Fragmentation by MS/MS of the respective $[M + H]^+$ ions and interpretation of the resulting daughter ions allowed the elucidation of the free polyamine structures: the series of $[M + H]^+$ ions at *m/z* 203, 260, and 317 (the respective masses differing by 57 Da each) correspond to the mixtures of tetramines PA343 and PA334, the pentamines PA3343 and PA3334, and the hexamines PA33433, PA33343, and PA33334, respectively (Table 1). The structure assignments are based on the comparison of the MS/MS data of the linear polyamines with those of the parent acylpolyamine compounds.

The second series of $[M + H]^+$ ions, recorded at *m/z* 219, 276, and 333, were identified as N-hydroxylated (+16 Da) derivatives of the tetramines, pentamines, and hexamines mentioned above. However, according to their fragmentation patterns, not all of the theoretically possible isomers of the hydroxylamines are present in the venoms. The OH group was solely found to be connected to the secondary N-atoms linked to terminal aminopropyl units. The compounds characterized are PA3(OH)43 and PA3(OH)34 for $[M + H]^+$ at *m/z* 219, PA3(OH)343 and PA3(OH)334 for $[M + H]^+$ at *m/z* 276, PA3(OH)3343 and PA3(OH)3334 for $[M + H]^+$ at *m/z* 333. To our knowledge, no free N-hydroxylated linear polyamines have been isolated from a natural source before.

Concentrating on the acetyl and guanidyl derivatives, the chromatogram of the venom of *P. birulai* shows two prominent signals at t_R = 12.3 and 12.9 min. The MS of the respective fractions reveal the presence of $[M + H]^+$ ions at *m/z* 302, 318 (t_R = 12.3 min) and at *m/z* 344, 359, and 401 (t_R = 12.9 min) (figure 1C).

Table 1. Polyamines and new polyamine derivatives found in *A. aperta*, *H. curta*, and *P. birulai*.

Spider	Trivial Name[a]	t_R [min]	$[M + H]^+$ *m/z*	m	n	o	b R[1]	R[2]	R[3]	Structure
A. aperta *H. curta*	PA343	5.4-5.5	203	1	2	1	H	–	–	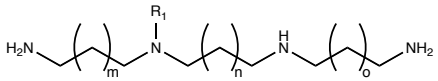
	PA334	5.4-5.5	203	1	1	2	H	–	–	
	PA4(OH)33	5.4-5.5	219	2	1	1	OH	–	–	
	PA3(OH)43	5.4-5.5	219	1	2	1	OH	–	–	
	PA3(OH)34	5.4-5.5	219	1	1	2	OH	–	–	
A. aperta *H. curta*	PA3343	5.4-5.5	260	2	1	–	H	H	H	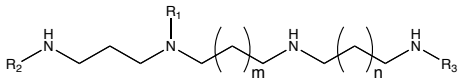
	PA3334	5.4-5.5	260	1	2	–	H	H	H	
	PA3(OH)343	5.4-5.5	276	2	1	–	OH	H	H	
	PA3(OH)334	5.4-5.5	276	1	2	–	OH	H	H	
P. birulai	PA3334Gu	12.3	302	1	2	–	H	H	Gu	
	PA3(OH)334Gu	12.3	318	1	2	–	OH	H	Gu	
	Ac3334Gu	12.9	344	1	2	–	H	Ac	Gu	
A. aperta *H. curta*	PA33433	5.4-5.5	317	2	1	1	H	H	H	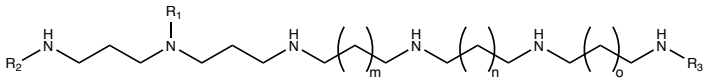
	PA33343	5.4-5.5	317	1	2	1	H	H	H	
	PA33334	5.4-5.5	317	1	1	2	H	H	H	
	PA3(OH)3343	5.4-5.5	333	1	2	1	OH	H	H	
	PA3(OH)3334	5.4-5.5	333	1	1	2	OH	H	H	
P. birulai	PA33334Gu	12.9	359	1	1	2	H	H	Gu	
	Ac33334Gu	12.9	401	1	1	2	H	Ac	Gu	
H. curta	Ac33343Ac	12.8	401	1	2	1	H	Ac	Ac	

[a]) PA stands for polyamine; the figures designate the numbers of methylene units in-between the several N-atoms.

[b]) Abbreviations for the substituents: Ac = CH_3CO; Gu = $H_2N–C=NH$.

MS/MS data of the first fraction allowed the deduction of the structures PA3334Gu[3] ($[M + H]^+$ *m/z* 302) and the N-hydroxylated derivative PA3(OH)334Gu ($[M + H]^+$ *m/z* 318); the major components of the second fraction were found to be the acetylated derivatives Ac3334Gu ($[M + H]^+$ *m/z* 344), PA33334Gu ($[M + H]^+$ *m/z* 359), and Ac33334Gu ($[M + H]^+$ *m/z* 401).The presence of the guanidyl group at the terminus of the polyamine backbone was already shown to be characteristic for toxins from *P. birulai* (Chesnov et al. 2000). *H. curta* revealed no guanidyl derivative but a bis-acetylated polyamine, Ac33343Ac ($[M + H]^+$ *m/z* 401), eluting with t_R = 12.8 min (figure 1B). Acetylated polyamines were previously isolated solely from bacteria, e.g. N^1-acetylcaldopentamine (Ac3333) from *Staphilothermus hellenicus* (Hamana et al. 2003).

Conclusion

The linear polyamines found in the three spider species are supportive for the biosynthesis previously proposed for the acylpolyamines (Manov et al. 2002). The linear polyamines arise probably from putrescine (PA4) by enzyme catalyzed repetitive addition of aminopropyl units, as described in the literature for mammalian cells (Tabor et al. 1984; Geneste et al. 1998). Once the linear polyamines are formed, they can be regiospecifically hydroxylated to the N-hydroxy derivatives. Interestingly, some bis-N-hydroxylated acylpolyamine toxins are described for *A. aperta* (Chesnov et al. 2001) although no free linear polyamine containing two N–OH moieties could be detected in the present study. Finally, the linear compounds are acylated at either end of the polyamine backbone with one of the known aromatic carboxylic acids 4-OH-BzOH, 2,5-$(OH)_2$-BzOH, 2,4-$(OH)_2$-PhAcOH, IndAcOH, 4-OH-IndAcOH, and 6-OH-IndAcOH (Schäfer et al. 1994) to yield the acylpolyamines.

As already mentioned, underivatized linear free polyamines are of low abundance in the case of *P. birulai*. All of the four compounds detected for this species possess a guanidyl end group attached to the aminobutyl portion of the polyamine backbone. However, 'regular' acylpolyamine toxins, having no guanidyl end group, are present in the venom cocktail of *P. birulai* (Chesnov et al. 2000). Elucidation of the complete biosynthetic route to acylpolyamines has yet to be confirmed, e.g. by *in-vivo* experiments.

[3] Gu designates a terminal guanidyl group instead of a primary amine.

References

Bienz, S., Detterbeck, R., Ensch, C., Guggisberg, A., Häusermann, U., Meisterhans, C., Wendt, B., Werner, C. and Hesse, M. (2002). "Putrescine, spermidine, spermine, and related polyamine alkaloids." *Alkaloids* **58**: 83-338.

Cabbiness, S. G., Gehrke, C. W., Kuo, K. C., Chan, T. K., Hall, J. E., Hudiburg, S. A. and Odell, G. V. (1980). "Polyamines in some tarantula venoms." *Toxicon* **18**: 681-683.

Chesnov, S., Bigler, L. and Hesse, M. (2000). "The spider *Paracoelotes birulai*: Detection and structure elucidation of new acylpolyamines by on-line coupled HPLC-APCI-MS and HPLC-APCI-MS/MS." *Helv. Chim. Acta* **83**: 3295-3305.

Chesnov, S., Bigler, L. and Hesse, M. (2001). "The acylpolyamines from the venom of the spider *Agelenopsis aperta*." *Helv. Chim. Acta* **84**: 2178-2197.

Chesnov, S., Bigler, L. and Hesse, M. (2002). "Detection and characterization of natural polyamines by high-performance liquid chromatography-atmospheric pressure chemical ionization (electrospray ionization) mass spectrometry." *Eur. J. Mass Spectrom.* **8**: 1-16.

Duffield, P. H., Duffield, A. M., Carroll, P. R. and Morgans, D. (1979). "Analysis of the venom of the Sydney funnel-web spider, *Atrax robustus* using gas chromatography mass spectrometry." *Biomed. Mass Spectrom.* **6**: 105-108.

Geneste, H. and Hesse, M. (1998). "Polyamines and polyamine derivatives in the nature. As manifold the functions of polyamines are in human, animals and plants, as manifold are their potential applications. In cancer therapy, as a tool in neurochemistry or as natural pesticide." *Chemie in unserer Zeit* **32**: 206-218.

Hagiwara, K. i., Tokita, A., Miwa, A., Kawai, N., Murata, Y., Uchida, A. and Nakajima, T. (1991). "Determination of biogenic amines in spider venom glands of nine typical Japanese species and chromatographic elution pattern analysis of venomous components." *Jpn. J. Sanit. Zool.* **42**: 77-84.

Hamana, K., Niitsu, M., Matsuzaki, S., Samejima, K., Igarashi, Y. and Kodama, T. (1992). "Novel linear and branched polyamines in the extremely thermophilic eubacteria *Thermoleophilum*, *Bacillus* and *Hydrogenobacter*." *Biochem. J.* **284**: 741-747.

Hamana, K., Niitsu, M., Samejima, K., Itoh, T., Hamana, H. and Shinozawa, T. (1998). "Polyamines of the thermophilic eubacteria belonging to the genera *Thermotoga*, *Thermodesulfovibrio*, *Thermoleophilum*, *Thermus*, *Rhodothermus* and *Meiothermus*, and the thermophilic archaebacteria belonging to the genera *Aeropyrum*, *Picrophilus*, *Methanobacterium* and *Methanococcus*." *Microbios* **93**: 7-21.

Hamana, K., Niitsu, M., Samejima, K. and Matsuzaki, S. (1990). "Thermopentamine, a novel linear pentaamine found in *Thermus thermophilus*." *FEMS Microbiol. Lett.* **68**: 27-30.

Hamana, K., Niitsu, M., Samejima, K. and Matsuzaki, S. (1991). "Novel polyamines in insects and spiders." *Comp. Biochem. Physiol.* **100B**: 399-402.

Hamana, K., Tanaka, T., Hosoya, R., Niitsu, M. and Itoh, T. (2003). "Cellular polyamines of the acidophilic, thermophilic and thermoacidophilic archaebacteria, *Acidilobus*, *Ferroplasma*, *Pyrobaculum*, *Pyrococcus*, *Staphylothermus*, *Thermococcus*, *Thermodiscus* and *Vulcanisaeta*." *J. Gen. Appl. Microbiol.* **49**: 287-293.

Horni, A., Weickmann, D. and Hesse, M. (2000). "The main products of the low molecular mass fraction in the venom of the spider *Latrodectus menavodi*." *Toxicon* **39**: 425-428.

Itagaki, Y. and Nakajima, T. (2000). "Acylpolyamines: mass spectrometric analytical methods for araneidae spider acylpolyamines." *J. Toxicol. Toxin Reviews* **19**: 23-52.

Lange, C., Paris, C. and Celerier, M.-L. (1992). "The components of the venom of a spider *Scodra griseipes*. 1. Analysis of low molecular weight products using gas chromatography/mass spectrometry." *Rapid Commun. Mass Spectrom.* **6**: 289-292.

Lange, C., Paris, C. and Celerier, M.-L. (1992). "The components of the venom of a spider *Scodra griseipes*. 2. Structural information on biogenic amines using tandem mass spectrometry." *Rapid Commun. Mass Spectrom.* **6**: 517-519.

Manov, N., Tzouros, M., Chesnov, S., Bigler, L. and Bienz, S. (2002). "Solid-phase synthesis of polyamine spider toxins and correlation with the natural products by HPLC-MS/MS." *Helv. Chim. Acta* **85**: 2827-2846.

Niitsu, M., Samejima, K., Matsuzaki, S. and Hamana, K. (1993). "Systematic analysis of naturally occurring linear and branched polyamines by gas chromatography and gas chromatography-mass spectrometry." *J. Chromatogr.* **641**: 115-123.

Oshima, T. and Kawahata, S. (1983). "Homocaldopentamine: a new naturally occurring pentaamine." *J. Biochem.* **93**: 1455-1456.

Schäfer, A., Benz, H., Fiedler, W., Guggisberg, A., Bienz, S. and Hesse, M. (1994). "Polyamine toxins from the venom of spiders and wasps." *Alkaloids* **45**: 1-125.

Tabor, C. W. and Tabor, H. (1984). "Polyamines." *Ann. Rev. Biochem.* **53**: 749-90.

5.2. Tandem Mass Spectrometric Investigation of Acylpolyamines of Spider Venoms and their ^{15}N-Labeled Derivatives

Abstract

The fragmentation mechanism of the acylpentamine toxins **1**-**4** found in the venom of the spider *Agelenopsis aperta* has been investigated in detail. To identify the origin of the two doublets of unexpected fragment ions at *m/z* 129/112 and *m/z* 115/98, three synthetic ^{15}N-labeled analogs **5**-**7** have been prepared and subjected to CID fragmentation on a triple quadrupole mass spectrometer. It appears that the unexpected doublet of fragment ions arises from an internal portion of the polyamine backbone after either a transaminative *Zip* reaction or a sequential fragmentation of the quasi-molecular ion. In-source CID experiments support the second alternative as more likely. The detailed knowledge of acylpentamine fragmentation mechanisms is essential for the correct characterization of isomeric compounds, particularly for co-eluting compounds within complex mixtures such as spider venoms.

Introduction

Polyamines and polyamine-containing alkaloids are widely found throughout the plant and animal kingdom (Schäfer et al. 1994; Bienz et al. 2002). Over the past decades, spider venoms, particularly those fractions containing acylpolyamine derivatives (Schäfer et al. 1994; Itagaki et al. 2000; Chesnov et al. 2002), have increasingly attracted the attention of scientists. With the advent of more sensitive and selective analytical methods — in particular of the modern mass spectrometric approaches — not only the major but also minor constituents of such trace toxin sources have become amenable to detection and structural elucidation. Recently, we demonstrated with the re-investigation of the venom of the spider *Agelenopsis aperta* (Agelenidae) that this toxin cocktail contains, in addition to the previously found 11 major acylpolyamines, 27 further minor components that evaded earlier investigations (Chesnov et al. 2001; Manov et al. 2002).

The detection and structural elucidation of these spider toxins relied particularly on the on-line coupled high-performance liquid chromatography, UV diode array detection, and atmospheric-pressure chemical ionization mass spectrometry (HPLC-UV(DAD)-APCI-MS and -MS/MS). This arrangement allowed the efficient separation and investigation of the several venom components, making most economical use of the precious sample material. The structural elucidations, however, would not have been possible if a profound knowledge of the fragmentation behavior of the parent class of compounds had not been available, especially in the case of co-eluting isomers. Although most of the toxins of *A. aperta* were disclosed on the basis of pure 'MS investigations' by comparison of fragmentation patterns observed and explained during previous investigations, five of them were only revealed by their comparison with synthetic material (Manov et al. 2002). Also in these cases, their identity could only be revealed due to the specific fragmentation behavior of the several structural isomers that could only be studied with the pure sample compounds. On the whole, the knowledge of the fragmentation patterns of polyamines and also the deeper understanding of the respective fragmentation mechanisms, proved an important prerequisite to allow efficient and definitive identification and characterization of known and new polyamine derivatives by MS methods.

In the course of our investigation of the venom of *A. aperta*, we have intensively studied the fragmentation behavior of acylpolyamines and have also discussed possible fragmentation paths and mechanisms (Chesnov et al. 2001). For some groups of isomeric

acylpentamines, however, inconsistencies with regard to expected fragmentation patterns surfaced. Fragments of the types **a** and **b** are formed upon collision induced dissociation (CID) by intramolecular nucleophilic substitutions (S_Ni) according to Scheme 1. Concentrating solely on the proposed fragmentation reaction for the 'loss of the terminal diaminopolymethylene unit, they were thought to be indicative for the identification of the terminal diamine portions of the toxins. However, the loss of these diamines as marker is only true with reservation. For instance, the toxins *IndAc4333*[1] (**1**) and *IndAc3433* (**2**) would be expected to give rise to fragments $\mathbf{a_{33}}$[2] (*m/z* 115) and $\mathbf{b_{33}}$ (*m/z* 98) and not to fragments $\mathbf{a_{43}}$/$\mathbf{a_{34}}$ (*m/z* 129) and $\mathbf{b_{43}}$ (*m/z* 112), while isomeric *IndAc3343* (**3**) and *IndAc3334* (**4**) should produce fragments $\mathbf{a_{43}}$/$\mathbf{a_{34}}$ and $\mathbf{b_{43}}$ instead, and none of the fragments $\mathbf{a_{33}}$ and $\mathbf{b_{33}}$.

Scheme 1. Mass spectral fragmentation of the terminal part of the $[M + H]^+$ ions of the *IndAc* pentamine derivatives **1**-**4**.

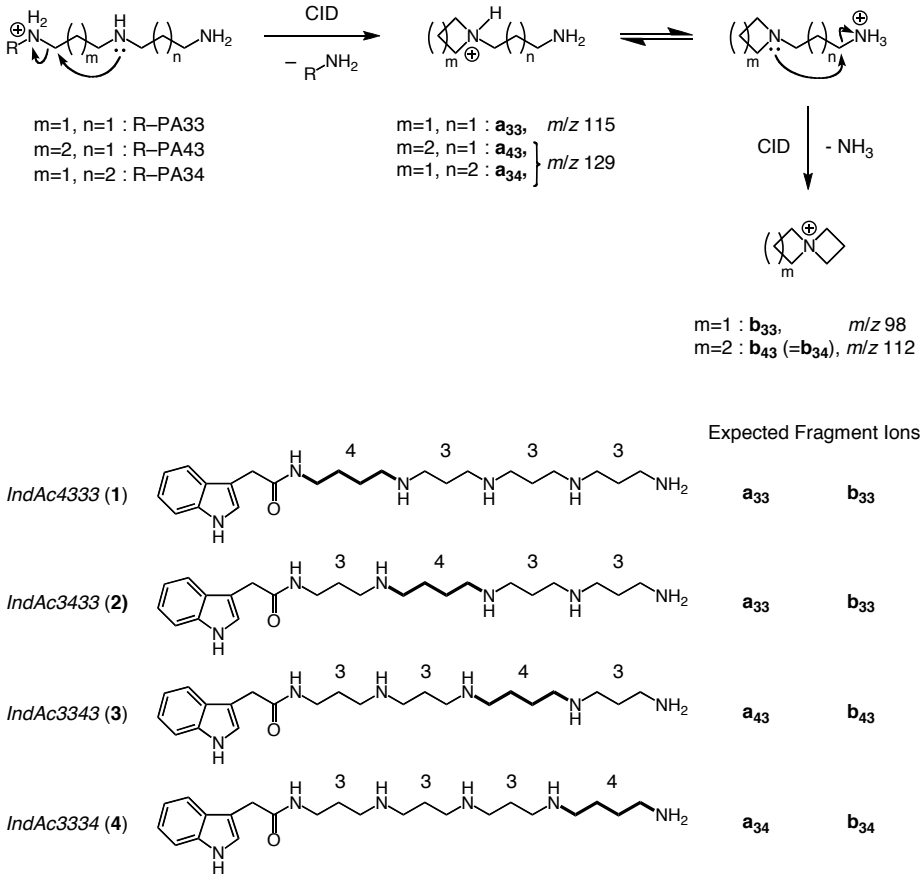

[1] The expression *IndAc4333* stands for a linear pentamine possessing 4, 3, 3, and 3 methylene units in-between the several N-atoms, whereby the *IndAc* group is located at the N-atom which is followed by the tetramethylene unit. *IndAc* is the abbreviation for 1*H*-indole-3-acetyl.

[2] The subscripts denote the number of methylene groups contained in the two chains or rings.

In reality, however, the CID spectra deriving from the two quasi-molecular ions of synthetic *IndAc4333* and *IndAc3433* showed also signals at *m/z* 129 and 112, which should be indicative for a terminal PA34 or PA43 unit[3], and in the case of *IndAc3334* (but not of *IndAc3343*!), signals at *m/z* 115 and 98 were additionally found, which would imply a PA33 end-portion for the molecule (figure 1).

The feature of exhibiting unexpected signals of such types is not specific to pentamines bearing the *IndAc* moiety; it is also characteristic for other pentamine derivatives that bear, *e.g.*, a 4-hydroxybenzoic or a 2,5-dihydroxybenzoic group in place of *IndAc*.

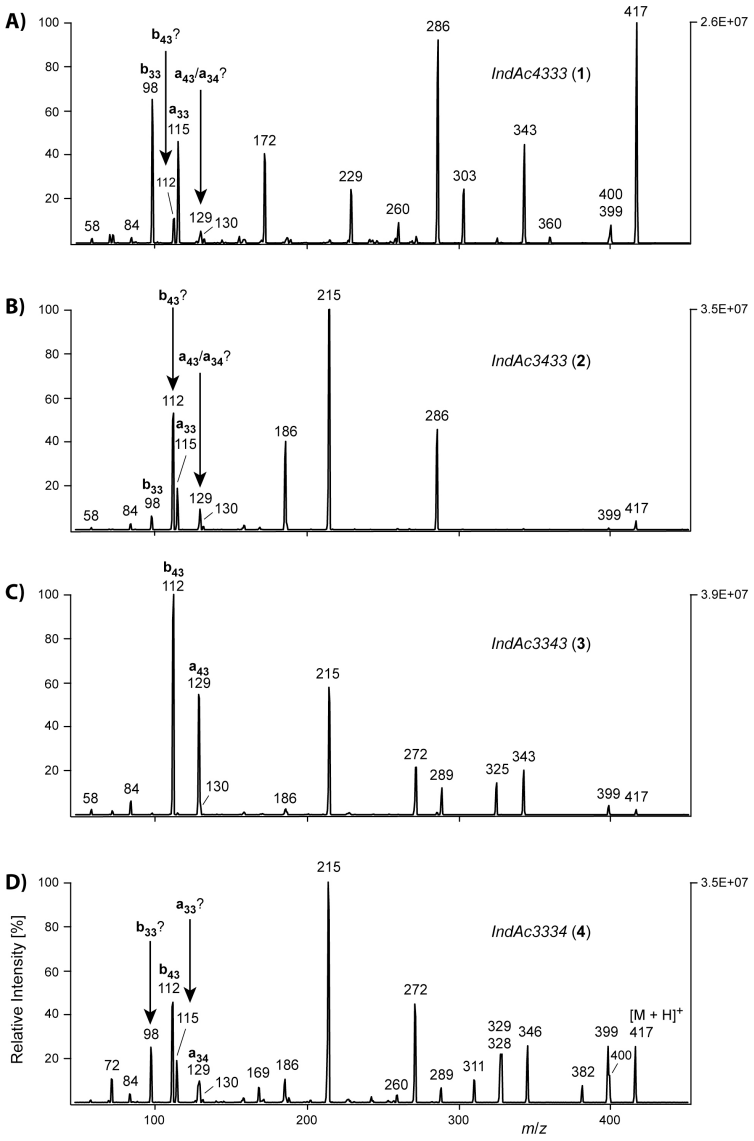

Figure 1. ESI-MS/MS of the $[M + H]^+$ ion at *m/z* 417 of (**A**) *IndAc3334* (**1**), (**B**) *IndAc3343* (**2**), (**C**) *IndAc3433* (**3**), and (**D**) *IndAc4333* (**4**). Unexpected fragment ions are indicated by an arrow.

[3] PA34 stands for a linear triamine with 3 and 4 methylene units (in this succession) in-between the terminal and internal N-atoms (Bienz et al. 2002). The nomenclature is also used for more extended polyamines.

As an explanation for the peculiar MS behavior of the acylpentamines, we offer two plausible reaction paths involving an acid promoted transamidative (A) or transaminative (B) *Zip* reaction (Kramer et al. 1977), as outlined in Scheme 2 in the case of *IndAc3334* (**4**). For both transformations, precedence is available in the MS literature: transamidation reactions were discussed with respect to the MS behavior of 4-hydroxycinnamoyl spermidines (Hu et al. 1996) as well as *N*,*N*'-bis(4-hydroxycinnamoyl) spermidines (Bigler et al. 1996), and transamination reactions were considered for polypropylenamine dendrimers (De Maaijer-Gielbert et al. 1999) and for monoimidazole polyamine conjugates (Zhu et al. 2002). The presence of the signal doublet at *m/z* 129/112 in the CID of *IndAc4333* would rather support the transamidative pathway A, whereas the lack of signals at *m/z* 115/98 for *IndAc3343* would suggest pathway B proceeding through transaminations.

Scheme 2. Possible gas phase rearrangements of the $[M + H]^+$ ions of *IndAc3334* (**4**).

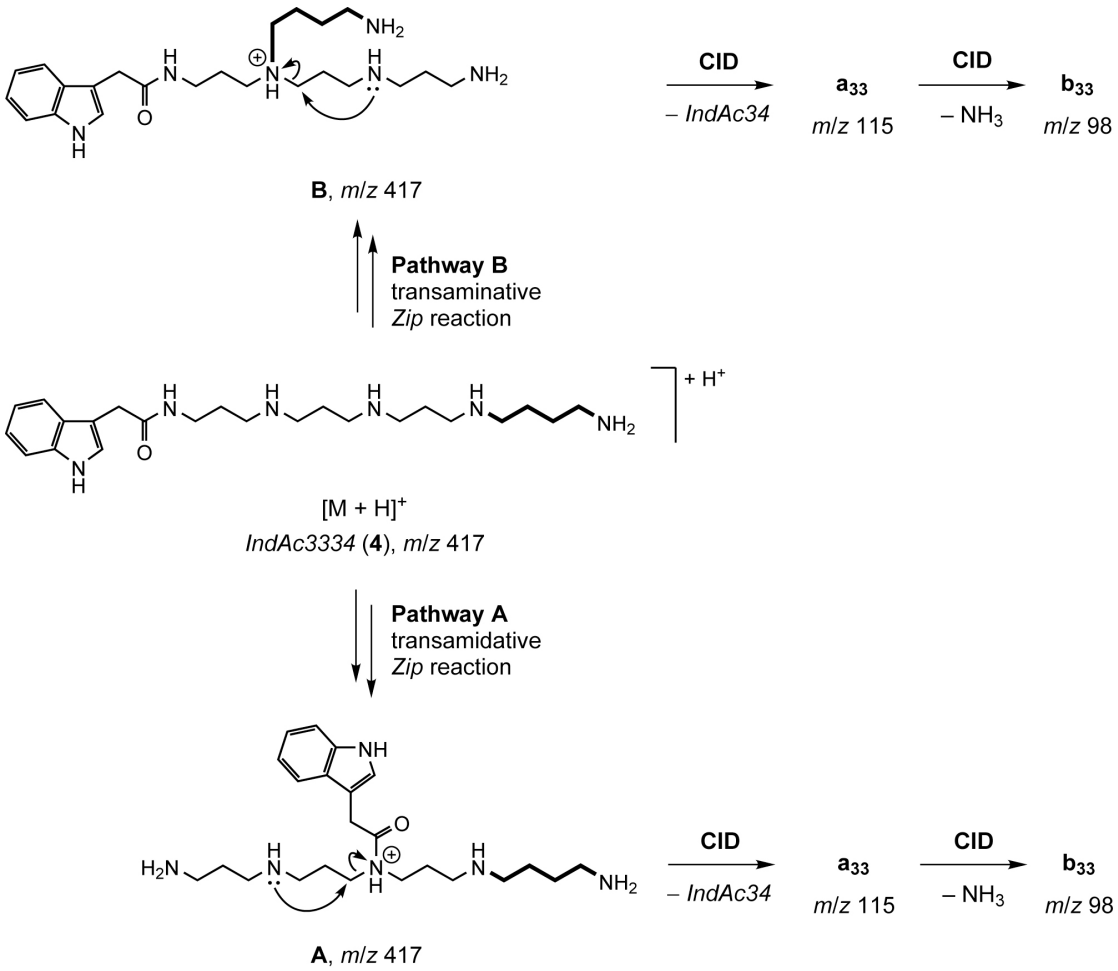

To distinguish between these two paths, we have synthesized the three ^{15}N-containing *IndAc3334* derivatives *IndAc^{15}N3334* (**5**), *IndAc3^{15}N334* (**6**), and *IndAc33^{15}N34* (**7**) (Manov et al.) (figure 2). The three labeled isomers were then analyzed by ESI-MS/MS, analogously to the unlabeled parent compound. The results of this MS investigation are presented below.

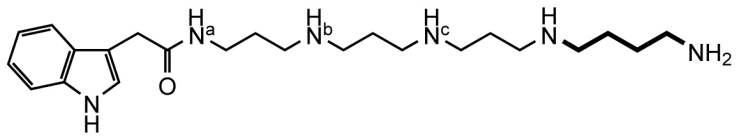

N^a = ^{15}N : *IndAc^{15}N3334* (**5**), $[M + H]^+$ *m/z* 418
N^b = ^{15}N : *IndAc3^{15}N334* (**6**)
N^c = ^{15}N : *IndAc33^{15}N34* (**7**)

Figure 2. Investigated ^{15}N-labeled *IndAc3334* derivatives **5**-**7**.

Experimental

Material

All ^{15}N-labeled acylpolyamine samples used were synthesized in our laboratory (Manov et al. 2004). For ESI-MS, all compounds were dissolved in a 1:1 mixture of HPLC grade MeOH (Scharlau, Barcelona, Spain) and H_2O (purified with a Milli-Q_{RG} apparatus, Millipore, Milford, MA) at a concentration of 50 nmol ml^{-1}.

Mass Spectrometry

ESI tandem mass spectra were recorded with a TSQ 700 triple quadrupole mass spectrometer (Finnigan MAT, San Jose, CA) equipped with a combined Atmospheric Pressure Ion (API) source. Samples were continuously introduced into the source with a

Syringe Pump 22 (Harvard Apparatus, Holliston, MA) at a flow rate of 5 μl min^{-1}. The ESI operating conditions in positive mode were: capillary voltage 4500 V; heated capillary temperature 210°C; sheath gas N_2 with an inlet pressure of 30 psi; electron multiplier: 1000 V; conversion dynode: –15 kV; resolution: 0.7 Da at half peak height; scan rate: 900 Da s^{-1}; 16 scans were averaged. For the CID experiments, Ar was used as the collision gas with a relative pressure of 2.5–3.3 mtorr. The collision-induced dissociation offset (Coff) was set to –27 V and the electron multiplier was set to 1500 V. In-source CID spectrum was obtained by setting the octopole voltage at –3 V, and fragment ions were further subjected to CID by setting the Coff voltage at –22 V.

Results and Discussion

The ESI-MS/MS of the three labeled compounds **5**–**7** and of the unlabeled parent compound **4** — all obtained under the same conditions from the respective $[M + H]^+$ parent ions — are shown in figure 3. Concentrating on the signals of type **a** and **b**, it is readily recognized that the signals for the respective fragment ions $\mathbf{a_{34}}$/$\mathbf{b_{43}}$[4] at *m/z* 129/112 remained unaffected for all the ^{15}N-containing compounds. However, the signals for the $\mathbf{a_{33}}$/$\mathbf{b_{33}}$ ions were recorded only for *IndAc*^{15}*N3334* (**5**) and *IndAc3*^{15}*N334* (**6**) at *m/z* 115/98. For *IndAc33*^{15}*N34* (**7**) the masses were higher by 1 Da (*m/z* 116/99) and consequently designated as ^{15}N-$\mathbf{a_{33}}$ and ^{15}N-$\mathbf{b_{33}}$ respectively.

[4] The fragment ion at *m/z* 130 has been previously described as 3-methylene-3*H*-indolium ($C_9H_8N^+$) (Chesnov et al. 2001) and is not considered as labeled ^{15}N-$\mathbf{a_{43}}$/$\mathbf{a_{34}}$.

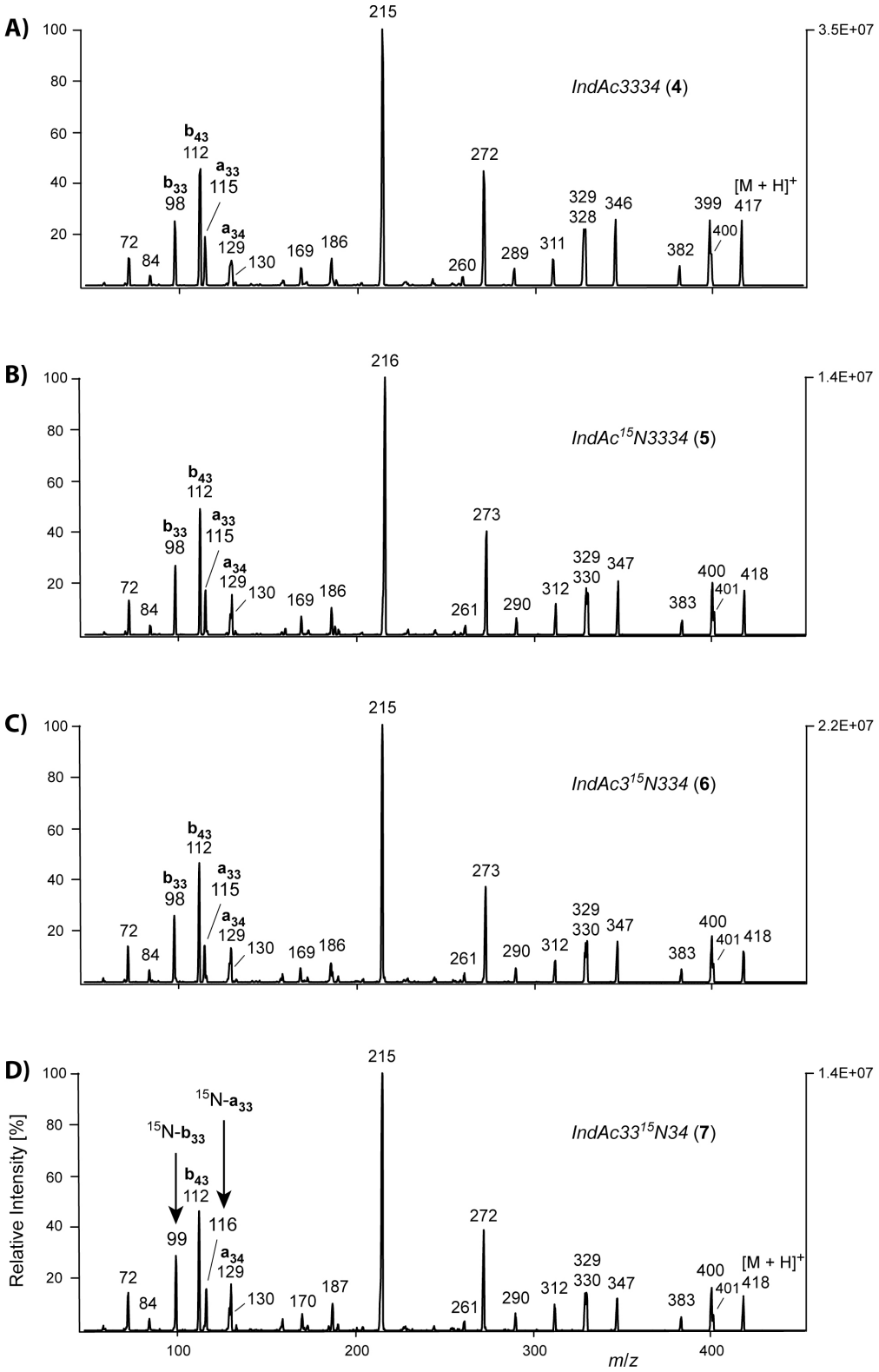

Figure 3. ESI-MS/MS of the $[M + H]^+$ ions at *m/z* 417 of (**a**) *IndAc4333* (**4**), and at *m/z* 418 of labeled (**b**) *IndAc*^{15}*N3334* (**5**), (**c**) *IndAc3*^{15}*N334* (**6**), and (**d**) *IndAc33*^{15}*N34* (**7**). ^{15}N-label containing **a** and **b** fragment ions are indicated by an arrow.

These results unambiguously show that the central portion of the polyamine moiety (as indicated by the surrounded part of the compound in figure 4) is incorporated in the fragments **a_{33}/b_{33}** deriving from **4.** Therefore, the transamidative pathway A for the formation of these fragments is certainly not operative and can be excluded. Otherwise, doublets for labeled fragments **a_{33}/b_{33}** at *m/z* 116/98 or 116/99 should have been found for isomers **5** and **6**, respectively. On the other hand, the doublet of signals at *m/z* 116/99 for the ^{15}N-containing fragments **a_{33}/b_{33}** deriving from isomer **7** is supportive for the transaminative pathway B.

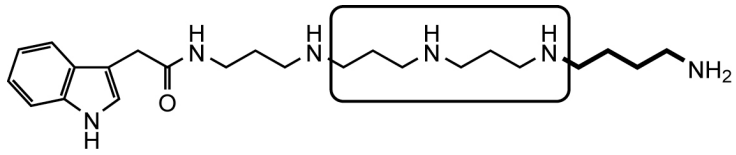

Figure 4. Portion of the polyamine backbone of *IndAc3334* responsible for the formation of the fragment ions **a_{33}/b_{33}** at *m/z* 115/98.

An alternative fragmentation path that was not seriously considered initially, but is also consistent with the experimental data, is the sequential fragmentation of acylpolyamines involving loss of a terminal aminoalkyl group in a first stage, forming e.g. for *IndAc3334* the ion [*IndAc333* + H]$^+$. Such a secondary parent ion could subsequently be fragmented according to the general rules (Scheme 3), and lead to fragments **a_{33}** and **b_{33}**. These fragment ions consist of the same portions of the parent molecule as those explained with the transamination/fragmentation pathway. However, if *IndAc3334* dissociates by the usual S_Ni reaction by attack of the terminal amino group at the CH_2 group in α-position to the protonated secondary N-atom, protonated pyrrolidine (see fragment ions at *m/z* 72 in figure 3) and neutral *IndAc333* is formed. Thus, the observed [*IndAc33^{15}N3* + H]$^+$ at *m/z* 347 from *IndAc33^{15}N34* (**7**) cannot directly derive from this S_Ni reaction. In order to retain the charge on the *IndAc*-end, a proton transfer process has to be operative. It is possible that a proton-bound complex is formed during fragmentation, where the *IndAc333*-unit and pyrrolidine compete for the H^+. This mechanism was postulated to explain the formation of the b_n/y_n ion series in the case of peptide fragmentation (Polce et al. 2000).

Scheme 3. Sequential mass spectral fragmentation of the $[M + H]^+$ ions of *IndAc33*^{15}*N34* (**7**).

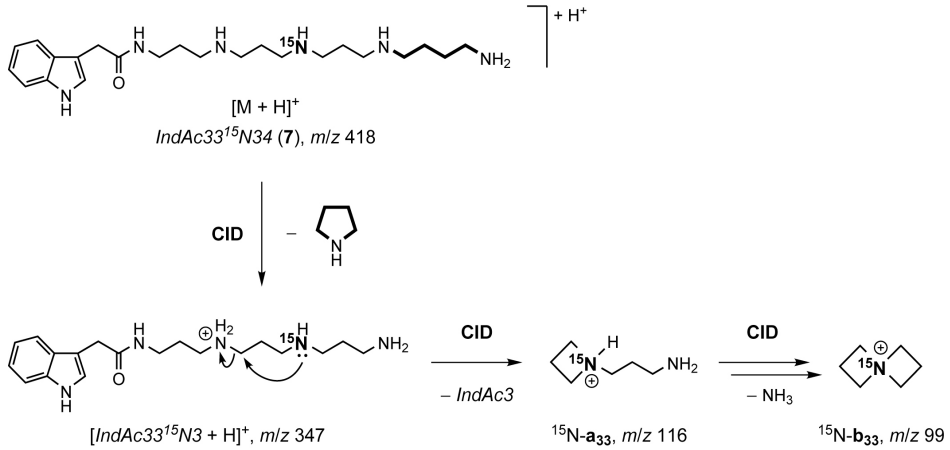

Support for the sequential fragmentation of **4**–**7** is found with the signals at *m/z* 346 and 347, corresponding to the proposed ions [*IndAc333* + H]$^+$ (figure 3). That these ions are formed rather easily is also demonstrated with the in-source CID experiment, which involves very mild energy transfer and thus very mild fragmentation conditions, performed with *IndAc33*^{15}*N34* (**7**) (figure 5). By in-source CID, almost exclusively the respective ions [*IndAc33*^{15}*N3* + H]$^+$ registered at *m/z* 347 were formed. These ions, selected by the first quadrupole and subjected to the usual CID by collision with Ar in the collision cell, gave rise to a spectrum that exhibited, not surprisingly, signals at *m/z* 116 and 99 for the ^{15}N-labeled fragments of type $\mathbf{a_{33}}$ and $\mathbf{b_{33}}$.

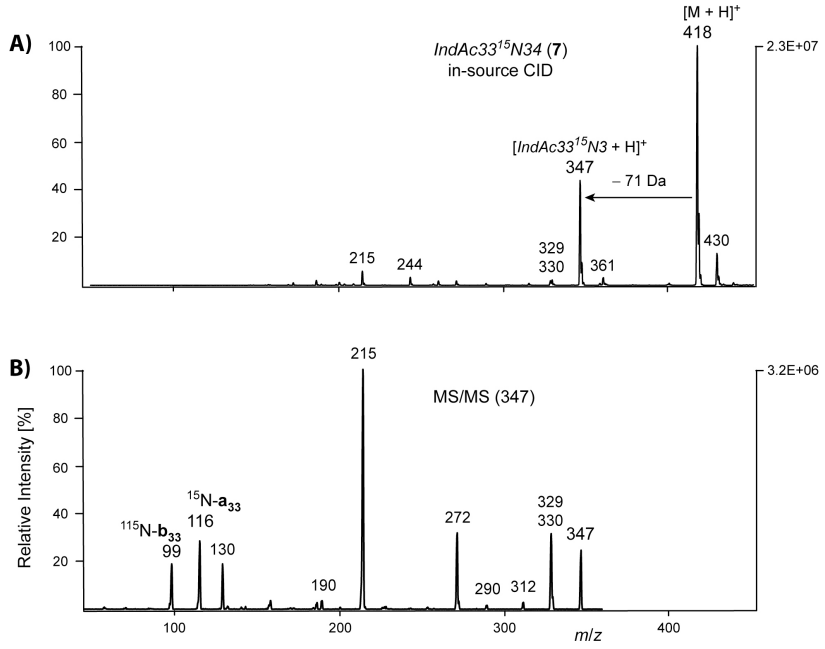

Figure 5. In-source CID of the $[M + H]^+$ ion at *m/z* 418 of labeled (**a**) *IndAc33*^{15}*N34* (**7**), and (**b**) MS/MS of the secondary parent [*IndAc33*^{15}*N3* + H]$^+$ ion at *m/z* 347.

Based on the experimental data acquired by the above experiments, both mechanisms — decomposition of [*IndAc3334* + H]$^+$ through transamination/fragmentation (pathway B) or by sequential fragmentation *via* intermediary [*IndAc333* + H]$^+$-ions — are feasible to explain to the formation of fragments $\mathbf{a_{34}}$/$\mathbf{b_{34}}$ detected at *m/z* 129/115 in the ESI-MS/MS of compound **4**. The fact that [*IndAc333* + H]$^+$ is formed quite easily by in-source CID and that this ion is also detected in the regular CID spectra talks in favor of the sequential fragmentation path.

The behaviors of *IndAc3433* (**2**) and *IndAc3343* (**3**) are consistent with the two fragmentation paths discussed above as well. In the case of *IndAc3433* (**2**), both loss of azetidine or transamination would form intermediates that could give rise to fragments $\mathbf{a_{43}}$ and $\mathbf{b_{43}}$ and thus to the observed signals at *m/z* 129/112 (see figure 1B). In this case, the signal for the secondary parent ion [*IndAc343* + H]$^+$ (*m/z* 360) proposed for the stepwise pathway is not found in the spectrum, which is possibly due to the fact that this ion should decompose immediately after its formation to fragment $\mathbf{a_{43}}$ — and subsequently $\mathbf{b_{43}}$ — through a favored five-membered transition structure as described above. For *IndAc3343* (**3**), the doublet at *m/z* 129/112 can be the response to the fragments $\mathbf{a_{43}}$/$\mathbf{a_{34}}$ and $\mathbf{b_{34}}$ deriving either by direct substitutive fragmentation or by the more complex pathways discussed above (see figure 1C). A doublet at *m/z* 115/98 for $\mathbf{a_{33}}$ and $\mathbf{b_{33}}$ is not observed for this compound, however, because [*IndAc33* + H]$^+$ (*m/z* 289), obtained by loss of terminal diaminoalkyl group, cannot undergo fragmentation to these ions similarly to a free triamine.

In the case of *IndAc4333* (**1**), the explanation for the formation of the ions of type $\mathbf{a_{43}}$/$\mathbf{a_{34}}$ and $\mathbf{b_{43}}$ (see figure 1A) is slightly different: loss of any portion of the molecule from the amino terminus of the compound and also transaminations would never lead to an intermediary species that could form these fragments. However, loss of the acyl group and liberation of the protonated polyamine itself seems to be a favorable CID-reaction for *Acyl4* derivatives (Manov et al. 2002). The respective signal for [PA4333 + H]$^+$ is in fact found at *m/z* 260 in the ESI-MS/MS of *IndAc4333* (**1**), and decomposition of the free polyamine can give rise to the fragments $\mathbf{a_{43}}$/$\mathbf{a_{34}}$ and $\mathbf{b_{43}}$. The corresponding [PA4333 +

$H]^+$ and $[PA3433 + H]^+$ signals for compounds **2**–**4** are of low abundance only or not observed at all (see figure 1A-D).

For *Acyl3* derivatives, the alternative formation of 4*H*-5,6-dihydro-1,3-oxazine species, represented in the spectra by the strong signals at *m/z* 215, is the dominant reaction of the head portion (Manov et al. 2002).

Conclusion

We have shown that acylpolyamines can form some fragments in ESI-MS/MS that are composed of internal portions of the polyamine moieties of the sample molecules. From a mechanistic point of view, a fragmentation path involving a transamidation was excluded. Two alternative mechanisms — by transamination followed by fragmentation, or by two subsequent fragmentations — are possible and cannot be distinguished. Signals of such fragments could lead to misinterpretations if they were regarded to be derived from the end-portion of the compounds. Thus, for the definite characterization and structural identification of acylpolyamines — particularly those natural products of low abundance that lack synthetic references —, such fragments are of little relevance. Of more relevance is the overall fragmentation pattern of the samples, which is dominated by the presence and location of 1,4-diaminobutane subunits. Such subunits allow some specific and predominant fragmentation reactions, occurring *via* five-membered transition structures. To deduce a specific sample structure on the basis of MS behavior, it is consequently necessary to judge the overall behavior of the considered compounds. In certain cases, the structural deduction might even not be feasible directly without the possibility to compare the sample compound with authentic samples.

References

Bienz, S., Detterbeck, R., Ensch, C., Guggisberg, A., Häusermann, U., Meisterhans, C., Wendt, B., Werner, C. and Hesse, M. (2002). "Putrescine, Spermidine, Spermine, and Related Polyamine Alkaloids." *Alkaloids* **58**: 83-338.

Bigler, L., Schnider, C. F., Hu, W. and Hesse, M. (1996). "Electrospray-Ionization Mass Spectrometry. Part 3. Acid-Catalyzed Isomerization of *N*,*N*′-bis[(*E*)-3-(4-Hydroxyphenyl)prop-2-enoyl]spermidines by the *Zip* Reaction." *Helv. Chim. Acta* **79**: 2152-2163.

Chesnov, S., Bigler, L. and Hesse, M. (2001). "The Acylpolyamines from the Venom of the Spider *Agelenopsis aperta*." *Helv. Chim. Acta* **84**: 2178-2197.

Chesnov, S., Bigler, L. and Hesse, M. (2002). "Detection and Characterization of Natural Polyamines by High-Performance Liquid Chromatography-Atmospheric Pressure Chemical Ionization (Electrospray Ionization) Mass Spectrometry." *Eur. J. Mass Spectrom.* **8**: 1-16.

De Maaijer-Gielbert, J., Gu, C., Somogyi, A., Wysocki, V. H., Kistemaker, P. G. and Weeding, T. L. (1999). "Surface-Induced Dissociation of Singly and Multiply Protonated Polypropylenamine Dendrimers." *J. Am. Soc. Mass Spectrom.* **10**: 414-422.

Hu, W., Reder, E. and Hesse, M. (1996). "Neighboring-Group Participation in the Mass-Spectral Decomposition of 4-Hydroxycinnamoyl-Spermidines." *Helv. Chim. Acta* **79**: 2137-2151.

Itagaki, Y. and Nakajima, T. (2000). "Acylpolyamines: Mass Spectrometric Analytical Methods for Araneidae Spider Acylpolyamines." *J. Toxicol. Toxin Reviews* **19**: 23-52.

Kramer, U., Guggisberg, A., Hesse, M. and Schmid, H. (1977). "Transamidation Reactions. 2. The "Zip"-reaction: A New Method for Ring Enlargement; Synthesis of 17- and 21-membered Polyaminolactams." *Angew. Chem.* **89**: 899-900.

Manov, N., Tzouros, M., Bigler, L. and Bienz, S. (2004). "Solid-Phase Synthesis of ^{15}N-Labeled Acylpentamines as Reference Compounds for MS/MS Investigation of Spider Toxins." *Tetrahedron* **60**: 2387-2391.

Manov, N., Tzouros, M., Chesnov, S., Bigler, L. and Bienz, S. (2002). "Solid-Phase Synthesis of Polyamine Spider Toxins and Correlation with the Natural Products by HPLC-MS/MS." *Helv. Chim. Acta* **85**: 2827-2846.

Polce, M. J., Ren, D. and Wesdemiotis, C. (2000). "Dissociation of the peptide bond in protonated peptides." *J. Mass Spectrom.* **35**: 1391-1398.

Schäfer, A., Benz, H., Fiedler, W., Guggisberg, A., Bienz, S. and Hesse, M. (1994). "Polyamine Toxins from the Venom of Spiders and Wasps." *Alkaloids* **45**: 1-125.

Zhu, C., Jiang, Y., Yang, X. and Zhao, Y. (2002). "Electrospray Ionization Mass Spectra of Monoimidazole/Polyamine Conjugates." *Rapid Commun. Mass Spectrom.* **16**: 2273-2277.

5.3. Pharmacokinetics of Taurolidine following Repetitive Intravenous Infusions Measured by HPLC-MS/MS of the Derivatives Taurultame and Taurinamide in Glioblastoma Patients

Abstract

Background: Taurolidine has a known antimicrobial activity. Furthermore, at lower concentrations, it has been found to exert a selective anti-neoplastic effect in vitro and in vivo. The aim of this study was to investigate the pharmacokinetics of taurolidine in vivo following repetitive intravenous infusion in a schedule used for the treatment of glioblastoma. As a prerequisite the pharmacokinetics of taurolidine in human blood plasma and whole blood in vitro was investigated.

Patients and Methods: The pharmacokinetics of taurolidine and its derivatives taurultame and taurinamide was investigated in human blood plasma and in whole blood in vitro using blood of a healthy male volunteer. During repetitive intravenous infusion therapy with taurolidine, plasma samples were taken every hour for a period of 13 hours per day in seven patients (3 male, 4 female, mean age: 48.4 ± 12.8 years, range: 27-66 years) with a glioblastoma. The concentrations of taurultame and taurinamide were determined using a

new method based on high-performance-liquid-chromatography (HPLC) online coupled to electrospray ionization tandem mass spectrometry (HPLC-ESI-MS/MS). The taurolidine concentration was below the level of detection due to rapid conversion, and was back-calculated from the taurultame and taurinamide values. After dansyl derivatization, the samples were analyzed by HPLC-ESI-MS/MS in the "multiple reaction monitoring" mode.

Results: The new HPLC-ESI-MS/MS method demonstrated a high accuracy and reproducibility. In blood plasma in vitro, concentrations of taurultame and taurinamide remained constant over the incubation period. In whole blood in vitro, a time-dependent formation of taurinamide was observed. At the start of the incubation, the taurultame-taurinamide-ratio was 0.95 at an initial taurolidine concentration of 50 µg/mL, and 1.69 at 100 µg/mL. The concentration of taurultame decreased at the same rate as the taurinamide concentration increased, showing a logarithmic kinetics. The calculated taurolidine concentration remained largely constant over the 6 hour incubation period. During repetitive infusions in patients, calculated serum concentrations of taurolidine showed a strong increase after the start of each infusion and continued to increase until the end of infusion, followed by a rapid decline. The taurultame-taurinamide-ratio was found to fluctuate between 0.1 and 0.3 depending on the relation to the previous or next infusion. The volume of distribution was markedly higher for taurolidine, taurultame and taurinamide than the plasma volume.

Discussion and conclusions: Taurolidine displayed a stable pattern of derivatives in blood plasma in vitro, whereas in whole blood a time- and concentration-dependent conversion was apparent. In patients, the calculated average taurolidine plasma concentration, achieved with the repetitive infusion regimen, was in the anti-neoplastic effective concentration range. The tissue concentrations of taurolidine and taurultame are expected to be higher than the plasma concentrations, taking into account the calculated volumes of distribution. Repetitive infusion of taurolidine is the therapeutically adequate mode of administration for the indication of glioblastoma multiforme.

Background

The synthetic agent taurolidine (bis-(1,1-dioxoperhydro-1,2,4-thiadiazinyl-4)methane) (Taurolin®,Geistlich Pharma, Wolhusen, Switzerland), a derivative of the non-essential aminoethyl-sulfonic acid taurine, has a known anti-microbial (Browne et al. 1977; Browne et al. 1978; Moser et al. 1978; Marti et al. 1980; Browne 1981; Knight et al. 1983; Wesch et al. 1983; McCartney et al. 1988; Bieselt 1997; Jurewitsch et al. 1998) and anti-endotoxin (Blenkharn 1987; Bedrosian et al. 1991; Watson et al. 1995) activity. Furthermore, taurolidine has been found to reduce the severity of peritoneal adhesions following abdominal surgery (Leaper 1985; Treutner et al. 1995). To exploit these effects, taurolidine was given systemically as an adjunct to treat severe infections and has been administered locally to prevent catheter infection (Jurewitsch et al. 2005), to treat pleural empyema (Bieselt 1997), to reduce postoperative adhesions (Leaper 1985) and to treat peritonitis (Browne et al. 1978; Moser et al. 1978; Blenkharn 1987).

Recently, a taurolidine dose far below the anti-microbial effective has been found to exert a direct and selective anti-neoplastic effect on tumor cells derived from the brain (Calabresi et al. 2001; Stendel et al. 2001; Stendel et al. 2002; Stendel et al. 2002; Rodak et al. 2005) and gastrointestinal tract (Calabresi et al. 2001). This anti-neoplastic effect was based the induction of mostly caspase-independent programmed cell death by the synergism with Fas-ligand (Stendel et al. 2003), the generation of reactive oxygen species (Rodak et al. 2005) concomitant with a change in mitochondrial membrane potential and the release of AIF (apoptosis-inducing factor) and the suppression of VEGF (vascular-endothelial-growth-factor) (Rodak et al. 2005). Furthermore, taurolidine exhibits anti-neoplastic activity in patients with glioblastoma (Stendel et al. 2004; Stendel et al. 2004) and other tumors (McCourt et al. 2000). For glioblastoma treatment, taurolidine has been administered by repetitive infusions (four infusions a day lasting for 2 hours each with an interval of 1 hour) (Stendel et al. 2002; Stendel et al. 2004).

In aqueous solution, taurolidine forms an equilibrium with taurultame and N-hydroxymethyl-taurultame (figure 1) with taurinamide being a downstream derivative (Knight et al. 1981; Erb et al. 1983; Waser et al. 1985). This equilibrium has been reported to bee mainly on the site of taurultame and N-hydroxymethyl-taurultame so that taurolidine is estimated to exist in very low concentrations in aqueous solution (Erb et al. 1982). Using pre-column derivatization and HPLC with fluorescence detection (Woolfson et al. 1989), a conversion of taurolidine with subsequent formation of taurinamide has been described following incubation of taurolidine in plasma (Jones et al. 1990). In order to substantiate these early findings and extend them to whole blood, experiments were carried out on the formation of the taurolidine derivatives in vitro using a newly developed quantification method. The knowledge of the pharmacokinetic behavior of taurolidine, taurultame and taurinamide following repetitive intravenous administration in humans is very limited (Vankemmel et al. 1982; Erb et al. 1983). Therefore the aim of the present study was to investigate the pharmacokinetics of taurolidine, taurultame and taurinamide in plasma and whole blood in vitro as well as in vivo following repetitive intravenous infusion in glioblastoma patients. For these analyses a new, highly sensitive quantification method was developed based on the combination of HPLC and tandem mass spectrometry (HPLC-ESI-MS/MS).

Scheme 1. Simplified representation of the formation of the derivatives of taurolidine.

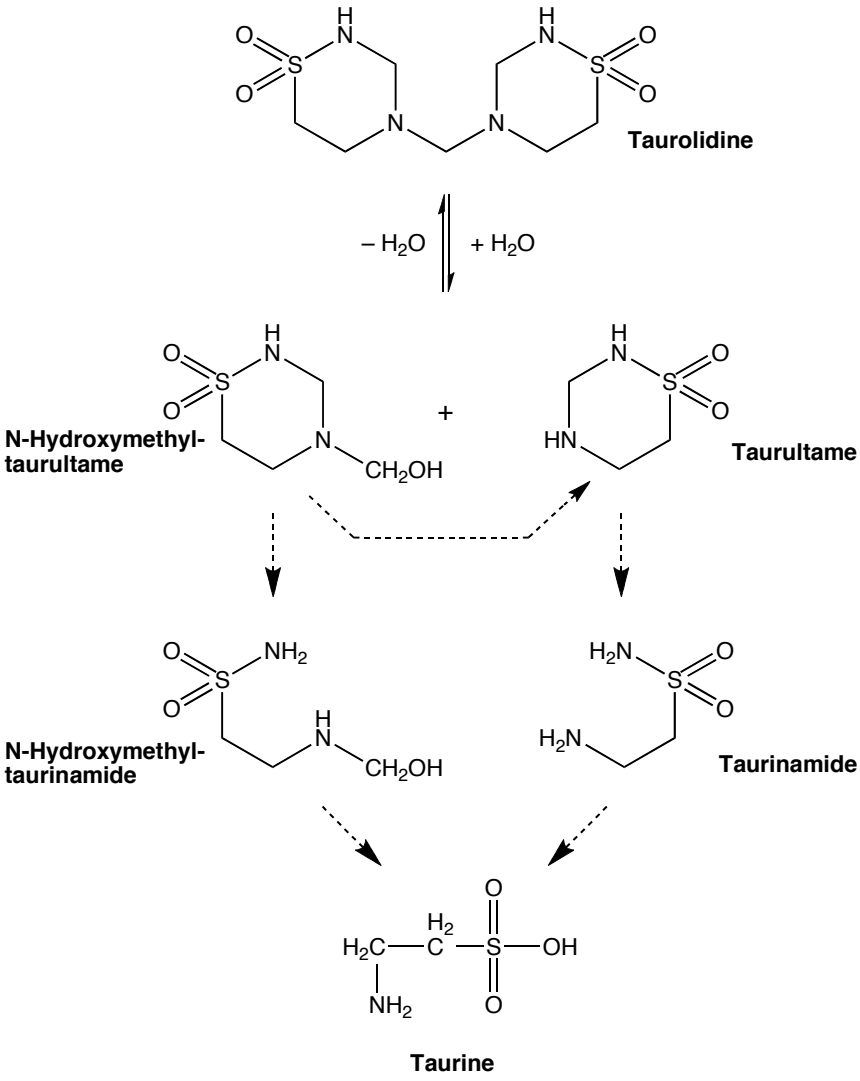

Patients and Methods

Patients

The pharmacokinetics of taurolidine in whole blood and plasma in vitro was investigated using blood of a healthy male volunteer (R.S.).

Plasma samples were drawn from 7 patients (3 male, 4 female, mean age: 48.4 ± 12.8 years, range: 27-66 years) with a glioblastoma. The patients received 4 daily infusions of a

2% taurolidine solution (provided by Geistlich Pharma AG, 6110 Wolhusen, Switzerland) with a volume of 250 mL, each administered over two hours with one hour interval between infusions (Stendel et al. 2004). The total daily dose was 20 g taurolidine. The investigations were performed as part of a study approved by the institutional ethics committee. All patients gave written consent to blood sampling and analysis. In 3 patients on two different days with one week interval and the arithmetic means of the corresponding values were used for the calculations. In 4 patients, samples were drawn on one therapy day only since the patients refused further taking of blood samples. The same dosing schedule regimen was used in all patients.

The renal and liver function was within normal limits in all patients at baseline conditions: AST (aspartate amino transferase): 18.6 ± 9.2 U/l, range: 8.0–33 U/l; ALT (alanine amino transferase): 25.0 ± 10.1, range: 13–40 U/l; GGT (gamma glutamyl transferase): 25.7 ± 10.7 U/l; 14–35 U/l; total protein: 65.0 ± 3.61 g/l, range: 60.0–70.0 g/l; creatinine: 80.4 ± 16.4 µmol/l, range: 57.0–98.0 µmol/l; urea: 4.9 ± 1.8 mmol/l, range: 2.9–6.0 mmol/l. Altogether, the following drugs were used as concomitant treatment: phenytoin, lamotrigine, clonazepam, valproic acid, diazepam, gabapentine, oxacarbazepine, captopril, metoprolol, ranitidine, pantoprazole, sertraline, dexamethasone. Five patients have received enzyme inducing anti-epileptic drugs (phenytoin, oxacarbazepine, clonazepam, diazepam, valproic acid), whereas two had not. There were no statistically significant differences of the plasma concentrations of taurultame and taurinamide between these two groups (t-test; $p>0.05$).

Methods

Determination of taurultame and taurinamide and calculation of taurolidine concentration

Taurolidine as well as taurultame were not stable under electrospray-ionization-mass spectrometry (ESI-MS) conditions (H_2O/CH_3CN + 0.05% HCOOH). Therefore, a new sensitive method for the quantification of taurultame and taurinamide has been developed. After dansyl derivatization according to Knight et al. (Knight et al. 1981), the samples were analyzed by HPLC-ESI-MS/MS in the "multiple reaction monitoring" (MRM) mode. This selective and sensitive approach allowed the calculation of taurolidine concentrations from the taurultame and taurinamide values in one run.

The concentrations of taurolidine were calculated as the sum of the taurultame quantification and the taurinamide using the following equation: Taurolidine concentration was calculated using the values of taurultame and taurinamide determined and the following equation:

$$C_{TAU} = C_{TTM} \cdot \frac{MW_{TAU}}{2 \cdot MW_{TTM}} + C_{TAA} \frac{MW_{TAU}}{2 \cdot MW_{TAA}}$$

where C_{TAU}= taurolidine concentration [µg/mL], C_{TTM} = taurultame concentration [µg/mL], C_{TAA} = taurinamide concentration [µg/mL], MW_{TAU} = molecular weight of taurolidine (= 284), MW_{TTM} = molecular weight of taurultame (= 136), MW_{TAA} = molecular weight of taurinamide (= 124).

Whole blood samples were taken using citrate tubes (Vacutainer™; Becton Dickinson, Heidelberg, Germany; containing 0.109M Natriumcitrat-solution 3.2%). These were then centrifuged for 10 min at 4°C and 3000 rpm (Eppendorf) to generate plasma samples for analysis. In order to be in the quantification range of the HPLC-MS method, the plasma samples were diluted with control human plasma depending on the expected concentration as follows (ex vivo samples: dilution factor 2, 5 or 10 and in vitro samples: dilution factor 10).

Experimentally, a total of 5 mL CH_3CN were added to 1 mL plasma sample and the mixture was shaken for 10 min at 300 rpm. After centrifugation for 10 min at 4°C and 3000 rpm (Eppendorf), the supernatant was decanted into a new tube and reduced in volume to approx. 2 mL under a stream of N_2 (45 min, 45°C). Derivatization was performed by addition of 1 mg of dansyl chloride dissolved in 3 mL CH_3CN. After shaking

for 10 min at 250 rpm and storage for 30 min at room temperature, 4 mL of dichloromethane were added and the tubes were shaken for further 10 min at 4°C with 300 rpm. After centrifugation (10 min at 4°C and 3000 rpm), the organic layer was transferred to a new tube and evaporated to dryness under a gentle stream of N_2 (40 min, 45°C). The residue was finally reconstituted in 0.5 mL CH_3CN and 5 µl were injected for HPLC-MS/MS analysis.

HPLC analyses were performed on an Agilent 1100 system (Agilent Technologies, Palo Alto, CA, U.S.A.) equipped with a binary pump, and fitted with a HTS PAL autosampler (CTC Analytics, Zwingen, Switzerland). Chromatographic conditions: Waters Symmetry C18 column (100-5 150 x 2.1mm); flow rate 200 µl/min; mobile phase: linear gradient within 4 min from 10 to 65% of solvent B, then isocratic at 65% of solvent B for another 4 min (solvent A: 0.05% HCOOH soln. in H_2O; solvent B: 0.05% HCOOH soln. in CH_3CN).

The ESI-MS experiments in the MRM-mode were performed on a Bruker ESQUIRE-LC quadrupole ion trap instrument (Bruker Daltonik GmbH, Bremen, Germany), equipped with a combined Agilent Atmospheric Pressure Ion source (Agilent Technologies, Palo Alto, CA, U.S.A.). The HPLC output was directly interfaced to the ESI ion source. The MS-conditions were: Nebulizer gas (N_2) 40 psi, dry gas (N_2) 9 l/min, dry temperature 300°C, HV capillary -4500 V, HV EndPlate offset –913 V, capillary exit 104 V, skimmer1 30 V, and trap drive 35. The MS/MS acquisitions were performed at normal resolution (0.6 u at half peak height), under ion charge control (ICC) conditions (10'000).

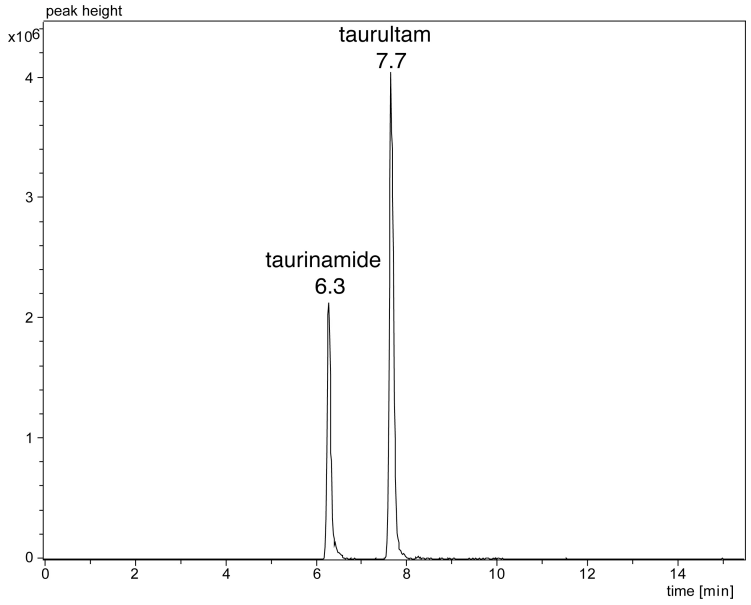

Figure 1. HPLC-ESI-MS of spiked human plasma containing 100 µg/mL taurolidine illustrating the selectivity of the method used for the quantification of taurinamide and taurultame

For taurinamide (Rt. 6.3 min) the MS/MS reaction from $[M+H]^+$ = *m/z* 358 to fragment ions *m/z* 170 (scan range *m/z* 160 – 180) was recorded and for taurultame (Rt. 7.7 min) from $[M+H]^+$ = *m/z* 370 to *m/z* 289 (scan range *m/z* 280 – 300). Extracted ion chromatograms were integrated for quantification (taurinamide: *m/z* 170, taurultame: *m/z* 289; figure 1). Calibration standards (n = 7) in the range from 0.2 – 20 µg/mL were prepared by diluting appropriate volumes (< 5% of plasma volume) of aqueous taurultame or taurinamide solutions in blank human plasma. The standards were aliquoted and deep-frozen.

Plotting the peak area versus the amount of each analyte generated calibration curves (figure 2).

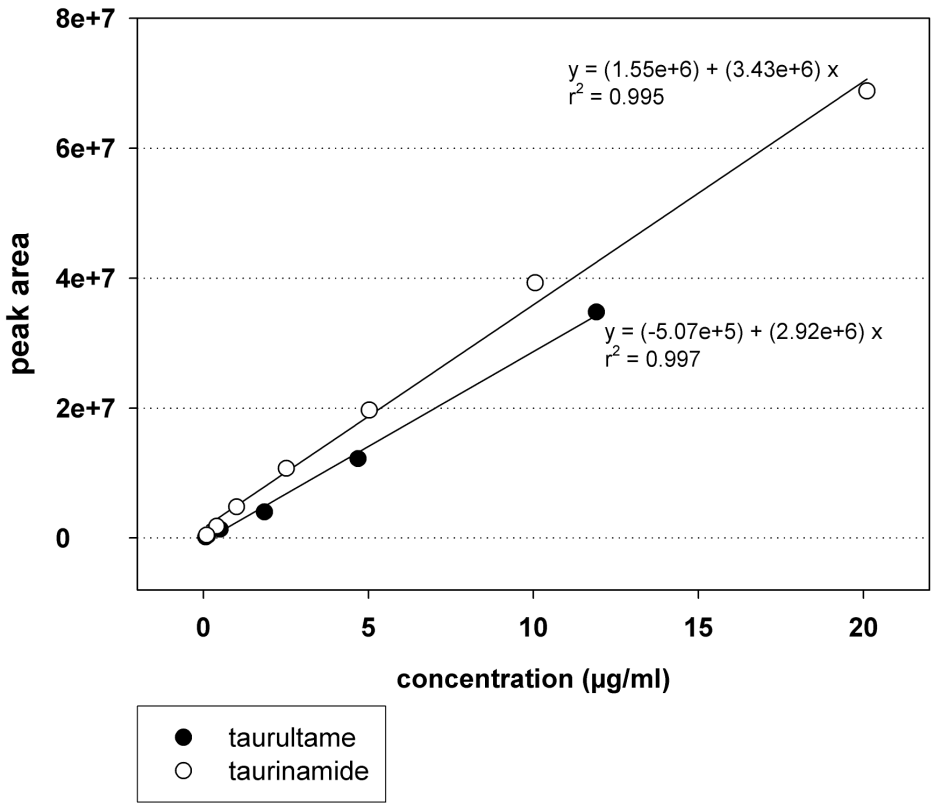

Figure 2. Calibration curves for the determination of taurinamide and taurultame in human blood serum in the range from 0.2–20 µg/mL. The relationship is linear. The sample volumes were 200 µl for the measurement in aqueous solution and 310 µl for the measurement in human plasma due to addition of the reagents for the precipitation of protein. These differences account for the slightly different courses of the curves. For details see Methods.

Validity of the detection of taurultame and taurinamide by HPLC-MS

The precision and accuracy of the method was evaluated by analysis of two replicates of human plasma samples spiked with taurinamide or taurultame at three different concentrations (0.2, 2.0 and 20 µg/mL) in two separate runs. The HPLC-MS method was able to detect taurultame with an accuracy of 5-9 % and taurinamide with an accuracy of 1-2 % in the concentration range of 2-20 µg/mL. The variation coefficient was 9.1 ± 0.8 % for taurultame and 4.8 ± 2.1 % for taurinamide in the concentration range of 0.2-20 µg/mL (table 1, figure 2).

Table 1. Precision and accuracy of the HPLC-MS method

	nominal concentration (µg/mL)	**CV between-batch** (%) n = 4	**ACC between-batch** (%) n = 4
taurinamide	0.2	5.6	86
	2.0	2.4	98
	20.0	6.5	101
taurultame	0.2	10.0	86
	2.0	8.4	95
	20.0	9.0	109

AAC = coefficient of variation as a measure of dispersion of a probability distribution
AAC = accuracy in % of the nominal concentration

Stability of taurolidine, taurultame and taurinamide in plasma

Whole blood (80 mL) was collected from a healthy male volunteer (R.S.) using citrate tubes (Vacutainer™; Becton Dickinson, Heidelberg, Germany; containing 0.109M Natriumcitrat-solution 3.2%). These were then centrifuged at 3000 rpm for 10 minutes (Eppendorf) for plasma extraction. Then 100 µg/mL of taurolidine were added to the plasma, followed by incubation at 37°C for 0, 5, 10, 20, 30, 60, 120, 240 or 360 min. All samples were immediately frozen and stored at -80 °C until analysis. The subsequent

sample preparation and analysis were performed as described in the section "Determination of taurultame and taurinamide and calculation of taurolidine concentration".

Stability of taurolidine, taurultame and taurinamide in whole blood

Whole blood (80 mL) was taken from a healthy male volunteer (R.S.). Then 50 or 100 µg/mL of taurolidine were added, followed by incubation at 37°C for 0, 5, 10, 20, 30, 60, 120, 240 or 360 min. The samples were collected using citrate tubes (Vacutainer™; Becton Dickinson, Heidelberg, Germany; containing 0.109M Natriumcitrat-solution 3.2%). These were centrifuged at 3000 rpm for 10 minutes (Eppendorf) for plasma extraction and immediately frozen and stored at -80 °C until analysis. Further sample preparation and analysis were performed using the method described in the section "Determination of taurultame and taurinamide and calculation of taurolidine concentration".

Extraction of plasma samples of the patients and detection of taurultame and taurinamide

Whole blood (6 mL) was collected every 60 minutes starting immediately before the first taurolidine infusion (8:00 a.m.) from each patient using citrate tubes (Vacutainer™; Becton Dickinson, Heidelberg, Germany; containing 0.109M Natriumcitrat-solution 3.2%). These were then centrifuged within 20 minutes of collection (Eppendorf, 3000 rpm, 10 min) and the supernatant of 2-4 mL frozen and stored at -80 °C until analysis. Further sample preparation and analysis were performed using the method described in the section "Determination of taurolidine".

Pharmacokinetic parameters

During steady-state-conditions the same amount of a substance is taken in and eliminated per period of time. This can only be achieved by a continuous infusion. As an approximation, repetitive infusions can be regarded as a continuous infusion which is "cutted into pieces" (Notari 1987). Then, an approximation of a steady-state-condition in kind of figures is reached after 5-6 half-life-periods (Notari 1987; Canal et al. 1998). This corresponds to the time period from 8.5-10.2 hours in the present study. Correspondingly,

analysis of the present data had shown that following the fourth infusion an approximation of a steady-state-condition has loomed. Probably the steady-state would have achieved after an additional fifth infusion. Taking into account these short-comings resulting from the data available, we tried to estimate pharmacokinetic parameters using an approximation of a steady-state-condition without assuming a compartment model.

A steady state was assumed for an interval of 4 hours comprising hours 9 through 12 following the start of infusion. The lowest ($C_{min\ (9\text{-}12\ h)}$) and highest ($C_{max\ (9\text{-}12\ h)}$) concentrations of taurolidine, taurultame and taurinamide, respectively during this interval were extracted from the individual concentration-time curves. The area under the curve during this interval was calculated using the trapezoidal rule. The mean concentrations were calculated according to the formula

$$C_{av(9-12h)} = \frac{AUC_{(9-12h)}}{approx.\ steady-state-interval}$$

where $C_{av\ (9\text{-}12\ h)}$ = average concentration of taurolidine, taurultame and taurinamide, respectively [µg/mL]; $AUC_{(9-12h)}$ = area under the curve during the approximated steady-state [µg·h/mL]; and *approx. steady-state-interval* = investigated 4-hour interval from hour 9 to 12 with approximated steady-state-conditions.

Peak trough flow fluctuation was calculated as

$$PTF_{(9-12h)} = \frac{100 \cdot (C_{max(9-12h)} - C_{(min(9-12h)})}{C_{av(9-12h)}}$$

Where $PTF_{(9\text{-}12h)}$ = peak trough flow fluctuation [%]; $C_{max\ (9\text{-}12\ h)}$ = maximal concentration of taurolidine, taurultame an taurinamide, respectively during the approximated steady-state-interval investigated [µg/mL]; and $C_{min\ (9\text{-}12\ h)}$ = minimal concentration of taurolidine, taurultame an taurinamide, respectively during the approximated steady-state-interval investigated [µg/mL].

The volume of distribution under steady-state conditions was calculated according to the formula

$$V_{D(9-12h)} = \frac{total\ dose\ administered}{C_{max(9-12h)}}$$

where $V_{D(9\text{-}12h)}$ = volume of distribution during the approximated steady-state-interval investigated [l]; *total dose administered* = total dose administered per day; and $C_{max(9\text{-}12h)}$ =

highest concentration of taurolidine, taurultame and taurinamide, respectively, during the approximated steady-state-interval investigated [µg/mL].

Clearance under the approximated steady-state-conditions was calculated according to the following formula:

$$Cl_{(9-12h)} = \frac{total\ dose\ administered}{AUC_{(9-12h)}}$$

where $Cl_{(9-12h)}$ = clearance under the approximated steady-state-conditions [l/h]; *total dose administered* = total dose administered per day; and $AUC_{(9-12h)}$ = area under the curve during the approximated steady-state-conditions [µg·h/mL].

The plasma half-life during the approximated steady-state-interval investigated was calculated as

$$t_{\frac{1}{2}(9-12h)} = \frac{\ln 2 \cdot V_{D(9-12h)}}{Cl_{(9-12h)}}$$

where $t_{\frac{1}{2}(9-12h)}$ = plasma half-life during the approximated steady-state-interval [h]; $V_{D(9-12h)}$ = volume of distribution of the approximated steady-state-interval investigated [l]; $Cl_{(9-12h)}$ = clearance under the approximated steady-state-conditions [l/h]).

Results

Validity of the detection of taurultame and taurinamide by HPLC-MS

The HPLC-MS/MS method (figures 1 and 2) was found to yield precise and reproducible results. For a within-study validation two replicates of human plasma samples spiked with taurolidine at two different concentrations (approx 2.5 and 20.0 µg/mL) in each run were analyzed. In all experiments, the concentration of taurolidine was back-calculated based on the measured concentration of taurultame and taurinamide. The calibration curves for taurultame and taurinamide could be described with linear functions with high precision (figure 2).

The mean between-batch accuracy was found to be 112 % at 2.52 µg/mL nominal concentration (n=6) and 107 % at 18.1 µg/mL nominal concentration (n=6) for the ex vivo samples. For the in vitro experiments, the mean between-batch accuracy was found to be 107 % at 2.66 µg/mL nominal concentration (n=6) and 115 % at 19.1 µg/mL nominal

concentration (n=6). The between batch variation coefficient was calculated as 8.7 ± 0.3 % for the ex vivo and 5.7 ± 0.6 % for the in vitro samples (Tables 1 and 2).

Stability of taurolidine, taurultame and taurinamide in plasma

In plasma, the concentrations of taurultame, taurinamide and taurolidine (back-calculated from the taurultame and taurinamide values) remained constant over a 6 hour period at 37 °C (repeated measures-ANOVA, n.s.; figure 3). The taurultame-taurinamide-ratio (TTR) did not change in a statistically significant way over the 6 hour period (2.25 vs. 2.85; repeated measures-ANOVA; n.s.).

Table 2. Within-study validation of the total taurolidine concentration

nominal concentration of taurolidine (µg/mL)	Between-batch CV (%) [n = 6]	Between-batch ACC (%) [n = 6]
Ex vivo		
2.52	8.9	112
18.1	8.5	107
In vitro		
2.66	5.2	107
19.1	6.1	115

ACC = accuracy of the nominal concentration; **CV** = coefficient of variation

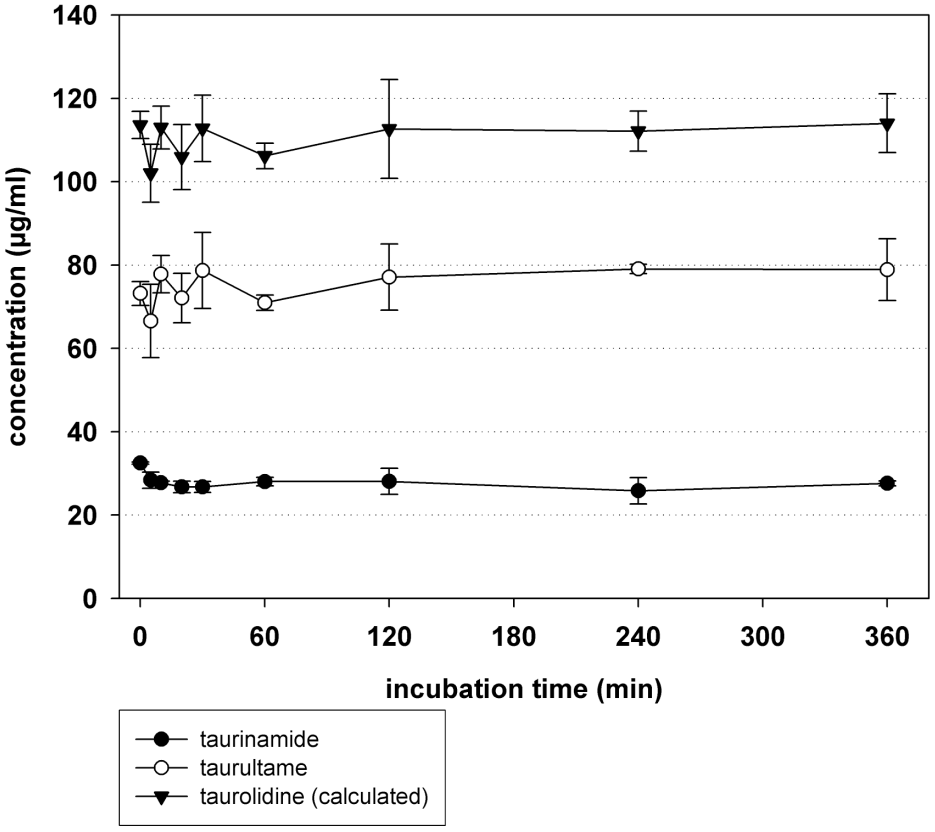

Figure 3. Concentration of taurultame, taurinamide and taurolidine (calculated from the taurultame and taurinamide values) in human plasma at 37 °C in vitro over 6 hours at an initial concentration of 100 µg/mL. There are no statistically significant changes of the concentrations. For details see methods.

Stability of taurolidine, taurultame and taurinamide in whole blood

In whole blood there was a time and concentration dependent conversion of taurolidine. During incubation at 37°C the concentration of taurultame decreased logarithmically at a rate which corresponded to the increase of the taurinamide concentration (figures 4 and 5).

Immediately following incubation the TTR was 0.95 at an initial taurolidine concentration of 50 µg/mL, and 1.69 at 100 µg/mL (t-test; $p<0.05$; figure 6). After 6h incubation, the TTR reached the value of 0.02, independent of the initial taurolidine concentrations (t-test, n.s.). The taurolidine concentration (back-calculated from the taurultame and taurinamide values) remained largely constant over the time period tested (figures 4 and 5).

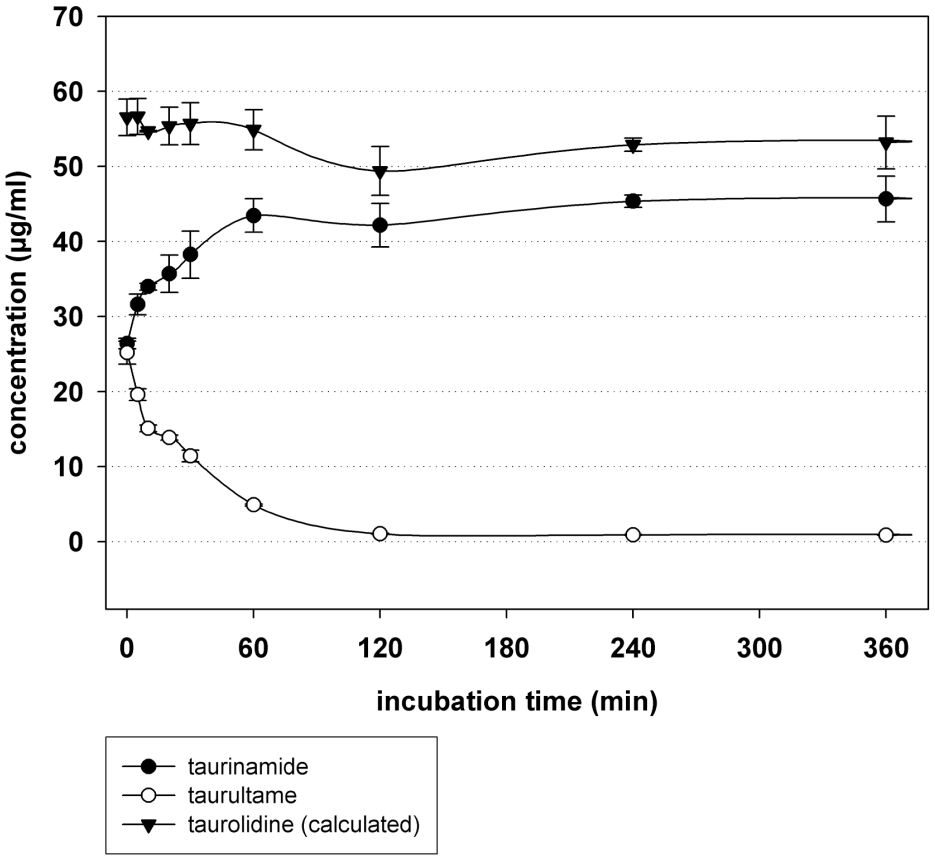

Figure 4. Concentration of taurultame, taurinamide and taurolidine (calculated from the taurultame and taurinamide values) in human whole blood in vitro at 37 °C over 6 hours (3 experiments) at an initial taurolidine concentration of 50 µg/mL. Mean values ± SEM are given.

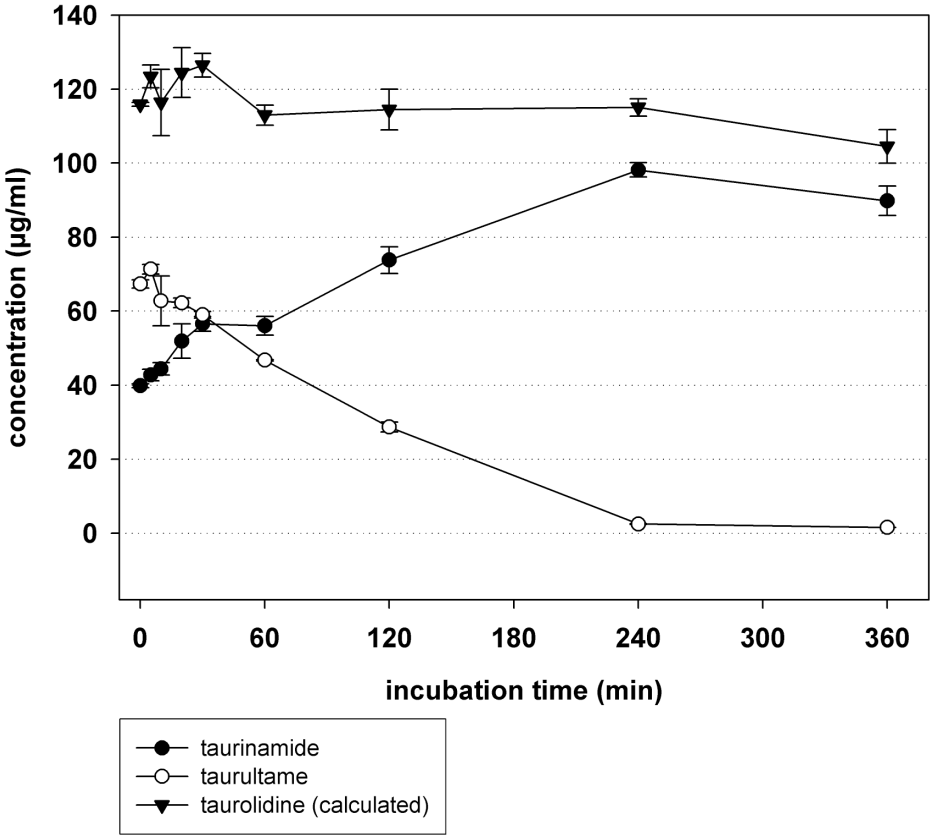

Figure 5. Concentration of taurultame, taurinamide and taurolidine (calculated from the taurultame and taurinamide values) in human whole blood in vitro at 37 °C over 6 hours at an initial taurolidine concentration of 100 µg/mL. Mean values ± SEM are given.

Concentration of taurolidine in plasma following repeated infusion

The calculated plasma concentration of taurolidine showed a strong increase after the start of each infusion and increased until the end of infusion, followed by a rapid decline (figure 7). The TTR was found to fluctuate between 0.1 and 0.3 depending on the relation to the previous or next infusion period (figure 6). Taurolidine and taurinamide showed a moderate accumulation over the 13 hour treatment period, whereas taurultame did not (figure 7).

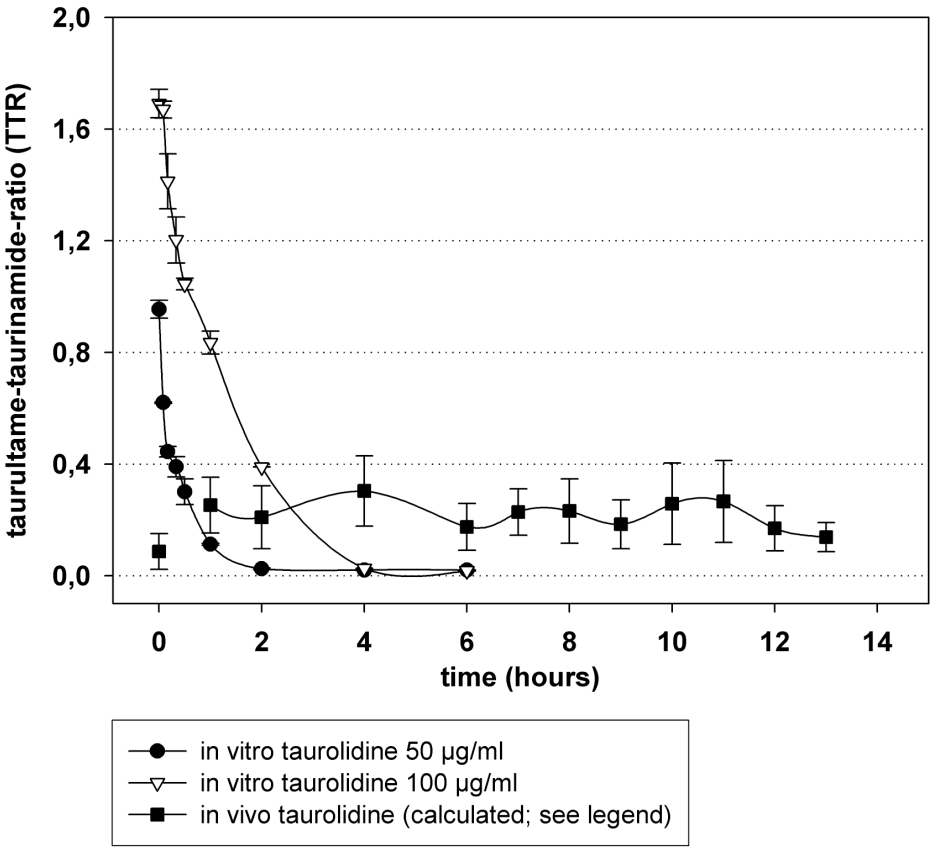

Figure 6. Time course of the taurultame-taurinamide-ratio (TTR) in whole blood over 6 hours (3 experiments) in vitro at 2 different initial taurolidine concentrations (filled circles and open triangles). Time course of the TTR in vivo over 13 hours during 4 repetitive taurolidine infusions in 7 patients (filled squares). The calculated mean plasma concentration of taurolidine in these patients was 83.0 µg/mL (for details see Methods, Results and table 3). Mean values ± SEM are given.

Pharmacokinetic parameters

The average patient plasma concentration (back-calculated from the taurultame and taurinamide values) of taurolidine was found to be 83.0 µg/mL (figure 7, table 3). Thus, the taurolidine concentration was within the anti-neoplastic effective concentration range determined in vitro (Calabresi et al. 2001; Stendel et al. 2002; Stendel et al. 2003; Rodak et al. 2005).

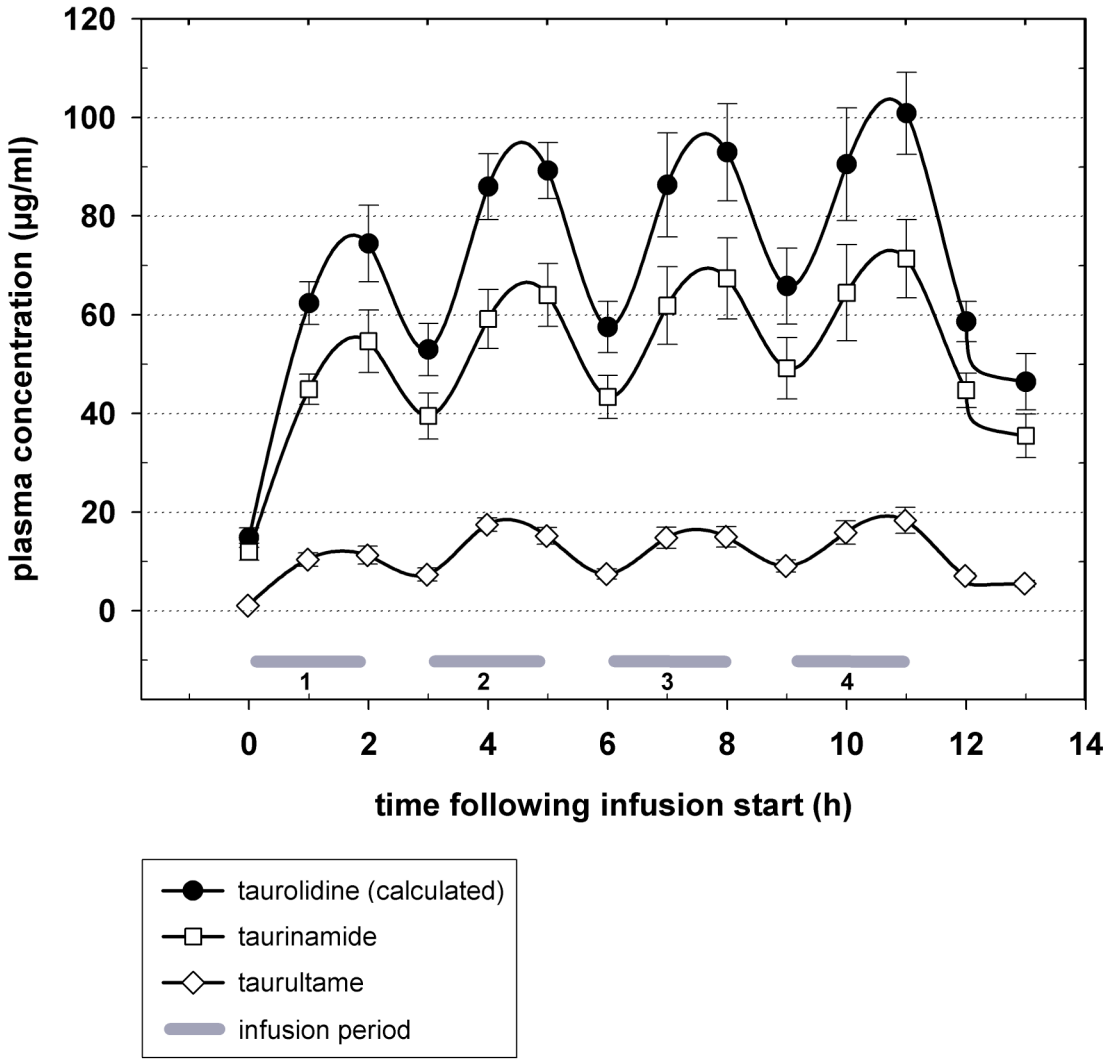

Figure 7. Plasma concentrations of taurultame, taurinamide and taurolidine (calculated from the taurultame and taurinamide values) during 4 repetitive taurolidine infusions (mean values and SEM of 7 patients; infusion over 2 hours with an interval of 1 hour between infusions). The calculated mean plasma concentration of taurolidine (83.0 µg/mL) is within the anti-neoplastic effective concentration range determined in vitro.

Table 3. Pharmacokinetic data of seven patients during repetitive intravenous administration of taurolidine comprising four 5g infusions every 24 hours[a].

Parameter	Taurolidine	Taurultame	Taurinamide
$C_{max\ (9\text{-}12)}$ (µg/mL)	95.8 ± 21.8	17.0 ± 8.1	69.1 ± 19.1
$C_{av\ (9\text{-}12)}$ (µg/mL)	83.0 ± 18.1	13.6 ± 5.6	58.5 ± 15.6
$C_{min\ (9\text{-}12)}$ (µg/mL)	61.3 ± 20.4	7.9 ± 4.6	46.9 ± 14.7
$t_{1/2\ (9\text{-}12)}$ (h)	1.7 ± 0.1	1.5 ± 0.2	1.7 ± 0.2
AUC $_{(9\text{-}12)}$ (µg h/mL)	249.2 ± 58.4	40.7 ± 16.7	175.5 ± 46.5
PTF $_{(9\text{-}12)}$ (%)	47.9 ± 18.8	80.1 ± 36.4	41.5 ± 15.4
$V_{d\ (9\text{-}12)}$ (L)	210.5 ± 45.8	289.6 ± 176.1	236.0 ± 67.4
Cl $_{(9\text{-}12)}$ (L/h)	84.8 ± 20.7	138.4 ± 10.3	95.6 ± 26.9

[a]) Values are expressed as mean ± SD

$AUC_{(9–12)}$ = area under the plasma concentration-time curve from hours 9 through 12 following the start of the infusion; **$Cav_{(9–12)}$** = average plasma concentration from hours 9 through 12 following the start of the infusion; **$Cmax_{(9–12)}$** = maximum plasma concentration from hours 9 through 12 following the start of the infusion; **$Cmin_{(9–12)}$** = minimum plasma concentration from hours 9 through 12 following the start of the infusion; **$CL_{(9–12)}$** = apparent clearance from hours 9 through 12 following the start of the infusion; **$PTF_{(9–12)}$** = peak trough flow fluctuation from hours 9 through 12 following the start of the infusion; **$t_{1/2(9–12)}$** = elimination half-life from hours 9 through 12 following the start of the infusion; **V** = volume of distribution from hours 9 through 12 following the start of the infusion.

Discussion

Using ^{1}H- and ^{13}C-NMR-spectroscopy (Erb et al. 1983; Hood et al. 1994), NMR spectroscopy and gas-chromatography (Knight et al. 1983) early studies have shown, that in aqueous solution taurolidine is present in an equilibrium of hydrolysis/hydration with taurultame and N-hydroxymethyl-taurultame.

Following incubation of taurolidine in human plasma or protein-free serum in vitro, taurultame and taurinamide, but not taurolidine, have been identified (Jones et al. 1990). Furthermore, following intraperitoneal (Knight et al. 1981; Vankemmel et al. 1982; Erb et al. 1983) and intravenous (Vankemmel et al. 1982; Erb et al. 1983) taurolidine application in vivo taurultame and taurinamide could be detected in human blood serum samples, so that taurultame and taurinamide are regarded as main derivatives of taurolidine (Skellern 1985; Waser et al. 1985). Similarly, using pre-column derivatization and HPLC with fluorescence detection (Woolfson et al. 1989), a conversion of taurolidine with subsequent formation of taurinamide has been observed in plasma (Jones et al. 1990). In the present study, taurolidine displayed a stable pattern of derivatives in plasma in vitro as nearly unchanged values of taurultame and taurinamide were found over 6 hours of incubation (figure 3). Taurolidine itself was below the limit of detection but was back calculated from the taurultame and taurinamide values. Since the ratio of metabolites was already stable at the first points of measurements (figure 3), the time period of plasma sample preparation (5 min.) before freezing appears to be sufficient for the conversion of taurolidine to taurultame and taurinamide.

In whole blood in vitro, a conversion of taurolidine was apparent in a time- and concentration-dependent manner (figures 4 and 5), with the TTR decreasing significantly (figure 6) as measured over a 6 hour period of incubation. These results point to two phases of taurolidine conversion in whole blood. During the first phase, the formation of taurultame and taurinamide occurs at a slower rate as compared to the nearly immediate formation of these two derivatives in plasma. The rate of conversion during the initial phase mainly depended on the initial concentration of taurolidine (figures 4 and 5) being significantly slower at the 50 µg/mL concentration than at 100 µg/mL. The second phase is characterized by a fairly linear kinetic profile and is markedly slower than the first one. Competitive binding of taurolidine to plasma proteins is unlikely, as indicated by the

results of experiments performed with radioactively labeled taurolidine dialyzed against human plasma (Steinbach-Lebbin et al. 1982). In whole blood in vitro binding of taurolidine to erythrocytes is postulated to explain the time course of the formation of its derivatives in whole blood in vitro.

A commercial preparation of taurolidine for intravenous infusion is available as a 2% solution (Taurolin®). Taurolidine treatment of human glioblastomas is performed by repetitive intravenous infusions comprising four daily infusions of 2% taurolidine solution, each administered over 2 hours with a 1-hour interval between infusions using a total daily dose of 20 g (Stendel et al. 2002; Stendel et al. 2004). In the present study, this infusion regimen was reflected by the intermittent rising and falling of the plasma concentrations of taurolidine, taurultame and taurinamide (figure 7). Correspondingly, the ratio of taurultame to taurinamide (TTR) did not vary significantly over the treatment period of 13 hours (figure 6). The average plasma concentration of taurolidine (83.0 µg/mL) as calculated from the taurultame and taurinamide values was within the anti-neoplastic effective concentration range (Calabresi et al. 2001; Stendel et al. 2002; Stendel et al. 2003; Rodak et al. 2005). Thus, the infusion protocol chosen for the treatment of glioblastoma provides an adequate anti-neoplastic concentration of taurolidine.

The previous knowledge on the pharmacokinetic behavior of taurolidine following repetitive intravenous administration in humans was very limited. Peak taurultame concentrations have been reported to be app. 4 µg/mL after continuous intravenous infusion of 15 g taurolidine (Vankemmel et al. 1982), and app. 5 µg/mL (Erb et al. 1983) - 8.1 µg/mL (Vankemmel et al. 1982) after the second of three repetitive intravenous infusions of each 5 g taurolidine. It is difficult to interpret in the cited studies (Vankemmel et al. 1982; Erb et al. 1983) that the peak taurultame concentration during the third infusion was markedly below that during the second infusion. In addition, these values are at least two-fold lower as measured in the present study using the same taurolidine dose per infusion (table 3). The overall lower serum concentrations of taurultame in the cited studies (Vankemmel et al. 1982; Erb et al. 1983) as compared to the results of the present study may possibly be attributable to the different way of sample processing after blood collection. In the present study the plasma concentrations of taurolidine and taurinamide showed a moderate accumulation with the increasing number of infusions, whereas the concentration of taurultame did not (figure 7). This is probably due to the higher volume of distribution indicating a much higher concentration in tissue. In addition, the

pharmacokinetic parameters must be interpreted with caution because only 3 blood samples were collected for each administration interval. Furthermore, the basis for the calculation of the pharmacokinetic parameters was only an approximation of a steady-state-condition.

Conclusions

A new method for quantitative determination of taurultame and taurinamide in human plasma has been developed. Taurultame and taurinamide concentrations were determined with high accuracies using HPLC and tandem mass spectrometry permitting a quantification of taurolidine concentrations.

Taurolidine displayed a stable pattern of derivatives in human plasma in vitro. In whole blood taurolidine is converted to taurultame and taurinamide in a time- and concentration-dependent manner.

The average taurolidine plasma concentration achieved with the repetitive infusion regimen in glioblastoma patients is within the anti-neoplastic effective concentration range. The volume of distribution is higher than plasma volume, suggesting that tissue concentrations of taurolidine, taurultame and taurinamide are markedly higher than plasma concentrations. Repetitive infusion of taurolidine is the therapeutically adequate mode of administration for the indication of glioblastoma.

References

Bedrosian, I., Sofia, R. D., Wolff, S. M. and Dinarello, C. A. (1991). "Taurolidine, an analogue of the amino acid taurine, suppresses interleukin 1 and tumor necrosis factor synthesis in human peripheral blood mononuclear cells." *Cytokine* **3**: 568-575.

Bieselt, R. (1997). "[Surgical therapy of pleural empyema with tauroline]." *Langenbecks Arch. Chir.* **382**: S42-6.

Blenkharn, J. I. (1987). "The antibacterial and antiendotoxin activity of taurolidine in combination with antibiotics." *Surgical Res. Commun.* **2**: 149-55.

Browne, M. K. (1981). "The treatment of peritonitis by an antiseptic - taurolin." *Pharmatherapeutica* **2**: 517-22.

Browne, M. K., Leslie, G. B., Pfirrmann, R. W. and Brodhage, H. (1977). "The in vitro and in vivo activity of Taurolin against anaerobic pathogenic organisms." *Surg. Gynecol. Obstet.* **145**: 842-846.

Browne, M. K., Mackenzie, M. and Doyle, P. J. A. (1978). "A controlled trial of Taurolin in established bacterial peritonitis." *Surg. Gynecol. Obstet.* **146**: 721-724.

Calabresi, P., Goulette, F. A. and Darnowski, J. W. (2001). "Taurolidine: cytotoxic and mechanistic evaluation of a novel antineoplastic agent." *Cancer Res.* **61**: 6816-21.

Canal, P., Gamelin, E., Vassal, G. and Robert, J. (1998). "Benefits of pharmacological knowledge in the design and monitoring of cancer chemotherapy." *Pathol. Oncol. Res.* **4**: 171-178.

Erb, F., Febvay, N. and Imbenotte, M. (1982). "Structural investigation of a new organic antiseptic: taurolidine. A Spectroscopic study of its stability and equilibria in various solvents." *Talanta* **29**: 953-958.

Erb, F., Imbenotte, M., Huvenne, J. P., Vankemmel, M., Scherpereel, P. and Pfirrmann, R. W. (1983). "Structural investigation of a new organic antispetic: taurolidine. Analytical study and application to identification and quantitation in biological fluids." *Eur. J. Drug Metab. Pharmacok.* **8**: 163-173.

Hood, H. T., Smail, G. A., Skellern, G. G., Jindal, D. P., Browne, M. K. and Pfirrman, R. W. (1994). "Studies of the thiadiazine, taurolidine. Identification of the molecular species present in aqueous solutions by H1 and C13-NMR Spectroscopy." *Talanta* **1**: 107-113.

Jones, D. S., McCafferty, D. F., Woolfson, A. D. and Gorman, S. P. (1990). "A study of the stability of taurolidine in plasma and protein-free serum." *Int. J. Pharmaceutica* **64**: R1-R4.

Jurewitsch, B. and Jeejeebhoy, K. N. (2005). "Taurolidine lock: the key to prevention of recurrent catheter-related bloodstream infections." *Clin. Nutr.* **24**: 462-5.

Jurewitsch, B., Lee, T., Park, J. and Jeejeebhoy, K. (1998). "Taurolidine 2% as an antimicrobial lock solution for prevention of recurrent catheter-related bloodstream infections." *JPEN J Parenter. Enteral. Nutr.* **22**: 242-4.

Knight, B. I., Skellern, G. G., Browne, M. K. and Pfirrmann, R. W. (1981). "The characterisation and quantitation by high-performance liquid chromatography of the metabolites of taurolin [letter]." *Br. J. Clin. Pharmacol.* **12**: 439-40.

Knight, B. I., Skellern, G. G., Smail, G. A., Browne, M. K. and Pfirrmann, R. W. (1983). "NMR Studies and GC analysis of the antibacterial agent taurolidine." *J. Pharmaceut. Sci.* **72**: 705-707.

Leaper, D. J. (1985). *Prevention of peritoneal adhesions after thermal injury using noxythiolin and Taurolin.* A new concept in antimicrobial chemotherapy for surgical infection. W. L. Bruckner and R. W. Pfirrmann. Baltimore, Urban & Schwarzenberg**:** 115-119.

Marti, M. C., Moser, G., Wicki, O., Linder, M. and del Ponte, F. (1980). "[Intravenous and intraperitoneal administration of an antiseptic: 65 cases of diffuse peritonitis treated with taurolin]." *Helv. Chir. Acta* **46**: 755-8.

McCartney, A. C. and Browne, M. K. (1988). *Clinical studies on administration of taurolidine in severe sepsis: a preliminary study.* Bacterial endotoxins: pathophysiological effects, clinical significance and pharmacological control. New York, Alan R.Liss Inc.**:** 130.

McCourt, M., Wang, J. H., Sookhai, S. and Redmond, H. P. (2000). "Taurolidine inhibits tumor cell growth in vitro and in vivo." *Ann. Surg. Oncol.* **7**: 685-91.

Moser, G. and Martin, M. D. (1978). "Forty cases of peritonitis treated without antibiotics:the intraperitoneal and intravenous use of Taurolin." *Praxis* **67**: 425-428.

Notari, R. E. (1987). *Biopharmaceutics and clinical pharmacokinetics.* New York, Basel, Marcel Dekker Inc.

Rodak, R., Kubota, H., Ishihara, H., Eugster, H. P., Konu, D., Mohler, H., Yonekawa, Y. and Frei, K. (2005). "Induction of reactive oxygen intermediates-dependent programmed cell death in human malignant ex vivo glioma cells and inhibition of the vascular endothelial growth factor production by taurolidine." *J. Neurosur.* **102**: 1055-68.

Skellern, G. G. (1985). *Pharmacokinetics of taurolidine.* Taurolin. Ein neues Konzept zur antimikrobiellen Chemotherapie chirurgischer Infektionen. W. L. Brückner and R. W. Pfirrman. München, Wien, Baltimore, Urabn & Schwarzenberg**:** 48-50.

Steinbach-Lebbin, C., Ganz, A. J., Chang, A. and Waser, P. G. (1982). "Pharmacokinetics of Taurolin." *Arzneimittelforschung* **32**: 1542-6.

Stendel, R., Picht, T., Schilling, A., Heidenreich, J., Loddenkemper, C., Janisch, W. and Brock, M. (2004). "Treatment of glioblastoma with intravenous taurolidine. First clinical experience." *Anticancer Res.* **24**: 1143-7.

Stendel, R., Scheurer, L., Schlatterer, K., Gminski, R. and Mohler, H. (2004). "Taurolidine-Fibrin-Sealant-Matrix using spray application for local treatment of brain tumors." *Anticancer Res.* **24**: 631-8.

Stendel, R., Scheurer, L., Stoltenburg-Didinger, G., Brock, M. and Mohler, H. (2003). "Enhancement of Fas-ligand-mediated programmed cell death by taurolidine." *Anticancer Res.* **23**: 2309-14.

Stendel, R., Stoltenburg-Didinger, G. and Brock, M. (2001). *The aminosulphonic acid derivative taurolidine induces apoptotic changes in brain tumor cells.* 12th World Congress of Neurosurgery, Sydney, Australia.

Stendel, R., Stoltenburg-Didinger, G. and Brock, M. (2002). "Apoptotic changes in brain tumor cells induced by taurolidine." *J. Cancer Res. Clin. Oncol.* **128**: 150.

Stendel, R., Stoltenburg-Didinger, G. and Brock, M. (2002). "Taurolidine - underestimated antineoplastic effect?" *J. Cancer Res. Clin. Oncol.* **128**: 140.

Stendel, R., Stoltenburg-Didinger, G., Lotte Al-Keikh, C., Wattrodt, M. and Brock, M. (2002). "The effect of taurolidine on brain tumor cells." *Anticancer Res.* **22**: 809-814.

Treutner, K. H., Bertram, P., Lerch, M. M., Klimaszewski, M., Petrovic-Kallholm, S., Sobesky, J., Winkeltau, G. and Schumpelick, V. (1995). "Prevention of postoperative adhesions by single intraperitoneal medication." *J. Surg. Res.* **59**: 764-71.

Vankemmel, M., Scherpereel, P., Erb, F., Sonnenfeld, H., Verkindre, A. M. and Brice, A. (1982). *Nouvelle approche fondamentale de la chimiothérapie anti-infectieuse en chirurgie abdominale: l´utilisation par voie locale et générale dún antiseptique: la taurolidine.*, Monographie de la Societé de Réanimation de Langue Francaise**:** 283-289.

Waser, P. G., Sibler, E. and Ganz, A. J. (1985). *Pharmakologie und Toxikologie von Taurolidin*. Taurolin. Ein neues Konzept zur antimikrobiellen Chemotherapie chirurgischer Infektionen. W. L. Brückner and R. W. Pfirrmann. München, Wien, Baltimore, Urban und Schwarzenberg**:** 24-37.

Watson, R. W., Redmond, H. P., Mc Carthy, J. and Bouchier-Hayes, D. (1995). "Taurolidine, an antilipopolysaccharide agent, has immunoregulatory properties that are mediated by the amino acid taurine." *J. Leukoc. Biol.* **58**: 299-306.

Wesch, G., Petermann, C. and Linder, M. M. (1983). "[Drug therapy of peritonitis. 6-year experience with the chemotherapeutic agent and anti-endotoxin taurolin]." *Fortschr. Med*. **101**: 545-50.

Woolfson, A. D., Gorman, S. P., McCafferty, D. F. and Jones, D. S. (1989). "Assay procedures for Taurolin solutions using pre-column derivatisation and high-performance liquid chromatography with fluorescence detection." *Int. J. Pharmac.* **49**: 135-140.

5.4. The Modified Flavonol Glycosylation Profile in the *Arabidopsis rol1* Mutants Results in Alterations in Plant Growth and Cell Shape Formation

Abstract

Flavonoids are secondary metabolites known to modulate plant growth and development. A primary function of flavonols, a subgroup of flavonoids, is thought to be the modification of auxin fluxes in the plant. Flavonols in the cell are glycosylated and the *rol1* mutants of *Arabidopsis thaliana,* affected in rhamnose biosynthesis, have a modified flavonol glycosylation profile. A detailed analysis of the *rol1-2* allele revealed hyponastic growth, aberrant pavement cell and stomatal morphology in cotyledons, and defective trichome formation. Blocking flavonoid biosynthesis suppresses the *rol1-2* shoot phenotype, suggesting that it is induced by the modified flavonol profile. The hyponastic cotyledons of *rol1-2* are likely to be the result of a flavonol-induced increase in auxin concentration. In contrast, the pavement cell, stomata, and trichome formation phenotypes appear not to be induced by the modified auxin distribution. Together, these results suggest that changes in the composition of flavonols can have a tremendous impact on plant development through both auxin-induced and auxin-independent processes.

Introduction

Flavonoids represent a highly diverse class of low molecular weight secondary metabolites, of which >6000 different compounds have been described. They are important for pigmentation and UV-protection. They serve as signals for pollinators and other beneficial organisms, participate in hormone signaling and function as phytoalexins. A number of biological processes such as transcriptional regulation, signal transduction, and cell-to-cell communication are influenced by flavonoids. Due to their antioxidant activity, flavonoids appear to play an important role in the control of reactive oxygen species (ROS) in plant cells (Lepiniec et al., 2006; Peer and Murphy, 2006). In *Arabidopsis thaliana*, 24 mutants have been identified on the basis of aberrant flavonoid accumulation (Routaboul et al., 2006). Frequently, mutants are defective in the biosynthesis of proanthocyanidins (Figure 1), the subgroup of flavonoids responsible for seed coloring (Korneef, 1990; Debeaujon et al., 2003; Lepiniec et al., 2006), and thus deviate from the typical brown seed color. The flavonols, kaempferol, quercetin, and isorhamnetin, constitute a subgroup of flavonoids that appears to be present in all tissues of Arabidopsis. They are *O*-glycosylated, mainly by glucose and rhamnose units at the C3 and C7 positions, resulting in a large number of different molecules (Veit and Pauli, 1999; Lepiniec et al., 2006).

Biochemical experiments and analyses of auxin fluxes in flavonoid-deficient mutants suggest that flavonols negatively regulate auxin transport (Jacobs and Rubery, 1988; Brown et al., 2001; Buer and Muday, 2004; Peer et al., 2004). There is also evidence that flavonols directly influence cell growth. In petunia and maize, *chalcone synthase* mutants are blocked in the first step of flavonoid-biosynthesis (Figure 1) and are defective in pollen tube growth. Kaempferol was identified as the pollen germination-inducing constituent when applied to mutant stigma (Mo et al., 1992). In addition, the petunia mutant is defective in root-hair development (Taylor and Grotewold, 2005).

Cell growth is largely determined by the extension rate of the cell wall, which is a complex structure composed of the polysaccharides cellulose, hemicellulose, and pectin, in addition to a number of structural proteins (Carpita and Gibeau, 1993; Cassab, 1998). Epidermal leaf pavement cells provide a model system in which to study the process of cell growth and determination of cell shape (Mathur, 2004). In *Arabidopsis*, pavement cells have a jigsaw puzzle-like shape where lobes extend into neighboring cells. This pattern is based on coordinated outgrowth at a given point in one cell, with inhibition of outgrowth in the

Previously, we identified two allelic *rol1* (*repressor of lrx1*) mutants, which suppress the *Arabidopsis* root-hair mutant *lrx1* (Diet et al., 2006). *LRX1* encodes an extracellular LRR-extensin protein, specifically expressed in root hairs (Baumberger et al., 2001; Ringli, 2005). While *lrx1* mutants develop defective root hairs, *lrx1 rol1* double mutants show a suppressed *lrx1* phenotype and form wild-type-like root hairs. The *ROL1* locus encodes *RHM1*, one of three rhamnose synthase proteins that convert UDP-D-Glucose to UDP-L-Rhamnose in *Arabidopsis* (Diet et al., 2006; Oka et al., 2007). The RHM1 protein encoded by the *rol1* mutants is unable to catalyze this conversion (Diet et al., 2006). Rhamnose is an important component of pectin (Ridley et al., 2001) and the *rol1* mutants exhibit modifications in pectin structure (Diet et al., 2006), which may provide the molecular basis of the observed suppression of the *lrx1* root-hair phenotype. Seedlings of both *rol1* alleles also develop cotyledons with an uneven surface and the peripheral zone that is bent upwards. This is referred to as hyponastic growth and is the result of asymmetric growth of the adaxial and abaxial (upper and lower, respectively) surfaces of the cotyledon (Kang, 1979). In addition, the stronger *rol1-2* allele develops slightly shorter roots and shorter root hairs than wild-type seedlings (Diet et al., 2006).

In this work, we show that the *rol1* mutants contain a modified flavonol glycosylation profile. A detailed analysis of the *rol1-2* allele revealed aberrantions in cell shape, which result in over-sized cotyledon pavement cells that lack typical lobes and have defective trichomes. Genetic experiments suggest that it is a change in the flavonol profile that induces the observed cotyledon and trichome phenotypes. Our results suggest that the shift in flavonol abundance results in a change of auxin concentration, inducing hyponastic growth in cotyledons. In addition, the modified flavonol profile appears to have a direct effect on cell formation that is independent of its effect on the auxin concentration. This suggests that flavonols can directly interfere with cell growth processes.

Results

Flavonol accumulation is modified in rol1 mutants

For the analysis of flavonol accumulation, wild-type, *rol1-1*, and *rol1-2* seedlings were grown for six days on MS-Agar plates in a vertical orientation. At this stage of seedling development, cotyledons are fully expanded and the first true leaves are about to form. Seedlings were cut in the hypocotyl, and shoot- and root tissues were separately pooled

adjacent cell. The underlying signaling network that controls this process involves a complex activation / inactivation interaction between ROP2 and RIC1 / RIC4 (Fu et al., 2005). ROP (Rho-related GTPase of plants) proteins regulate the organization of cortical microtubules and actin microfilaments (Smith, 2003; Fu et al., 2005). Indeed, interfering with actin filament nucleation changes pavement cell shape (Frank et al., 2003; Mathur et al., 2003; Djakovic et al., 2006). Recently, the TREHALOSE-6-PHOSPHATE SYNTHASE mutant, *csp1,* was shown to cause a pavement cell phenotype, though the function of trehalose-6-phosphate in this process remains unclear (Chary et al., 2007). The importance of the cell wall in cell-shape determination is well know and is reflected by the fact that the cellulose synthase mutant *rsw1* lacks lobe formation in pavement cells, resulting in straight cell boundaries (Williamson et al., 2001).

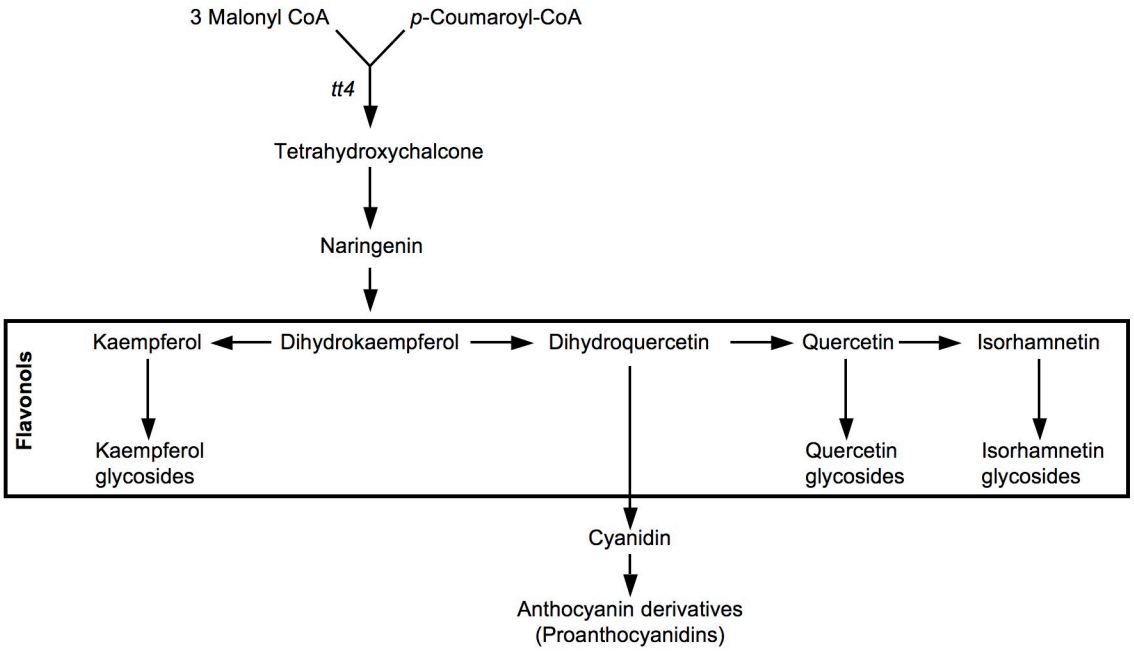

Figure 1. Biosynthesis of flavonoids in Arabidopsis.

Flavonoids are made of three molecules of Malonyl CoA and one molecule of p-Coumaroyl CoA. Flavonols are a subgroup of flavonoids and commonly consist of glycosylated kaempferol, quercetin, and isorhamnetin derivatives. transparent testa (tt) mutants of Arabidopsis are flavonoid biosynthesis mutants characterized by a change in seed color due to the absence of proanthocyanidins. The tt4 mutant is deficient in chalcone synthase, resulting in the absence of flavonoids.

and analyzed. The targeted metabolite analysis was performed by HPLC-MS, as described in the METHODS section. Most flavonol glycosides were identified by their UV-absorption spectra, MS/MS analysis, and by comparison with reference compounds of known structure. Recently published data was also used to interpret results (Kerhoas et al., 2006; Le Gall et al., 2006; Stobiecki et al., 2006; Veit et al., 1999). Flavonol levels were obtained by calculating the area below each HPLC-peak per milligram dry weight of plant material.

Figure 2A shows the elution profile of shoot extracts. Several changes were observed between wild type and the *rol1* mutants. Some flavonols were less abundant than in wild-type tissues, while others were elevated in the *rol1* mutants. Flavonol aglycones were not detected in any of the plant lines analyzed.

Fig. 2(A)

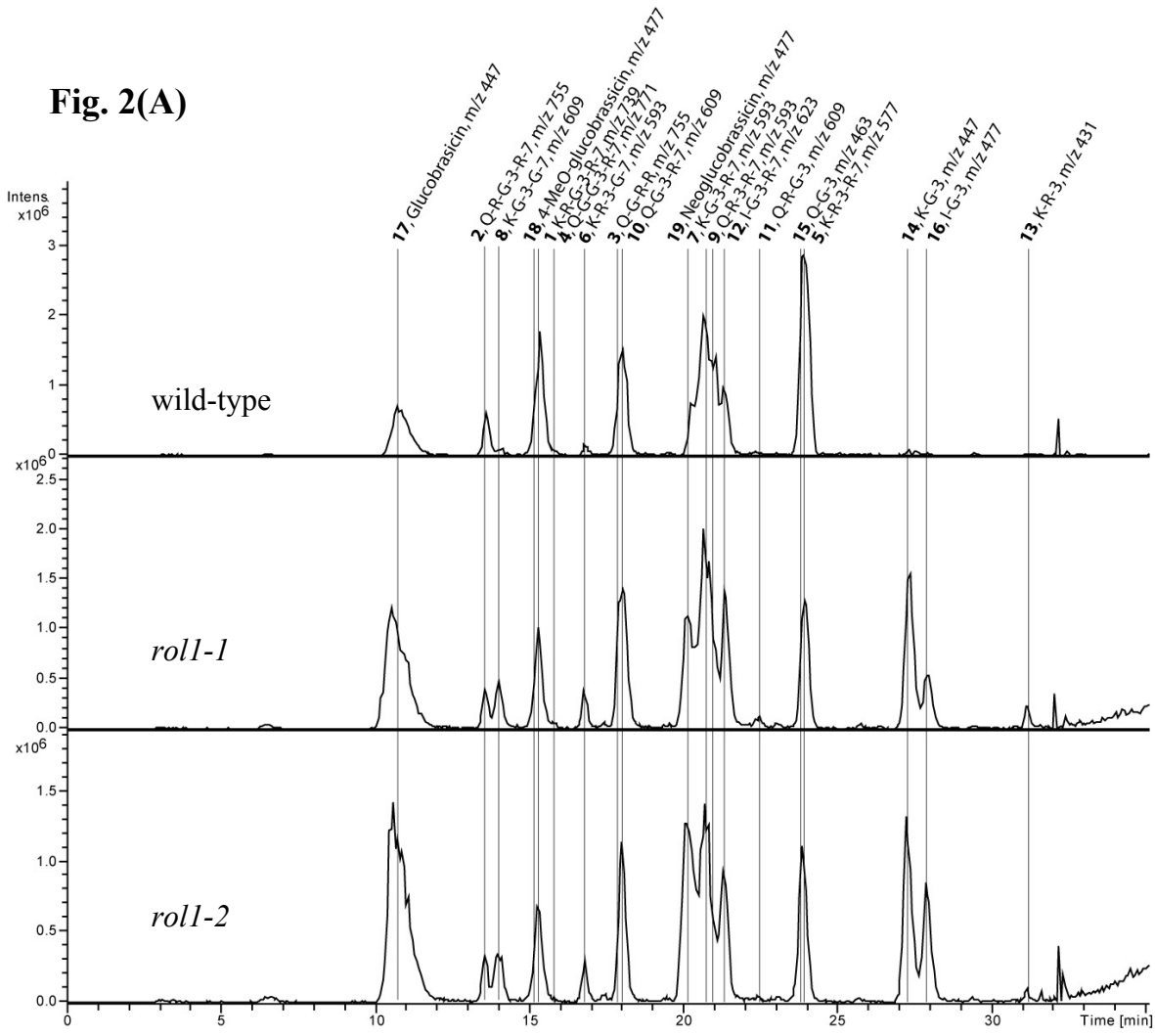

Fig. 2(B)

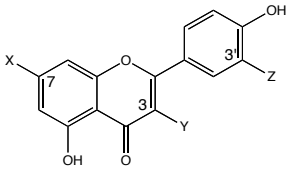

Com-pound	MW	X	Y	Z	Trivial Name	accumulation in *rol1-1* seedlings	accumulation in *rol1-2* seedlings	tissue of detection in wild-type
1	740	α-rha	α-rha(1→2)β-glc	H	K-R-G-3-R-7	0.5	0.4	shoot and root
2	756	α-rha	α-rha(1→2)β-glc	OH	Q-R-G-3-R-7	0.6	0.6	shoot and root
3	756	?	?	OH	Q-G-R-R *	0.1	0.1	mainly root
4	772	α-rha	β-glc(1→6)β-glc	OH	Q-G-G-3-R-7	1.1	0.4	mainly root
5	578	α-rha	α-rha	H	K-R-3-R-7	0.2	0.1	mainly shoot
6	594	β-glc	α-rha	H	K-R-3-G-7	2.6	2.1	mainly shoot
7	594	α-rha	β-glc	H	K-G-3-R-7	**	**	
8	610	β-glc	β-glc	H	K-G-3-G-7	4.7	4.3	shoot and root
9	594	α-rha	α-rha	OH	Q-R-3-R-7	**	**	
10	610	α-rha	β-glc	OH	Q-G-3-R-7	0.9	0.6	shoot and root
11	610	OH	α-rha(1→2)β-glc	OH	Q-R-G-3	2.7	0.8	root
12	624	α-rha	β-glc	OCH3	I-G-3-R-7	1.6	1.2	shoot and root
13	432	OH	α-rha	H	K-R-3	10	4	shoot
14	448	OH	β-glc	H	K-G-3	40	40	shoot and root
15	464	OH	β-glc	OH	Q-G-3	40	50	shoot and root
16	478	OH	β-glc	OCH3	I-G-3	34	58	mainly root

Figure 2. Flavonol accumulation is modified in *rol1* mutants.

Flavonols were extracted from Arabidopsis seedlings grown for six days in a vertical orientation. **(A)** Flavonol elution profiles obtained from HPLC-(–)-ESI-MS analyses. In order to improve the selectivity, the sums of the extracted ion chromatograms corresponding to flavonoid derivatives **1** to **16** are displayed (EIC of *m/z* 431, 447, 463, 477, 577, 593, 609, 623, 739, 755, 771). Glucobrassicin derivatives [peaks Nr. 17 (*m/z* 447), 18, and 19 (both *m/z* 477)] are non-flavonoid compounds that are listed because they show the same mass spectra as some flavonoid derivatives. **(B)** The flavonol structure is given. The groups at the C7, C3, and C3' positions are listed in the table (X, Y, Z, respectively). The flavonoid accumulation of the single components is represented by the factor of induction / repression in *rol1* mutants compared to wild type that was determined on whole-seedling extracts. The substances are numbered according to the chromatograms in **(A)**. To determine tissue-specificity of flavonol accumulation, seedlings were cut in the hypocotyl and upper (shoot) and lower (root) tissue was collected and extracted separately. Detection in mainly one tissue was defined as a ≥5 fold overaccumulation of the compound in one tissue compared to the other. Only two compounds accumulated exclusively in one tissue (**11** and **13**). K= kaempferol, Q=quercetin, I=isorhamnetin, G=Glucose, R=Rhamnose. * The exact structure of this compound could not be identified. ** The factor of induction / repression could not be determined because peak Nr. 7 and 9 are coeluting and have identical molecular weights.

Figure 2B shows the exact structure of each of the identified flavonol species and the induction/repression factor in the *rol1* mutants compared to the wild type. The two *rol1* alleles revealed a comparable profile. A reduction of up to tenfold was found in *rol1* mutants for flavonols glycosylated with several rhamnose units. Some flavonols containing single rhamnose units, such as kaempferol-3-*O*-rhamnose (K-R-3; Figure 2, peak #1), however, are increased several-fold. The clearest alteration in *rol1* mutants was found for the 3-*O*-glucosides of kaempferol (kaempferol-3-*O*-glucose; K-G-3), quercetin (quercetin-3-*O*-glucose; Q-G-3), and isorhamnetin (isorhamnetin-3-*O*-glucose; I-G-3) (Figure 2, peaks #3, 4, 5, respectively). While the first two are strongly induced, particularly in the shoot (factor of 57 to 92), I-G-3 newly accumulates in shoots and overaccumulates in roots of *rol1* mutants. One flavonol (MW 490; Figure 2, peak #6) has yet to be identified in Arabidopsis. Based on MS/MS analysis and the analysis of the *rol1-2 tt7* double mutant (see below), this flavonol is a kaempferol and therefore referred to as K-uk (unknown kaempferol). According to the literature, it may be a kaempferol-3-*O*-(6''-acetyl-glucoside), which has been found in needles of *Pinaceae* species (Slimestad, 2003).

The relative abundance of each flavonol compound in the different lines is shown in Supplemental Figure 1A. Calculating the total amounts of shoot and root flavonols revealed a decrease by 25% in the shoot of the *rol1* mutants and an increase by 30% (*rol1-1*) and 10% (*rol1-2*) in roots (Supplemental Figure 1B) compared to wild type. Since the two *rol1* alleles showed comparable changes in the flavonol profile, we decided to limit further analyses to the *rol1-2* allele, which shows a stronger phenotype (Diet et al., 2006).

Flavonoids were visualized in vivo with diphenylboric acid-2-aminoethyl ester (DPBA), a flavonoid-specific stain, which binds flavonols (Buer et al., 2007). In agreement with previous reports (Peer et al., 2001), fluorescence was found in the cotyledonary node, the root/shoot transition zone, the root elongation zone, and very faintly in trichomes of wild-type plants. In *rol1-2* mutants, increased fluorescence was detected in the root-elongation zone and in trichomes (Supplemental Figure 2). No increase in DPBA-staining was observed in the cotyledonary node. To confirm that the observed fluorescence was due to the presence of flavonoids, a *rol1-2 tt4* double mutant was generated and analyzed. *tt4* plants carry a mutation in the *CHALCONE SYNTHASE* gene and are thus blocked in the first step of flavonoid biosynthesis (Shirley et al., 1995; Figure 1). As shown in Figure 2A, the flavonol-peaks are indeed absent in *rol1-2 tt4* extracts. These plants also fail to produce fluorescence, other than a faint background staining in root tissue (Supplemental Figure 2).

Fig. S1 (A)

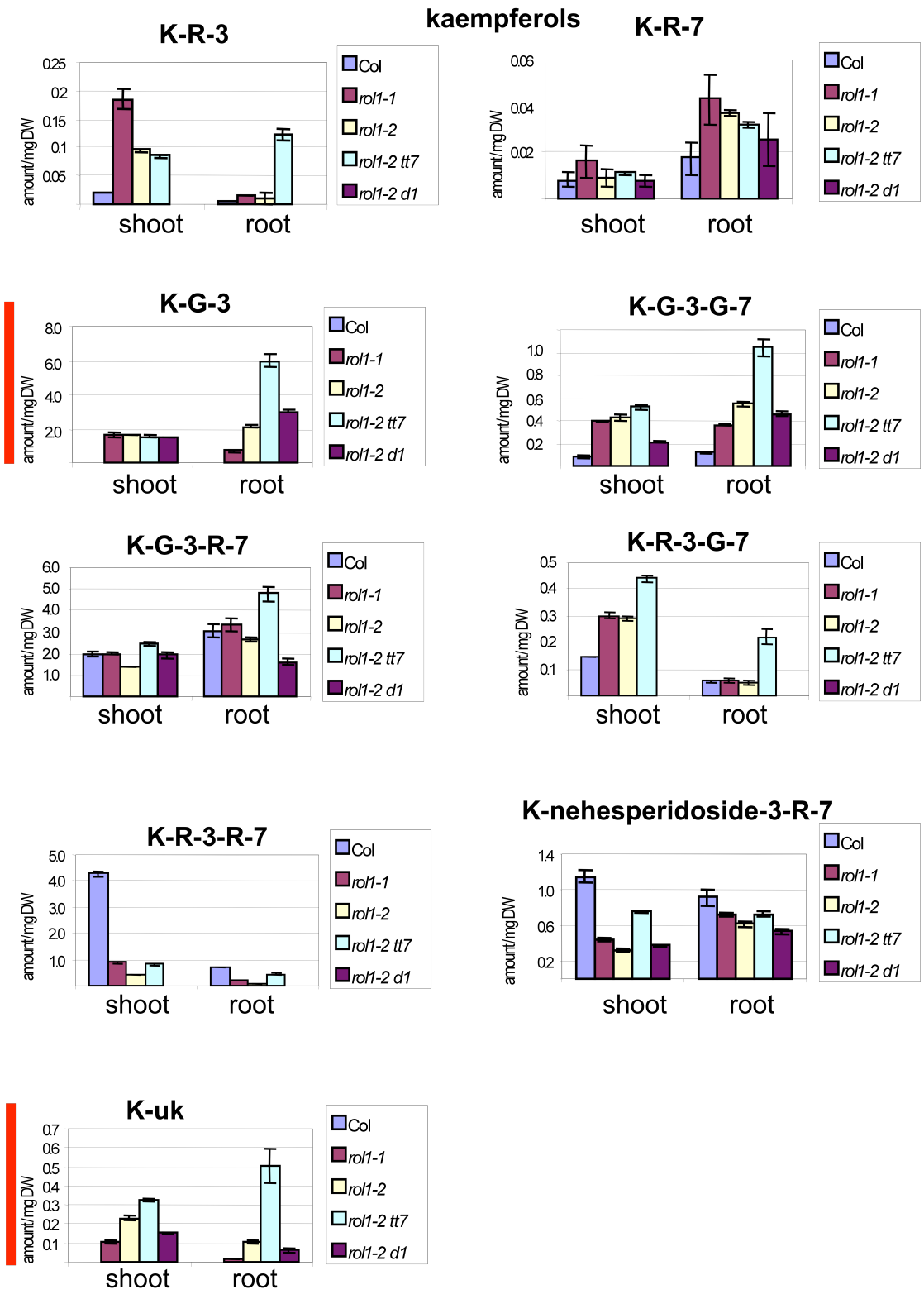
kaempferols
K-R-3
K-R-7
K-G-3
K-G-3-G-7
K-G-3-R-7
K-R-3-G-7
K-R-3-R-7
K-nehesperidoside-3-R-7
K-uk
amount/mgDW
shoot
root
Col
rol1-1
rol1-2
rol1-2 tt7
rol1-2 d1

Fig. S1 (B)

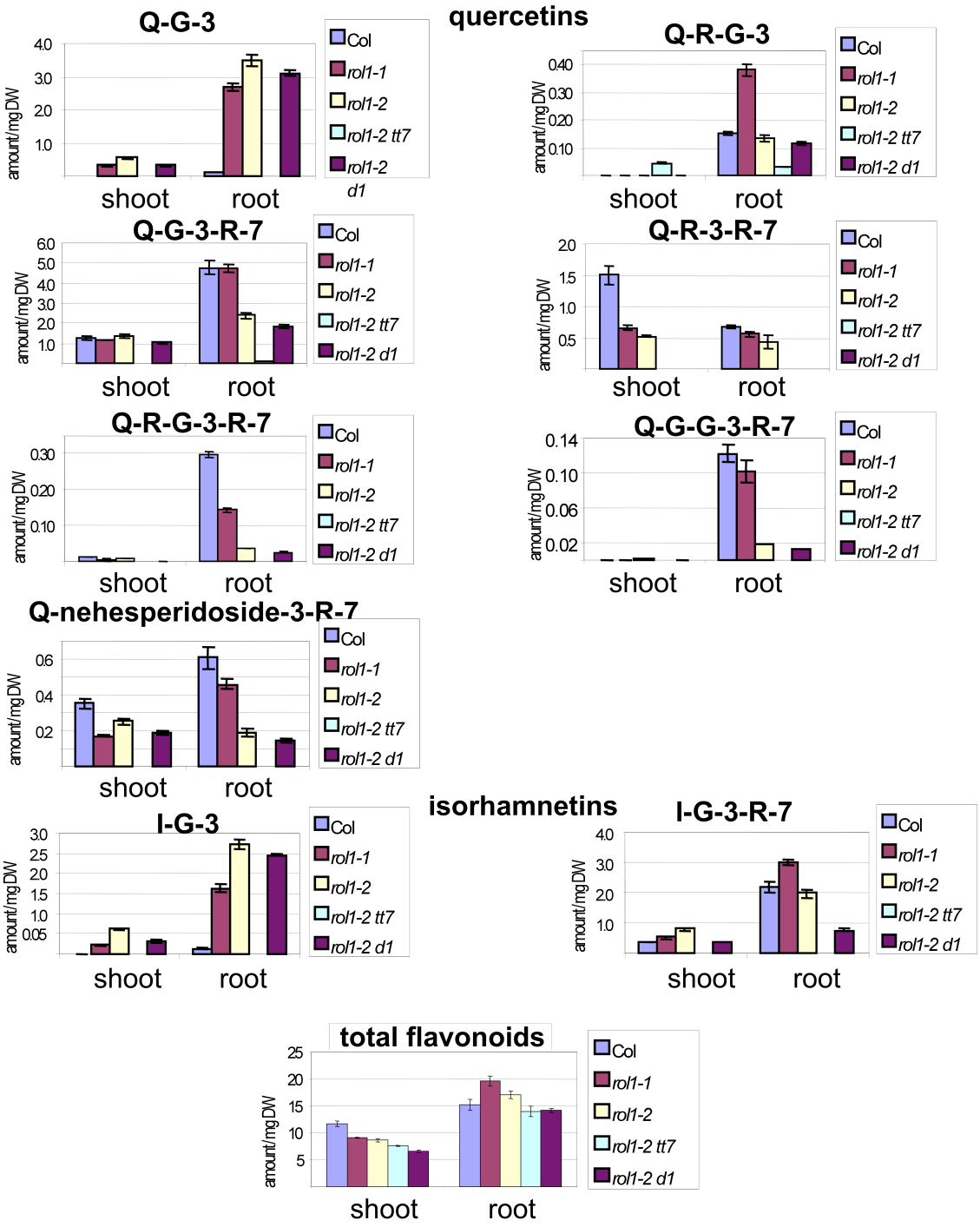

Supplemental Figure 1. Graphical representation of flavonol abundance in wild type and *rol1* mutant seedlings.

(A) The distribution of the flavonol species in shoots and roots in the different lines is shown for each identified flavonol. The amount of flavonol was defined as the area under the corresponding HPLC-peak and calculated per milligram dry weight. Note the difference in the scale, i.e. the abundance of the different flavonols. Red bar: Two obvious candidates for a function in *rol1-2*. They accumulate to higher levels in *rol1* mutants compared to the wild type and are present in all lines showing the *rol1-2* phenotype. **(B)** Total amounts of flavonols in the different lines. Means ± SE of 3 samples are shown.

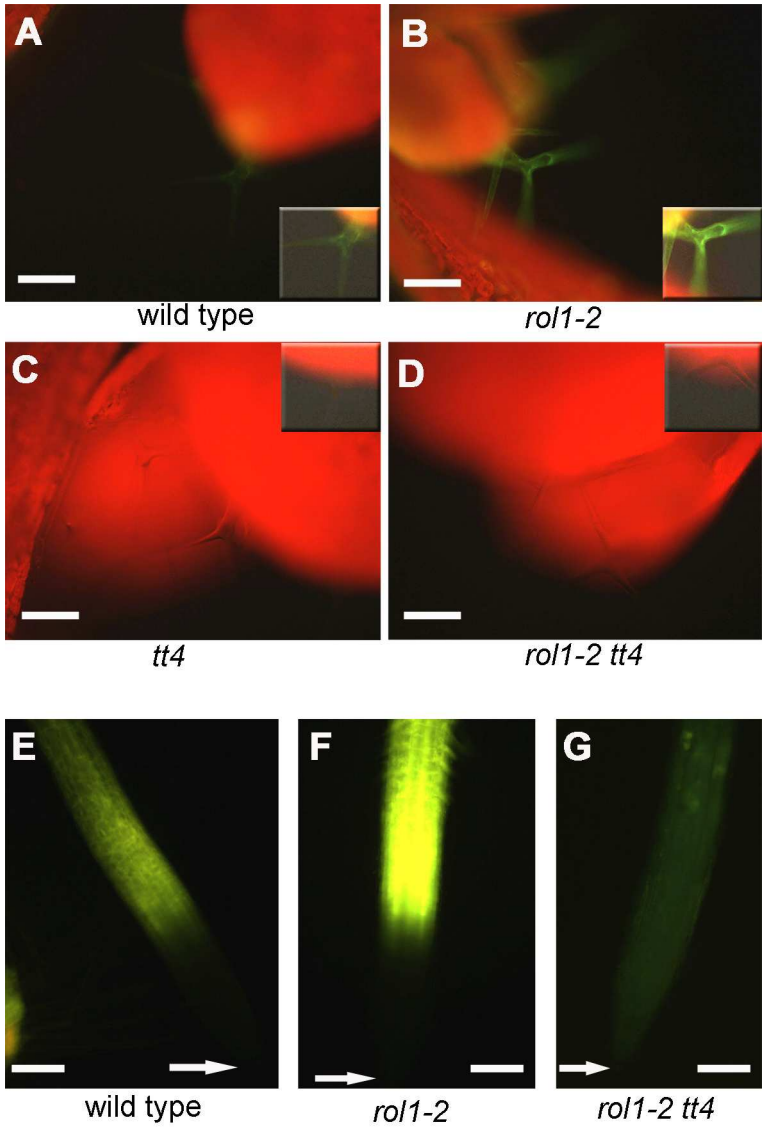

Supplemental Figure 2. Flavonoid staining by DPBA in *Arabidopsis* seedlings.

Seedling shoots [**(A)-(D)**] of wild type, *rol1-2*, *tt4*, and *rol1-2 tt4* mutants were stained with DPBA and analyzed by fluorescence microscopy. DPBA fluorescence is shown in green while the red color represents chlorophyll autofluorescence. Flavonoids are more abundant in trichomes of *rol1-2* mutants, and absent in *tt4* or *rol1-2 tt4* mutants. The insets show better visualization of trichome flavonol fluorescence. Wild type roots **(E)** show weaker fluorescence than do *rol1-2* roots **(F)** while *rol1-2 tt4* double mutant roots **(G)** reveal only background staining of the dye. The root tips are indicated by arrows. All photographs were taken at identical settings to allow comparisons in the fluorescence intensities. Bar [**(A)-(D)**] = 0.5 mm, Bar [**(E)-(G)**] = 0.5 mm To investigate the distribution of flavonoids in vivo, wild-type and *rol1-2* seedlings were stained with diphenylboric acid-2-aminoethyl ester (DPBA), which forms fluorescent complexes with flavonoids. In agreement with previous reports (Peer et al., 2001), fluorescence in wild-type plants was found in the cotyledonary node, the root/shoot transition zone, and the root elongation zone. In *rol1-2* mutants, fluorescence was strongly increased in the root and observed in trichomes, which in wild-type plants are void of DPBA-detectable flavonoids (Figure S1). No increase in DPBA-staining could be observed in the cotyledonary node.

The rol1-2 mutant develops several shoot phenotypes

rol1-2 mutants show aberrant cotyledon development, with an uneven cotyledon surface and hyponastic growth. In addition, trichomes of the first rosette leaves are strongly deformed in *rol1-2* (Diet et al., 2006; Figure 3A and 3B). The cotyledon growth phenotype was investigated in more detail by scanning electron microscopy (SEM). Compared to the wild type, the size of adaxial pavement cells is frequently increased (Figure 4A and 4B) and the typical jigsaw puzzle-like cell shape of pavement cells is absent in *rol1-2* mutants (cell borders are straight and the characteristic lobes are absent, see Figure 4C and 4D). This phenotype is restricted to the abaxial site of the cotyledon. In the SEM analysis, stomatal distribution appeared to be affected in *rol1-2* cotyledons. Stomata were therefore visualized by confocal microscopy using FM4-64. *rol1-2* plants have fewer stomata than wild-type plants (34 ± 8 per mm^2 versus 163 ± 26) and the stomata are frequently larger than those of wild type (Figure 4I and 4J).

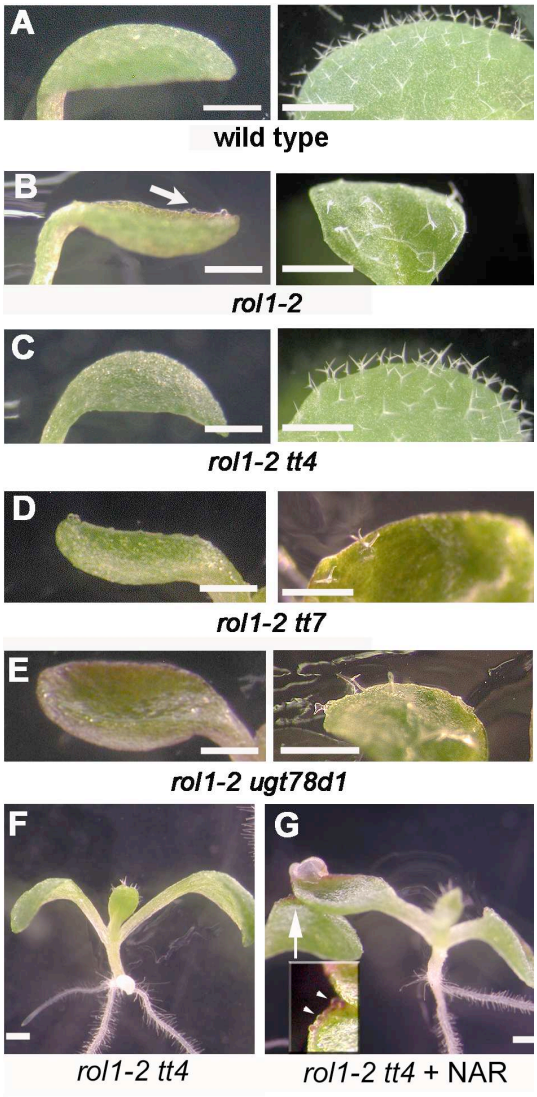

Figure 3. Aberrant cotyledon and trichome formation in *rol1-2* mutants.

(A) to **(E)** Cotyledons and leaves of 5- and 8-d-old Arabidopsis plants.

(A) Wild type.

(B) *rol1-2*. The periphery of cotyledons is bent upward, referred to as hyponastic growth. Also, the surface of *rol1-2* mutant cotyledons is rough and contains bulging epidermal cells (arrow). Trichomes are frequently deformed.

(C) The features of the *rol1-2* phenotype are suppressed by the tt4 mutation in *rol1-2 tt4* double mutants.

(D) and **(E)** No suppression of the *rol1-2* phenotype is observed in *rol1-2 tt7* **(D)** *or rol1-2 ugt78d1* **(E)** double mutants.

(F) and **(G)** The anthocyanin-less *rol1-2 tt4* mutant **(F)** is chemically complemented by naringenin **(G)**. The arrow in **(G)** indicates the area shown in the inset. Colocalization of anthocyanin and epidermal bulging is indicated by arrowheads in the inset.

Bars = 1 mm.

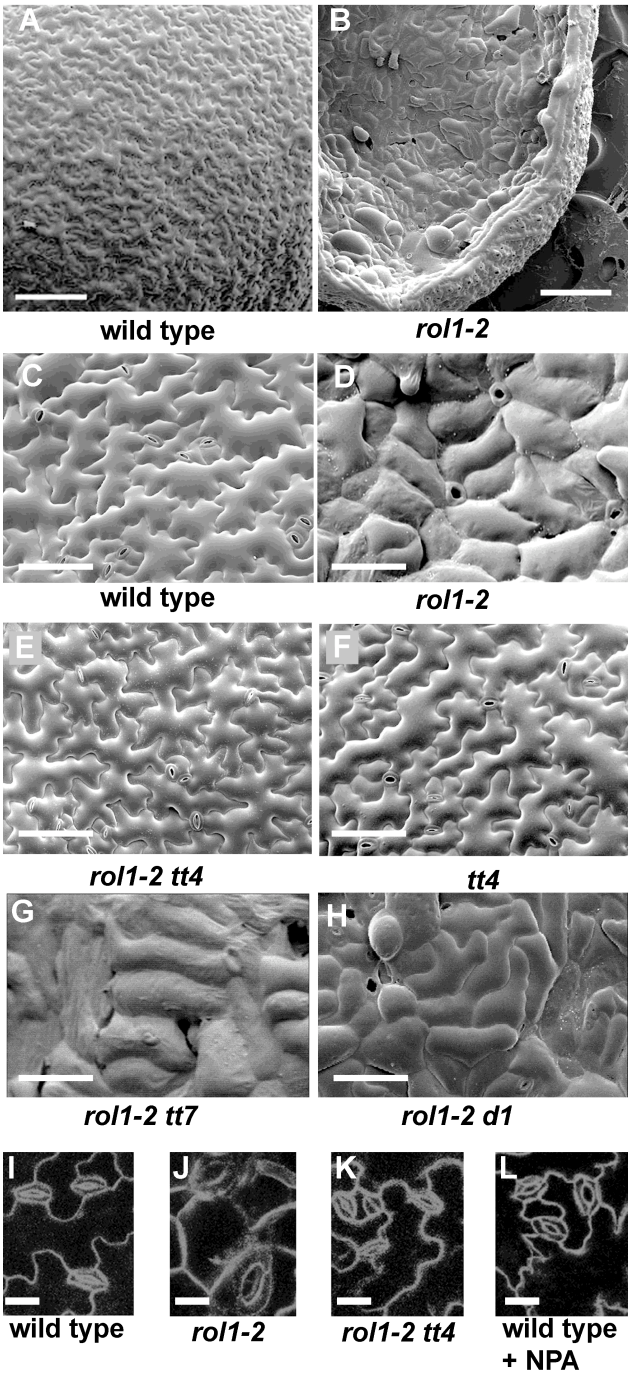

Figure 4. Pavement cell and stomata phenotypes in *rol1-2* mutants.

Scanning electron micrographs from 5-d-old cotyledons. Wild-type plants develop jigsaw puzzle–like pavement cells (**[A]** and **[C]**), whereas lobe formation is suppressed in *rol1-2* mutants (**[B]** and **[D]**), resulting in brick-like cells. Also, cells are frequently oversized compared with those in the wild type. The pavement cell phenotype induced by the *rol1-2* mutation is suppressed by the tt4 mutation **(E)**. *tt4* single mutants develop pavement cells that are indistinguishable from those in the wild type **(F)**. *tt7* and *ugt78d1* do not suppress the *rol1-2* phenotype in the corresponding double mutants (**[G]** and **[H]**). Compared with the wild type **(I)**, stomata of cotyledons are larger in *rol1-2* **(J)**, an effect that is suppressed in the *rol1-2 tt4* double mutant **(K)**. Treatment of the wild type with NPA does not change the size of stomata **(L)**.

Bars = 250 μm in **(A)** and **(B)**, 100 μm in **(C)** to **(H)**, and 20 μm in **(I)** to **(L)**.

The rol1-2 shoot phenotypes are flavonoid-dependent

To investigate the role of modified flavonoid accumulation in the development of the *rol1-2* phenotype, the flavonoid-less *rol1-2 tt4* double mutant was characterized. In the double mutant, the hyponastic growth and trichome formation phenotypes observed in the *rol1-2* single mutants were fully suppressed (Figure 3C). This indicates that the *rol1-2* mutant shoot phenotypes are related to the change in flavonol accumulation, a finding that was confirmed by SEM analysis. In *rol1-2 tt4* double mutants, pavement-cell shape is reverted

to wild type (Figure 4E). *tt4* single mutant plants also develop wild type-like pavement cells (Figure 4C and 4F). Furthermore, the size (Figure 4K) and density (142 ± 13 per mm^2) of stomata in *rol1-2 tt4* cotyledons is again comparable to wild type.

To confirm co-segregation of the *tt4* mutation with suppression of the *rol1-2* mutant phenotypes, seedlings homozygous for *rol1-2* but segregating for *tt4* were grown. Of 460 seedlings analyzed, 126 showed a lack of anthocyanin accumulation, typical of homozygous *tt4* mutants (Shirley et al., 1995), and suppression of the *rol1-2* shoot phenotypes. This corresponds to the expected 3:1 wild-type:mutant segregation of the recessive *tt4* mutation (χ^2-test, P=0.05) and indicates a close linkage between the *tt4* mutation and the locus that suppresses the *rol1-2* mutant shoot phenotypes.

In a second approach, we tested the chemical complementation of the *tt4* mutation in the *rol1-2 tt4* double mutant using naringenin, a flavonoid precursor positioned downstream of *tt4* (Figure 1; Shirley et al., 1995). Growing *rol1-2 tt4* double mutants in the presence of naringenin induced the accumulation of anthocyanin, confirming the uptake and metabolic processing of naringenin in the seedlings. At the same time, naringenin induced hyponastic growth and the irregular cell shapes characteristic of the *rol1-2* mutation (Figure 3F and 3G), indicating that the effect of the *tt4* mutation is suppressed in the presence of naringenin. Together, our genetic and chemical complementation experiments suggest that the *tt4* mutation suppresses the *rol1-2* mutation and, hence, that flavonols are involved in the development of the *rol1-2* shoot phenotype.

The rol1-2 *phenotype is modified by kaempferol derivatives*

In order to restrict flavonol accumulation more specifically, the *rol1-2* mutation was crossed into the *tt7* mutant background. The *tt7* mutant is defective in flavanone-3'-hydroxylase, which converts dihydrokaempferol to dihydroquercetin, and thus inhibits the accumulation of quercetin and isorhamnetin, while kaempferol accumulates to higher levels (Figure 1; Peer et al., 2001). The effect of *tt7* on flavonol accumulation was confirmed in *rol1-2 tt7* double mutants (Supplemental Figure 1A), which show almost no accumulation of quercetin or isorhamnetin. The increase in kaempferol accumulation is more pronounced in roots than in shoots, indicating that the *tt7* mutation might have distinct effects on the activity of the flavonoid biosynthesis pathway in these tissues. *rol1-2 tt7* seedlings develop a *rol1-2* phenotype (Figure 3D and 4G), suggesting that the *rol1-2*

phenotype-inducing flavonols are kaempferols. The *tt7* single mutant and the corresponding wild type Landsberg *erecta* do not develop a *rol1-2* phenotype (Supplemental Figure 3), thus demonstrating that the increased accumulation of kaempferols, per se, does not cause the *rol1-2* phenotype.

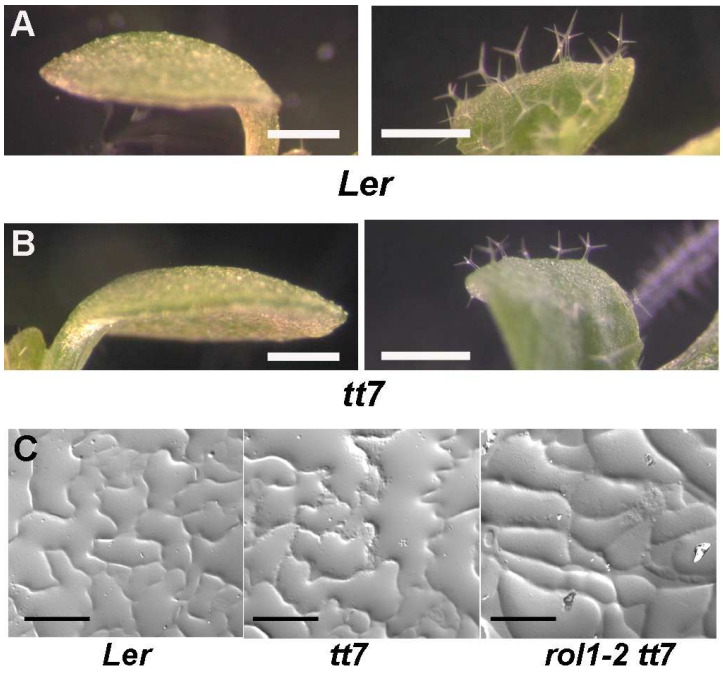

Supplemental Figure 3. The *tt7* mutation does not develop *rol1-2* like phenotypes.

Wild type Landsberg *erecta* (*Ler*) **(A)** and *tt7* **(B)** seedlings develop epinastic cotyledons and normal trichomes. Gel prints of pavement cells **(C)** reveal no difference between wild type and the *tt7* mutant. For comparison, a gel print of a *rol1-2 tt7* double mutant reveals the absence of the typical jigsaw puzzle-like cell shapes due to the *rol1-2* mutation.
Bars = 1 mm [**(A)** and **(B)**], 100 μm **(C)**.

rol1-2 was also combined with the UDP-rhamnose:flavonol-3-*O*-rhamnosyltransferase mutant *ugt78d1* (Jones et al., 2003). This double mutant contains reduced amounts of 3-*O*-rhamnosylated flavonols (Supplemental Figure 1A), but develops a *rol1-2* like phenotype (Figure 3E and 4H).

The flavonol(s) that cause the observed *rol1-2* phenotype should be more abundant in the *rol1* mutants than in wild-type plants and they should also be present in the *rol1-2 tt7* and *rol1-2 ugt78d1* double mutants. Based on these assumptions, K-G-3 and K-uk are the best candidates as causal agents for the *rol1-2* phenotype. In Landsberg *erecta* and *tt7,* these flavonols are absent or present in very small amounts compared to *rol1-2* (Figure 5).

Hence, the abundance of these two flavonol glucosides correlates with, and therefore may be responsible for the observed *rol1-2* phenotype.

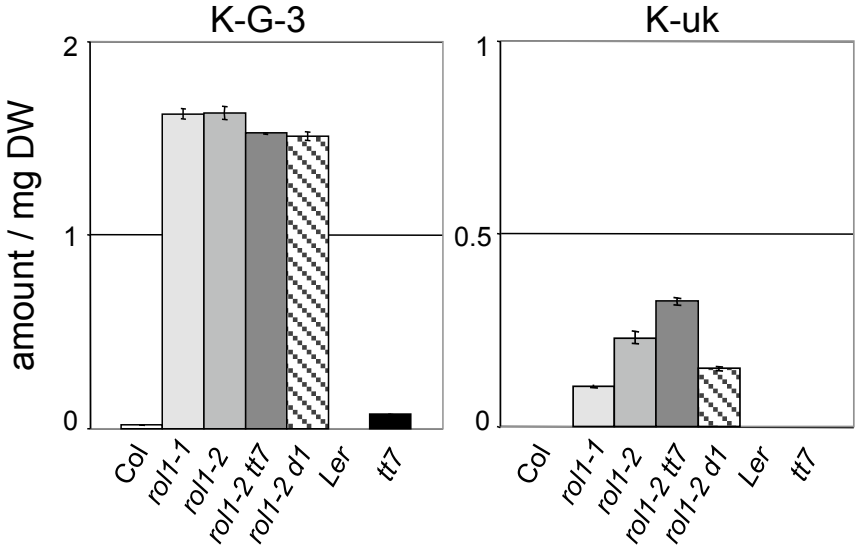

Figure 5. The abundance of K-G-3 and K-uk correlates with the rol1-2 shoot phenotype.

K-G-3 and K-uk [potentially kaempferol-3-O-(6''-acetyl-glucoside)] fulfill the predicted requirements for the flavonol species that cause the *rol1-2* shoot phenotypes. Both are found in small amounts (K-G-3) or are absent (K-uk) in the wild type (Columbia and Landsberg erecta) and *tt7* but are present in *rol1*, *rol1-2 tt7*, and *rol1-2 ugt78d1*. Mean ± SE amounts of shoot flavonols are shown (n = 3). The area under the HPLC peak was used as the measurement for the amount of the flavonols.

The modified flavonol profile of rol1-2 does not influence root-hair formation.

Suppression of the *lrx1* root-hair formation phenotype in the *lrx1 rol1-2* double mutant was attributed to *rol1-2* induced modifications in the cell wall (Diet et al., 2006). The drastic effect on cell growth caused by the modified flavonols prompted us to investigate their role in root-hair development and the suppression of *lrx1*. The *lrx1* mutant root-hair phenotype (Figure 6A and 6B; Baumberger et al., 2001) is suppressed in the *lrx1 rol1-2* double mutant, where root hairs form, though with reduced length compared to wild type (Figure 6C; Diet et al., 2006). The absence of flavonoids in the *lrx1 rol1-2 tt4* triple mutant does not influence suppression of *lrx1* through *rol1-2* (Figure 6D).

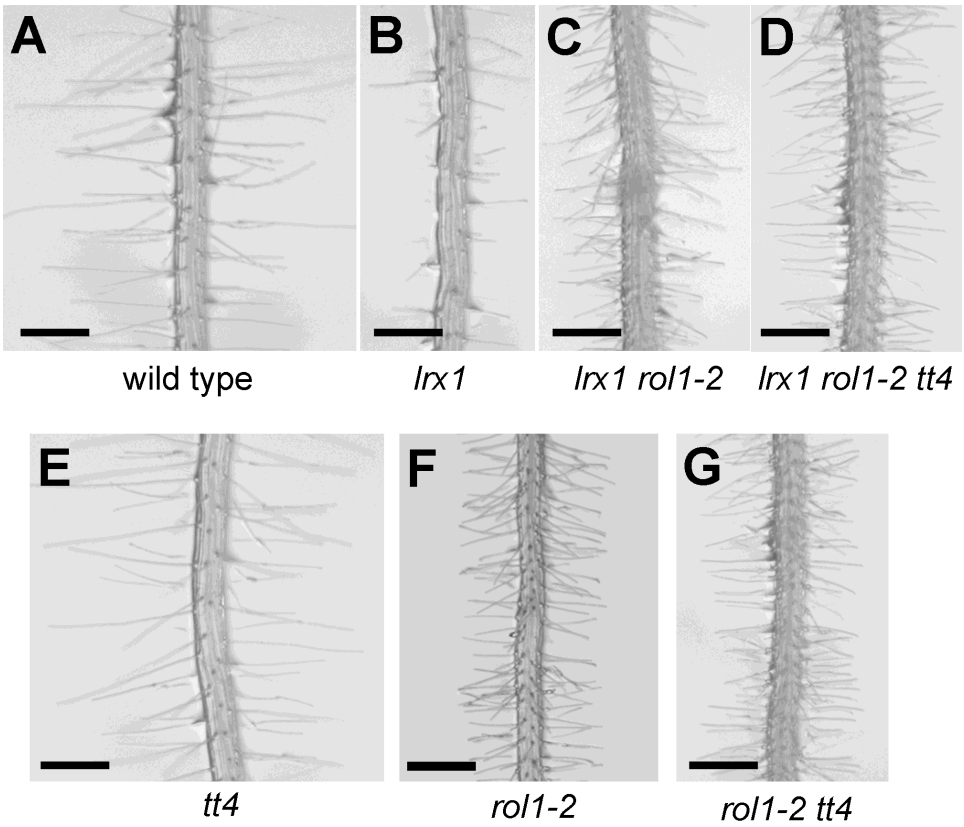

Figure 6. Flavonoid independence of root hair development.

Seedlings were grown for 5 d in a vertical orientation. The *lrx1* mutant root hair phenotype (compare **[A]** and **[B]**) is suppressed by the *rol1-2* mutation **(C)**. This suppression is not dependent on the flavonols in *rol1-2*, since the *lrx1* phenotype is also suppressed in *lrx1 rol1-2 tt4* triple mutants **(D)**. The absence of flavonoids in the *tt4* mutant does not have a significant effect on root hair formation **(E)** or on the *rol1-2* mutant phenotype (compare **[F]** and **[G]**). Bar = 0.5 mm

To investigate the effect of *tt4* on root development, the visual root-hair phenotype, root length and root-hair length and density was determined in wild-type, *rol1-2*, *tt4*, and *rol1-2 tt4* seedlings. *tt4* mutants show a wild-type-like root-hair phenotype and the *tt4* mutation does not influence the *rol1-2* root-hair phenotype (Figure 6E-G). Measuring root-hair length confirmed that neither the wild type nor *rol1-2* mutant root-hair length is influenced by the *tt4* mutation (Figure 7A). While root length is comparable between wild type and *tt4* mutants, the *tt4* mutation partially (t-test, P=0.01) suppresses the short-root phenotype of the *rol1-2* mutant (Figure 7B). The root-hair density is reflected by the length of root-hair-forming trichoblasts. *rol1-2* mutants develop shorter trichoblasts compared to wild type (Figure 7C; Diet et al., 2006), resulting in a higher root-hair density. While the length of trichoblasts of *tt4* mutants and the wild type are comparable, the *tt4* mutation partially (t-test, P=0.01) suppresses this aspect of the *rol1*-2 mutant. The same result was found for atrichoblasts, which lack root hairs (Figure 7C).

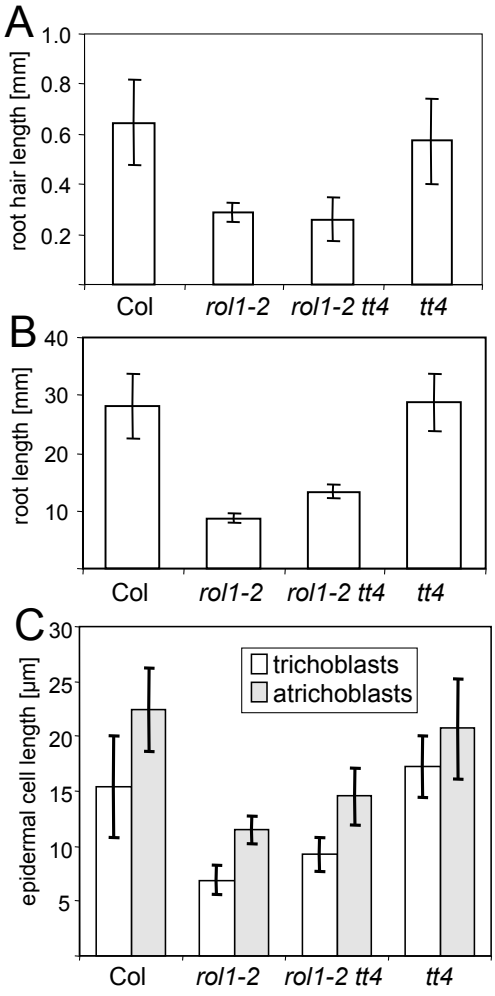

Figure 7. Quantification of the root phenotypes in the different lines.

Five-day-old seedlings were used for the quantification of root hair length **(A)**, root length **(B)**, and epidermal cell length **(C)**. Trichoblasts are root hair–forming root epidermal cells, and atrichoblasts are root hair–less root epidermal cells. Means ± SE are shown (n = 25). Col, Columbia wild type.

Hence, the increase in root length of *rol1-2 tt4* double mutants compared to *rol1-2* is paralleled by an increased length of the root epidermal cells. Together, these results indicate that the root phenotype of *rol1-2*, including the suppression of the *lrx1* phenotype, is largely determined by the effect of the *rol1-2* mutation on the cell-wall structure. The modified flavonol profile of *rol1-2* seedlings has a small but significant influence on root development.

Auxin levels are increased in rol1-2 mutants

Flavonols are known to be negative regulators of auxin transport (Buer and Muday, 2004; Peer et al., 2004). In order to establish whether the modified flavonol profile in *rol1-2* mutants influences auxin distribution, we measured free auxin concentrations in cotyledons and roots of six-day-old seedlings. As shown in Figure 8A, the amount of auxin was increased in cotyledons of *rol1-2* mutants compared to that of wild type plants, and was restored to wild-type levels in *rol1-2 tt4* double mutants. In the roots of the same plants, no significant changes in auxin levels were observed.

These results indicate that the increased levels of auxin in *rol1-2* shoots correlate with the observed mutant phenotypes. To investigate this further, we inhibited auxin transport using 1-*N*-naphthylphthalamic acid (NPA) to determine whether this could phenocopy the *rol1-2* mutation. Wild type seedlings grown for six days in the presence of 5 μM NPA developed hyponastic cotyledons (Figure 8B), mimicking the effects of the *rol1-2* mutation. Trichome and pavement cell shape were not affected by this treatment (Figure 8B and 8C), neither was the size of the stomata (Figure 4L). However, the density of stomata was reduced (i.e.119 ± 10 per mm^2 for treated versus 163 ± 26 per mm^2 for untreated seedlings), yet this reduction in density was not to the same degree as that observed in *rol1-2* (34 ± 8 per mm^2). These results suggest that the increase in auxin concentration affects stomatal density, while having no effect on the shape of pavement cells, trichomes, or the size of stomata. In a control experiment using Columbia wild type seedlings transformed with the auxin-sensitive *DR5*:*GUS* construct (Ulmasov et al., 1997), treatment with 5 μM NPA resulted in hyponastic cotyledons and strongly increased GUS activity when compared to un-treated sibling plants (Supplemental Figure 4).

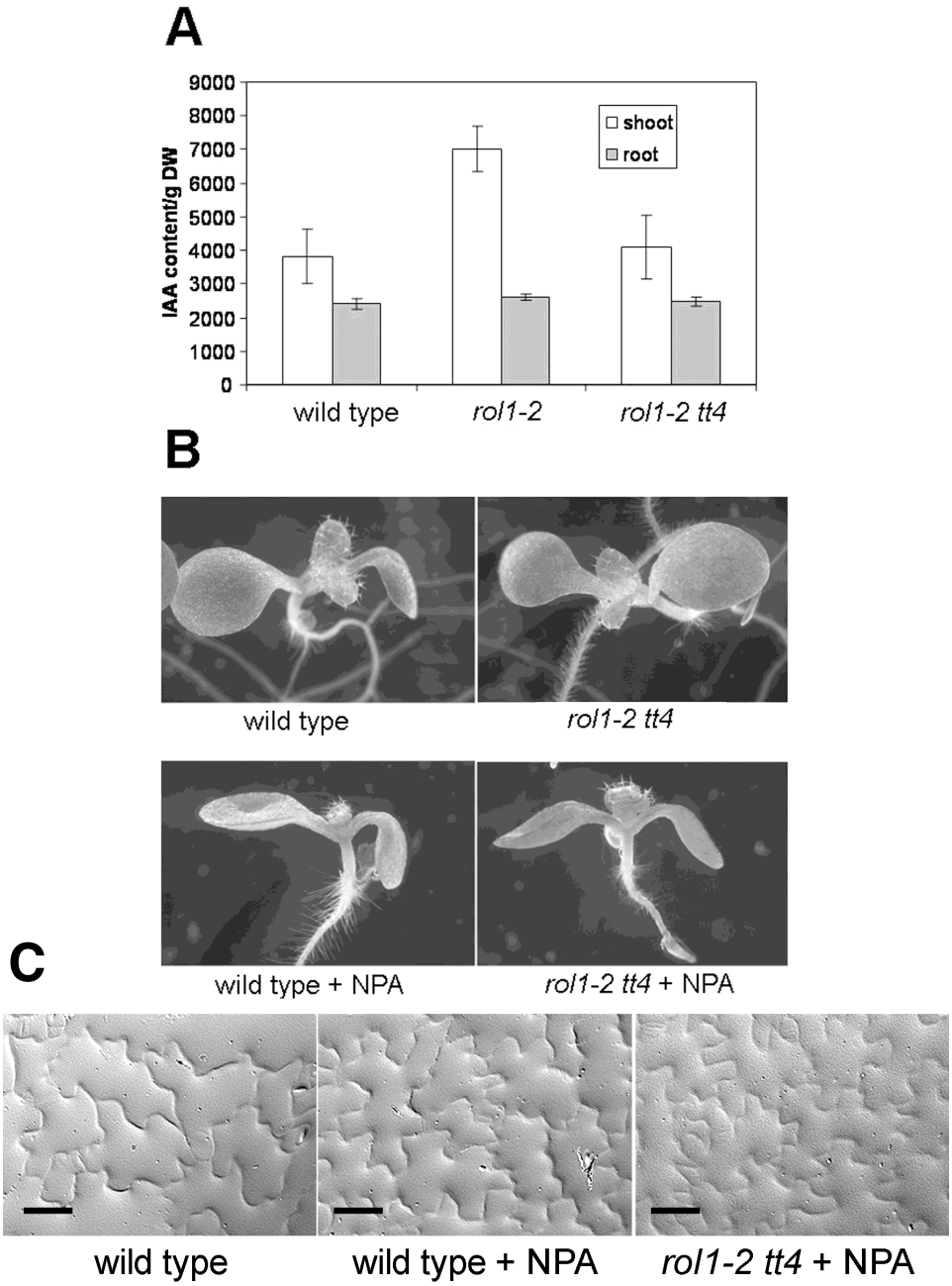

Figure 8. Auxin levels are modified in the *rol1-2* mutant.

(A) Auxin concentration in the different plant lines was measured for shoots and roots of 6-d-old seedlings. Means ± SE are shown (n = 3). The *rol1-2* mutation causes a significantly increased concentration of auxin in the shoot compared with the Columbia wild type. This effect is reversed by the presence of the *tt4* mutation. DW, dry weight.

(B) The hyponastic growth of *rol1-2* cotyledons can be mimicked by growing wild-type or *rol1-2 tt4* plants on 5 mM NPA (an auxin transportinhibitor).

(C) NPA does not influence pavement cell shape in wild-type or *rol1-2 tt4* plants. Gel prints taken from the adaxial side of cotyledons are shown.

Bars = 100 µm

To determine whether alterations in pavement cell shape and trichome formation, in *rol1-2* mutant plants, are caused by the combination of the effect of the *rol1-2* mutation on the cell-wall structure (Diet et al., 2006) and auxin concentration, *rol1-2 tt4* double mutants were grown in the presence of 5 μM NPA. The NPA treatment of these double mutants induced hyponastic cotyledons, but did not affect trichome development or pavement cell shape (Figure 8B and 8C). These data suggest that the hyponastic cotyledon phenotype of *rol1-2* mutants results from increased auxin levels caused by the altered flavonol profile of these plants. These changes to the flavonol profile affect trichome and pavement cell shapes, through an unknown mechanism, independent of auxin.

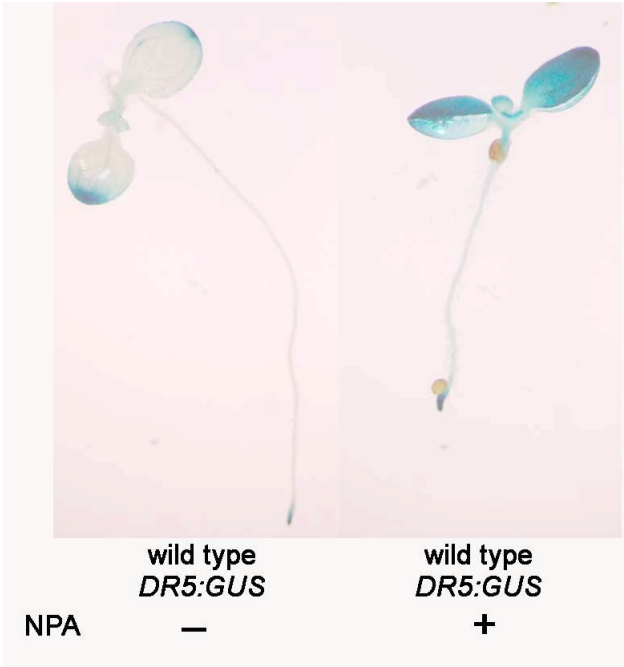

Figure S4. Effect of NPA on seedling development and *DR5*:*GUS* activity.

Wild-type seedlings containing the auxin-sensitive *DR5*:*GUS* reporter construct were grown with (right) or without (left) 5 μM NPA in a vertical orientation and stained for GUS activity. In the presence of NPA, seedlings show hyponastic growth and strongly increased GUS activity.

Discussion

The *Arabidopsis UDP-L-RHAMNOSE SYNTHASE* mutant alleles of *rol1* are affected in the flavonol glycosylation profile. Compared to wild type, *rol1* mutants contain strongly reduced amounts of flavonols glycosylated with multiple rhamnose units, while flavonols with single rhamnose units are, sometimes, even more abundant in *rol1* mutants. The concomitant strong increase in mono-glucosylated flavonols in *rol1* seedlings might be a compensatory effect of the limited rhamnose availability. The metabolite analysis suggests that flavonol glycosylation is altered with preferential conjugation at the C3-position and a redirection towards glucosylation. Compared to the wild type, there is a reduction in total amounts of flavonols in the shoots and an increase in the roots of the *rol1* mutants. The increase of DPBA-induced fluorescence in *rol1-2* trichomes seems to be at odds with the reduced amounts of flavonols in the shoot. This discrepancy can be explained by the small number of cells represented by trichomes compared to the total number of cells in the shoot The increased amounts may reflect a difference in the biosynthesis or turn-over rate of different flavonol species. Alternatively, flavonols may accumulate differentially in certain tissues by a directed transport mechanism (Buer et al., 2007). The possibility that the *rol1-2* phenotype is induced by a non-flavonoid compound that is modified as a secondary indirect effect of *rol1-2* can not be ruled out. However, the suppression of *rol1-2* by *tt4* and chemical complementation by naringenin, makes this scenario less plausible. Our data suggest that changes in the flavonol conjugation pattern in *rol1-2*, i.e. an increase of one or several flavonol species, may interfere mainly with shoot development, while the complete removal of these conjugates may allow the plant to resume normal shoot development. Even though there is a measurable effect of the flavonols on *rol1-2* root development, this process appears to be predominantly influenced by the modified cell-wall composition of *rol1-2* (Diet et al., 2006). Indeed, cell walls are known to be a key determinant of cell expansion (Martin et al., 2001).

The changes in the pavement cell shape are only observed on the adaxial side of cotyledons, whereas the abaxial side appears to be unaffected. This may be due to overlapping expression patterns of the (assumed) functionally redundant genes *RHM1* (i.e. *ROL1*) to *RHM3* (Reiter and Vanzin, 2001). A very similar pavement cell phenotype is restricted spatially to the adaxial side of cotyledons, in the ROP-interacting protein mutant

icr1 (Lavy et al., 2007), suggesting a coordinated regulation of this process. It is an attractive hypothesis that under natural conditions, plants have the potential to modify the flavonol glycosylation profile as a mean to modulate growth and development. Interestingly, the absence of flavonoids appears to have no significant effect on cell growth or cell shape in Arabidopsis. This is in contrast to other plant species such as maize, petunia, or tomato, in which flavonoid deficiency leads to aberrant pollen tube growth, root hair growth, pavement cells, and stomata density (Mo et al., 1992; Liu-Gitz et al., 2000; Taylor and Grotewold, 2005; Schijlen et al., 2007).

The rol1-2 phenotype is modified via auxin-dependent and –independent processes

Auxin is a phytohormone involved in a plethora of plant developmental processes. Modifying auxin transport directly affects plant growth (Friml, 2003). The *rol1-2* mutation causes an increase in auxin concentration in cotyledons, which induces hyponastic growth and a reduction in stomatal density. This conclusion is based on the finding that treatment of wild type plants with the auxin transport inhibitor NPA can at least partly mimic the *rol1-2* mutant phenotype. A hyponastic growth phenotype is also found in the *Arabidopsis* mutants *msg1* and *cnr1* that are both impaired in their auxin response (Watahiki and Yamamoto, 1997; Laxmi et al., 2006). Although the influence of auxin on stomata distribution is known (Vandenbussche and Vanderstraaten, 2007), the stomatal density is much more affected in *rol1-2* than in the NPA-treated wild type. This suggests that flavonols also play an auxin-independent role in the patterning of stomata. The *tt4* mutation, which blocks flavonoid biosynthesis (Shirley et al., 1995), neutralizes the effect of *rol1-2* on auxin distribution and suppresses the *rol1-2* cotyledon phenotype. Auxin transport has been shown to be negatively regulated by flavonols and is increased in *tt4* mutants when compared to wild type (Jacobs and Rubery, 1988; Brown et al., 2001; Buer and Muday, 2004; Peer et al., 2004). Recent experiments have shown that unglycosylated kaempferol and quercetin are particularly able to compete with the auxin transport inhibitor NPA for a high affinity-binding site found in a protein complex containing AtPGP1, AtPGP2, and AtMDR1/AtPGP19. Among these proteins a role in auxin transport for AtPGP1 and AtMDR1/AtPGP9 has been demonstrated (Noh et al., 2001; Murphy et al., 2002; Geisler et al., 2005; Multani et al., 2003). Flavonols are likely then to directly modulate auxin transport, a process that is reduced in the kaempferol over-accumulating mutant *tt7* (Peer et al., 2004). It is possible, therefore, that the change in auxin

concentration observed in *rol1-2* is caused by kaempferol-induced modulation of auxin transport.

Our data indicate that the aberrant size of stomata, pavement cell shape, trichome formation, and part of the stomatal density phenotype in *rol1-2* plants is not caused by modified auxin distribution, but rather flavonols play a role in auxin-independent cell growth and development.

The observed mutant phenotypes are specific for rol1-2

A number of flavonoid accumulation mutants have been described (Lepiniec et al., 2006). There are no reports of *rol1-2* -like phenotypes for *tt* mutants, suggesting that the aberrant development of *rol1-2* seedlings is induced by the modified flavonol glycosylation profile or the combination of aberrant cell-wall development (Diet et al., 2006) and the modified flavonol profile. K-G-3 and K-uk are the two flavonol glycosides whose accumulation in shoots correlates with the development of the *rol1-2* phenotype. In lines developing a wild-type shoot phenotype, they are present in very low amounts or not at all, respectively. While K-G-3 (kaempferol-3-*O*-glucose) has been identified in Arabidopsis, K-uk, might be kaempferol-3-*O*-(6''-acetyl-glucoside) that has so far only been found in needles of *Pinaceae* species (Slimestad, 2003). Unfortunately, it is not possible to provide these flavonols exogenously since glycosylated flavonols are not taken up by the plant (Klein et al., 2000). It is not possible, therefore, to define these flavonols as the *rol1-2* phenotype-inducing compounds. It is possible that unglycosylated kaempferol, present in amounts below the detection limit, is the biologically active compound. The turnover-rate of K-G-3 and K-uk might be different from other kaempferol glycosides, leading to abnormal levels of free aglycone kaempferol, which in turn affects plant development.

The mechanism(s) by which the flavonol(s) modify cell growth remains to be elucidated. A number of processes can be influenced by flavonoids (Peer and Murphy, 2006). Here, we could show a change in shoot auxin concentration and provide evidence for an auxin-independent mechanism. One interesting aspect is the function of flavonoids in ROS homeostasis (Peer and Murphy, 2006), since ROS are known to influence cell growth (Gapper and Dolan, 2006). In mammalian cell systems, flavonoids have been shown to interfere with actin (Peer and Murphy, 2006). This is of interest since mutations affecting the actin cytoskeleton in Arabidopsis and maize have been shown to result in aberrant

pavement cells (Frank et al., 2003; Mathur et al., 2003; Djakovic et al., 2006). Having established that flavonols can interfere with cell development it will be necessary to unravel the mechanisms by which they influence these processes.

Methods

Plant material and growth conditions

The *lrx1*, *rol1*, *tt4* (*2YY6* allele), and *ugt78D1* mutants are Columbia accessions and *tt7* is a Landsberg *erecta* accession. These lines are described elsewhere (Shirley et al., 1995; Baumberger et al., 2001; Jones et al., 2003; Diet et al., 2006). The *2YY6* allele of *tt4* contains a *max4* mutation which affects auxin-dependent processes (Bennett et al., 2006). Using a molecular marker (see below), *MAX4 tt4* single mutants were selected in the F2 generation of a back-cross with a Columbia plant. Molecular markers for all mutations (see below) were used to establish the different lines used in this study. For *tt4* and *tt7*, the lack of anthocyanin staining in young seedlings and the yellow seed color were used as visual markers for selecting homozygous mutants, which were confirmed using molecular markers.

For growth of plants in sterile conditions, seeds were surface sterilized with 1% sodium hypochlorite, 0.03% Triton X -100, stratified 3-4 days at 4°C, and grown for 5 days on half-strength MS-medium containing 0.6% Phytagel (Sigma), 2% sucrose, 100 mg/l myo-inositol with a 16 h light / 8 h dark cycle at 22°C. For crosses and propagation of the plants, seedlings were transferred to soil and grown in growth chambers with a 16 h light / 8 h dark cycle at 22°C.

For the chemical complementation of the *rol1-2 tt4* double mutant, seedlings were grown for 7 days on agar plates as described above, complemented with 30 μM naringenin, in a horizontal orientation. Since this amount of naringenin is not fully soluble in water, the exact final concentration in the agar-medium is not certain.

Molecular markers for **tt4, tt7***, and* **max4**

Molecular markers for *lrx1* and *rol1-2* were previously described (Diet et al., 2004; 2006). The point mutations in *tt4*, *tt7*, and *max4* were confirmed by amplification of genomic DNA, comparing mutants to the wild type DNA. Based on this information, CAPS

markers could be established for all mutations. For *tt4* and *max4*, point mutations had to be introduced in one primer (underlined positions) to create a restriction site polymorphism. *tt4*: *tt4_F* CCAACAGTGAACACATGACCGAC and *tt4_R* GTTTCCGAATTGTCG ACTTAGCGC; digested with *Eco* 47III.
tt7: *tt7_F* CAAACCCAACACTATGGCAACTC and *tt7_R* GTTTGAAATCTTCGAGA GCTTTAG; digested with *Mse* I.
max4: max4_F GCGGGTGAGGTGTCGAAGTGGTACGT and max4_R AACCATCCATAAACTATGATCTAC; digested with *Sna* BI.

Microscopy and root measurements

Light microscopic observations were made using a Leica stereomicroscope MZ125. For measurements of root epidermal cells, pictures were taken of fully elongated root sections of 6-day-old seedlings by DIC microscopy using an axioplan microscope (Zeiss, Jena, Germany). Low temperature SEM was performed as described in Baumberger et al. (2001).

Gel prints of epidermal cells were produced following an established protocol (Horiguchi et al., 2006), and observed by DICP microscopy using a Leica DMR microscope.

For root length and cell length measurements, seedlings were grown in a vertical orientation for 5 days. For root length, 25 seedlings per line were used. For root hair, trichoblast, and atrichoblast measurements, at least 25 cells originating from at least 4 different seedlings were used.

GUS- and DABP-staining

GUS staining was performed in 50 mM sodium phosphate pH 7.0, 10 mM EDTA, 0.5 mM $K_3Fe(CN)_6$, 0.5 mM $K_4Fe(CN)_6$, 0.1% Triton X-100, and 1 mM 5-bromo-4-chloro-3-indolyl-β-D-glucuronic acid between 2 h and 16 h at 37°C.

Flavonoids were visualized by the fluorescence of flavonoid-conjugated DPBA after excitation with blue light (Peer et al., 2001). Plants were grown for six days prior to staining. Fluorescent staining of whole seedlings was performed according to Buer and Muday (2004). Fluorescence was achieved by excitation with FITC filters (450 to 490 nm, suppression long pass 515 nm) on a Leica DMR fluorescence microscope and 10X or 20 X objectives. Digital images were captured with a Leica DC300 F charge coupled device (CCD) camera.

Flavonoid analysis and auxin measurement

For the analysis of the flavonol accumulation profile, seedlings were grown in a vertical orientation for six days on half-strength MS as described above. One hundred intact seedlings were cut in the hypocotyl region and roots and shoots pooled separately, frozen in liquid nitrogen and lyophilized to determine the dry weight. The dried material was incubated in 500 µl 80% methanol overnight at 4°C and subsequently macerated with a pestle, followed by vigorous vortexing. After pelleting the cell debris by centrifugation, the supernatant was transferred to a fresh tube and evaporated in a speed-vac centrifuge, with the temperature being limited to a maximum of 43°C. After evaporation, the pellet was resuspended in 100 µl fresh 80% methanol and used for analysis.

Flavonoid derivatives used as reference were commercially available (I-G-3, Q-G-3; Extrasynthese), or obtained from Dr. Veit (K-G-3, K-G-3-G-7, K-G-3-R-7, Q-R-G-3-R-7).

The flavonoid profile analyses were performed by HPLC-MS on an Agilent 1100 HPLC system (Agilent Technologies) fitted with a HTS PAL autosampler (CTC Analytics), and an ESQUIRE-LC ion trap mass spectrometer (Bruker Daltonics). Chromatographic conditions: Nucleosil 100-3 C18 column (3 µm, 2 x 250 mm, Macherey-Nagel); flow rate 0.170 mL min-1. Mobile phase: gradient within 25 min from 10 to 25% of solvent B, and then within 10 min from 25 to 70% of B (solvent A: 0.1% (v/v) HCOOH in H_2O), solvent B: 0.1% (v/v) HCOOH in MeCN). MS conditions: Nebulizer gas (nitrogen) 40 psi, dry gas (nitrogen) 9 l/min, dry temperature 300°C, HV capillary 4000 V, HV EndPlate offset -500 V, capillary exit -100 V, skimmer1 -28.9 V, and trap drive 53.4. The electrospray MS were acquired in the negative mode, at normal resolution (0.6 u at half peak height), under ion charge control conditions (ICC = 10'000) in the mass range from m/z 100 to 1000. MS/MS experiments were performed at 4u isolation width, the fragmentation cut-off set by "fast calc", and 0.9V fragmentation amplitude in the "SmartFrag" mode.

For auxin measurement, 250 mg root or hypocotyl/cotyledon tissue was collected, frozen in liquid nitrogen, macerated, suspended in 100% methanol, briefly warmed to 70°C, and kept for 30 min with continuous gentle shaking. Prior to warming to 70°C, 100 pmol $[^2H]_2$-IAA was added as the internal standard. After centrifugation, the pellet was dried to determine the dry weight and the supernatant was used for auxin quantification. The GC-MS/MS analysis of IAA contents was carried out according to Müller et al. (2002). In brief, the samples were pre-cleaned by microscale solid-phase extraction on custom-made

cartridges containing a silica-based aminopropyl matrix. After application of the samples and washing the microcolumn with 250 µL $CHCl_3$:2-propanol = 2:1 (v/v), the IAA fraction was eluted twice with 200 µL diethyl ether containing 2% acetic acid. Thereafter, the samples were dried, re-dissolved in 20 µL methanol, and treated with ethereal diazomethane. Subsequently samples were transferred to autosampler vials and excessive diazomethane and solvent was removed in a gentle stream of nitrogen. The methylated samples were then taken up in 10 µL of chloroform. Aliquots of 1 µL of each sample were injected into the GC-MS system for separation and mass fragment analysis using the autosampler and system quoted in the following. All spectra were recorded on a Varian Saturn 2000 ion-trap mass spectrometer connected to a Varian CP-3800 gas chromatograph equipped with a CombiPal autoinjector (Varian).

Acknowledgments

We would like to thank Dr. A. Schaeffer for the *ugt78d1* mutant, Dr. Markus Geisler for $[^2H]_2$-IAA, and Dr. Heller (GSF, Munich) and Dr. Veit (Kaufering) for providing us with flavonol standards that were invaluable for the flavonol structure analysis. We also thank Dr. Celia Jäger-Baroux, Petra Düchting, and Barbara Weder for technical assistance and Dr. Mark Curtis for critical reading of the manuscript. This work was supported by the Swiss National Science Foundation grants No 31-61419.00 and 3100A0-103891 (C.R., R.-M.L., and A.D.), 3100A0-116051 (M.K.), the SNF-NCCR “Plant Survival” grant of Prof. Dr. E. Martinoia (D.S.), the Julius-Klaus Stiftung (R.-M.L.) and the Forschungskommission der Universität Zürich (B.M.K.).

References

Baumberger, N., Ringli, C., and Keller, B. (2001). The chimeric leucine-rich repeat/extensin cell wall protein LRX1 is required for root hair morphogenesis in *Arabidopsis thaliana*. Genes Dev. **15,** 1128-1139.

Bennett, T., Sieberer, T., Willett, B., Booker, J., Luschnig, C., and Leyser, O. (2006). The Arabidopsis MAX pathway controls shoot branching by regulating auxin transport. Curr. Biol. **16,** 553-563.

Bolte, S., Talbot, C., Boutte, Y., Catrice, O., Read, N.D., and Satiat-Jeunemaitre, B. (2004). FM-dyes as experimental probes for dissecting vesicle trafficking in living plant cells. Journal of Microscopy-Oxford **214,** 159-173.

Bovy, A., Schijlen, E., and Hall, R.D. (2007). Metabolic engineering of flavonoids in tomato (Solanum lycopersicum): the potential for metabolomics. Metabol. **3,** 399-412.

Brown, D.E., Rashotte, A.M., Murphy, A.S., Normanly, J., Tague, B.W., Peer, W.A., Taiz, L., and Muday, G.K. (2001). Flavonoids act as negative regulators of auxin transport in vivo in Arabidopsis. Plant Physiol. **126,** 524-535.

Buer, C.S., and Muday, G.K. (2004). The *transparent testa4* mutation prevents flavonoid synthesis and alters auxin transport and the response of Arabidopsis roots to gravity and light. Plant Cell **16,** 1191-1205.

Buer, C.S., Muday, G.K., and Djordjevic, M.A. (2007). Flavonoids are differentially taken up and transported long distances in Arabidopsis. Plant Physiol. **145,** 478-490.

Carpita, N.C., and Gibeaut, D.M. (1993). Structural models of primary cell walls in flowering plants: consistency of molecular structure with the physical properties of the walls during growth. Plant J. **3,** 1-30.

Cassab, G.I. (1998). Plant cell wall proteins. Annu. Rev. Plant Physiol. Plant Mol. Biol. **49,** 281-309.

Chary, S.N., Hicks, G.R., Choi, Y.G., Carter, D., and Raikhel, N.V. (2008). Trehalose-6-phosphate synthase/phosphatase regulates cell shape and plant architecture in Arabidopsis. Plant Physiol. **146,** 97-107.

Debeaujon, I., Nesi, N., Perez, P., Devic, M., Grandjean, O., Caboche, M., and Lepiniec, L. (2003). Proanthocyanidin-accumulating cells in Arabidopsis testa: Regulation of differentiation and role in seed development. Plant Cell **15,** 2514-2531.

Diet, A., Brunner, S., and Ringli, C. (2004). The *enl* mutants enhance the *lrx1* root hair mutant phenotype of *Arabidopsis thaliana*. Plant Cell Physiol. **45,** 734-741.

Diet, A., Link, B., Seifert, G.J., Schellenberg, B., Wagner, U., Pauly, M., Reiter, W.D., and Ringli, C. (2006). The Arabidopsis root hair cell wall formation mutant *lrx1* is suppressed by mutations in the *RHM1* gene encoding a UDP-L-rhamnose synthase. Plant Cell **18,** 1630-1641.

Djakovic, S., Dyachok, J., Burke, M., Frank, M.J., and Smith, L.G. (2006). BRICK1/HSPC300 functions with SCAR and the ARP2/3 complex to regulate epidermal cell shape in Arabidopsis. Development 133, 1091-1100.

Frank, M.J., Cartwright, H.N., and Smith, L.G. (2003). Three *BRICK* genes have distinct functions in a common pathway promoting polarized cell division and cell morphogenesis in the maize leaf epidermis. Development 130, 753-762.

Friml, J. (2003). Auxin transport - shaping the plant. Curr. Op. Plant Biol. 6, 7-12.

Fu, Y., Gu, Y., Zheng, Z.L., Wasteneys, G., and Yang, Z.B. (2005). Arabidopsis interdigitating cell growth requires two antagonistic pathways with opposing action on cell morphogenesis. Cell 120, 687-700.

Gapper, C., and Dolan, L. (2006). Control of plant development by reactive oxygen species. Plant Physiol. 141, 341-345.

Geisler, M., Blakeslee, J.J., Bouchard, R., Lee, O.R., Vincenzetti, V., Bandyopadhyay, A., Titapiwatanakun, B., Peer, W.A., Bailly, A., Richards, E.L., Ejenda, K.F.K., Smith, A.P., Baroux, C., Grossniklaus, U., Muller, A., Hrycyna, C.A., Dudler, R., Murphy, A.S., and Martinoia, E. (2005). Cellular efflux of auxin catalyzed by the Arabidopsis MDR/PGP transporter AtPGP1. Plant J. 44, 179-194.

Horiguchi, G., Fujikura, U., Ferjani, A., Ishikawa, N., and Tsukaya, H. (2006). Large-scale histological analysis of leaf mutants using two simple leaf observation methods: identification of novel genetic pathways governing the size and shape of leaves. Plant J. 48, 638-644.

Jacobs, M., and Rubery, P.H. (1988). Naturally-Occurring Auxin Transport Regulators. Science 241, 346-349.

Jones, P., Messner, B., Nakajima, J.I., Schaffner, A.R., and Saito, K. (2003). UGT73C6 and UGT78D1, glycosyltransferases involved in flavonol glycoside biosynthesis in Arabidopsis thaliana. J. Biol. Chem. 278, 43910-43918.

Kang, B.G. (1979). Epinasty. In Physiology of Movements, W. Haupt and M.E. Feinleib, eds (Berlin: Springer-Verlag), pp. 647-667.

Kerhoas, L., Aouak, D., Cingoz, A., Routaboul, J.M., Lepiniec, L., Einhorn, J., and Birlirakis, N. (2006). Structural characterization of the major flavonoid glycosides from Arabidopsis thaliana seeds. Journal of Agricultural and Food Chemistry 54, 6603-6612.

Klein, M., Martinoia, E., Hoffmann-Thoma, G., and Weissenbock, G. (2000). A membrane-potential dependent ABC-like transporter mediates the vacuolar uptake of rye flavone glucuronides: regulation of glucuronide uptake by glutathione and its conjugates. Plant J. 21, 289-304.

Koornneef, M. (1990). Mutations affecting the testa color in Arabidopsis. Arabidopsis Inf Serv 19, 113-115.

Lavy, M., Bloch, D., Hazak, O., Gutman, I., Poraty, L., Sorek, N., Sternberg, H., and Yalovsky, S. (2007). A novel ROP/RAC effector links cell polarity, root-meristern maintenance, and vesicle trafficking. Curr. Biol. 17, 947-952.

Laxmi, A., Paul, L.K., Raychaudhuri, A., Peters, J.L., and Khurana, J.P. (2006). Arabidopsis cytokinin-resistant mutant, *cnr1*, displays altered auxin responses and sugar sensitivity. Plant Mol. Biol. 62, 409-425.

Le Gall, G., Metzdorff, S.B., Pedersen, J., Bennett, R.N., and Colquhoun, I.J. (2006). Metabolite profiling of *Arabidopsis thaliana* (L.) plants transformed with an antisense chalcone synthase gene. Metabol. 1, 181-198.

Lepiniec, L., Debeaujon, I., Routaboul, J.M., Baudry, A., Pourcel, L., Nesi, N., and Caboche, M. (2006). Genetics and biochemistry of seed flavonoids. Annu. Rev. Plant Biol. 57, 405-430.

Li, G., and Xue, H.W. (2007). Arabidopsis PLD zeta 2 regulates vesicle trafficking and is required for auxin response. Plant Cell 19, 281-295.

Liu-Gitz, L., Britz, S.J., and Wergin, W.P. (2000). Blue light inhibits stomatal development in soybean isolines containing kaempferol-3-O-2(G)-glycosyl-gentiobioside (K9), a unique flavonoid glycoside. Plant Cell and Environment 23, 883-891.

Martin, C., Bhatt, K., and Baumann, K. (2001). Shaping in plant cells. Curr. Op. Plant Biol. 4, 540-549.

Mathur, J. (2004). Cell shape development in plants. Trend in Plant Sci. 9, 583-590.

Mathur, J., Mathur, N., Kernebeck, B., and Hülskamp, M. (2003). Mutations in actin-related proteins 2 and 3 affect cell shape development in Arabidopsis. Plant Cell 15, 1632-1645.

Mo, Y.Y., Nagel, C., and Taylor, L.P. (1992). Biochemical complementation of *chalcone synthase* mutants defines a role for flavonols in functional pollen. Proc. Natl. Acad. Sci. USA 89, 7213-7217.

Müller, A., Düchting, P., and Weiler, E.W. (2002). A multiplex GC-MS/MS technique for the sensitive and quantitative single-run analysis of acidic phytohormones and related compounds, and its application to *Arabidopsis thaliana*. Planta 216, 44-56.

Multani, D.S., Briggs, S.P., Chamberlin, M.A., Blakeslee, J.J., Murphy, A.S., and Johal, G.S. (2003). Loss of an MDR transporter in compact stalks of maize *br2* and sorghum *dw3* mutants. Science 302, 81-84.

Murphy, A.S., Hoogner, K.R., Peer, W.A., and Taiz, L. (2002). Identification, purification, and molecular cloning of N-1-naphthylphthalmic acid-binding plasma membrane-associated aminopeptidases from Arabidopsis. Plant Physiol. 128, 935-950.

Noh, B., Murphy, A.S., and Spalding, E.P. (2001). Multidrug resistance-like genes of Arabidopsis required for auxin transport and auxin-mediated development. Plant Cell 13, 2441-2454.

Oka, T., Nemoto, T., and Jigami, Y. (2007). Functional analysis of *Arabidopsis thaliana* RHM2/MUM4, a multidomain protein involved in UDP-D-glucose to UDP-L-rhamnose conversion. J. Biol. Chem. 282, 5389-5403.

Peer, W.A., and Murphy, A.S. (2006). Flavonoids as signal molecules. In The Science of Flavonoids, E. Grotewold, ed (Berlin: Springer-Verlag), pp. 239-268.

Peer, W.A., Brown, D.E., Tague, B.W., Muday, G.K., Taiz, L., and Murphy, A.S. (2001). Flavonoid accumulation patterns of transparent testa mutants of Arabidopsis. Plant Physiol. 126, 536-548.

Peer, W.A., Bandyopadhyay, A., Blakeslee, J.J., Makam, S.I., Chen, R.J., Masson, P.H., and Murphy, A.S. (2004). Variation in expression and protein localization of the PIN family of auxin efflux facilitator proteins in flavonoid mutants with altered auxin transport in *Arabidopsis thaliana*. Plant Cell 16, 1898-1911.

Reiter, W.D., and Vanzin, G.F. (2001). Molecular genetics of nucleotide sugar interconversion pathways in plants. Plant Mol. Biol. 47, 95-113.

Ridley, B.L., O'Neill, M.A., and Mohnen, D.A. (2001). Pectins: structure, biosynthesis, and oligogalacturonide-related signaling. Phytochem. 57, 929-967.

Ringli, C. (2005). The role of extracellular LRR-extensin (LRX) proteins in cell wall formation. Plant Biosyst. 139, 32-35.

Routaboul, J.M., Kerhoas, L., Debeaujon, I., Pourcel, L., Caboche, M., Einhorn, J., and Lepiniec, L. (2006). Flavonoid diversity and biosynthesis in seed of *Arabidopsis thaliana*. Planta 224, 96-107.

Schijlen, E., de Vos, C.H.R., Martens, S., Jonker, H.H., Rosin, F.M., Molthoff, J.W., Tikunov, Y.M., Angenent, G.C., van Tunen, A.J., and Bovy, A.G. (2007). RNA interference silencing of Chalcone synthase, the first step in the flavonoid biosynthesis pathway, leads to parthenocarpic tomato fruits. Plant Physiol. 144, 1520-1530.

Shirley, B.W., Kubasek, W.L., Storz, G., Bruggemann, E., Koornneef, M., Ausubel, F.M., and Goodman, H.M. (1995). Analysis of Arabidopsis mutants deficient in flavonoid biosynthesis. Plant J. 8, 659-671.

Slimestad, R. (2003) Flavonoids in buds and young needles of *Picea*, *Pinus* and *Abies*. Biochem. Sys. Ecol. 31, 1247-1255.

Smith, L.G. (2003). Cytoskeletal control of plant cell shape: getting the fine points. Curr. Op. Plant Biol. 6, 63-73.

Staiger, C.J. (2000). Signaling to the actin cytoskeleton in plants. Annu. Rev. Plant Physiol. Plant Mol. Biol. 51, 257-288.

Stobiecki, M., Skirycz, A., Kerhoas, L., Kachlicki, P., Muth, D., Einhorn, J., and Mueller-Roeber, B. (2006). Profiling of phenolic glycosidic conjugates in leaves of *Arabidopsis thaliana* using LC/MS. Metabol. 2, 197-219.

Taylor, L.P., and Grotewold, E. (2005). Flavonoids as developmental regulators. Curr. Op. Plant Biol. 8, 317-323.

Ulmasov, T., Murfett, J., Hagen, G., and Guilfoyle, T.J. (1997). Aux/IAA proteins repress expression of reporter genes containing natural and highly active synthetic auxin response elements. Plant Cell 9, 1963-1971.

Vandenbussche, F., and Van Der Straeten, D. (2007) One for all and all for one: Cross-talk of multiple signals controlling the plant phenotype. J. Plant Growth Reg. 26, 178-187.

Veit, M., and Pauli, G.F. (1999). Major flavonoids from *Arabidopsis thaliana* leaves. J. Nat. Prod. 62, 1301-1303.

Watahiki, M.K., and Yamamoto, K.T. (1997). The *massugu1* mutation of Arabidopsis identified with failure of auxin-induced growth curvature of hypocotyl confers auxin insensitivity to hypocotyl and leaf. Plant Physiol. 115, 419-426.

Williamson, R.E., Burn, J.E., Birch, R., Baskin, T.I., Arioli, T., Betzner, A.S., and Cork, A. (2001). Morphology of *rsw1*, a cellulose-deficient mutant of Arabidopsis thaliana. Protoplasma 215, 116-127.

Yang, Z.B. (1998). Signaling tip growth in plants. Curr. Op. Plant Biol. 1, 525-530.